Global mapping of nature based flood risk reduction solutions

MSc. thesis

T. R. Krijger

MSC. Thesis

Delft University of Technology

Global mapping of nature based flood risk reduction solutions

Author:
Tjerk Krijger (4481909)

Date:
November 4, 2021

TU Delft

Prof. dr. ir. S.N. (Bas) Jonkman **(Chair of committee)**
Prof. dr. ir. S.G.J. (Stefan) Aarninkhof
Ir. A.G.M. (Alejandra) Gijón Mancheño

Van Oord

Dr. ir. Gerben J. de Boer

TUDelft

Van Oord
Marine ingenuity

Preface

This thesis concludes my Master of Science program of Hydraulic Engineering with specialization of Coastal Engineering at the Delft University of Technology, conducted in cooperation with Van Oord.

During one of the lectures of Coastal and Basin-scale Physical Oceanography, Gerben de Boer performed a guest lecture where I was introduced to the Climate Adaptation Program of Van Oord. It immediately caught my intention as it involved a research subject from two angles, namely large data sets and specific coastal engineering problems. By combining those two facets, I think future predictions of coastal vulnerability on a global scale can be improved.

I would like to thank Gerben de Boer for choosing to work with me for a period of eight months and providing me with feedback about anything at anytime. Secondly, I would like to thank Alejandra Gijón Mancheño for providing me with key insights from her Mangrove expertise during our bi-weekly meetings. I would like to thank Bas Jonkman for his feedback especially related to the flood risk sections that really helped shaping and scoping this research. Also, even though William de Lange was only part of the committee shortly, I would still like to thank William for bringing me a lot of enthusiasm at the early stages of the work. Furthermore, I would like to thank Stefan Aarninkhof for the feedback that was provided during the consequent committee meetings.

Finally, I would like to thank my family and friends for their continuous support throughout my studies.

T.R. (Tjerk) Krijger
Delft, November 2021

Abstract

Coastal flood risk is expected to increase over the 21st century as a result of climate change and economic growth, which makes low-lying regions especially vulnerable. Global screening techniques are needed for a more widespread use of NBS in these flood prone coastal regions. This research expands on the current assessments done by developing a quantitative global screening method that evaluates the costs and benefits for two defence approaches; 1) increasing the dike height, 2) a hybrid solution that includes increasing of the dike height in combination with restoring mangroves and/or corals. The screening method is based on Van Oord's Climate Risk Overview tool, in which, globally, coastal hotspots are indicated that have a predefined risk of flooding in the 21st century. The steps added by my screening method include; 1) determining which NBS can be applied depending on the local physical conditions, 2) determining the costs for both NBS and conventional hard solutions, 3) determining the increase/decrease in flood risk of the different interventions for current and future conditions, 4) monetizing additional benefits that NBS provide, 5) assessing the benefits and costs to determine if NBS are the most optimal solution. The results of this global method are inherently limited by several simplifying assumptions and by the lack of high resolution local data, which influences the cost/risk estimates and corresponding site identification. For 2.6-3.3% of the coastal hotspots, NBS can reduce the investment costs in addition to being cost-beneficial. There is potential for expanding this work by adding sea grasses, salt marshes and oyster reefs as vegetated foreshore systems, and by including more thresholds to make the criterion for potential sites to apply NBS more strict.

Summary

Coastal flood risk is expected to increase over the 21st century as a result of climate change and economic growth, which makes low-lying regions especially vulnerable. Long-term coastal adaptation strategies and mitigation measures are required considering this uncertain future. Hard coastal structures such as dikes and breakwaters are the most common mitigation measures, but are neither resilient as they cannot keep up with SLR nor sustainable as it can damage the local ecosystems. Nature-based solutions (NBS) can serve as important elements in adaptive coastal management, as they can maintain ecological values and mitigate flood risk. NBS can reduce the flood risk by by attenuating waves and storm surge and by reducing erosion. However, they are not yet widely used due to a combination of factors such as a lack of quantitative knowledge about their efficacy for coastal protection, but also about their contribution to flood risk reduction and fit to economic considerations.

In order to promote and increase more widespread use of NBS in flood prone coastal regions, global screening techniques are required. Currently global assessments have been done to evaluate to evaluate the global costs and/or benefits for dikes (Hinkel et al., 2014; Tiggeloven et al., 2020), mangroves (van Zelst, 2018; Menéndez et al., 2020) and corals (Beck et al., 2018) all over the world, under several scenarios of SLR. However, these studies did not consider potential sites for mangrove and coral restoration, did not all use the latest information on current protections, and did not investigate the combination of dikes with mangroves and corals.

This research expands on the current assessments done by developing a quantitative global screening method that evaluates the costs and benefits for two defence approaches; 1) increasing the dike height, 2) a hybrid solution that includes increasing of the dike height in combination with restoring mangroves and/or corals. These approaches explain the intervention that is taken to go from the current towards the new situation. The aim is to target cost-effective risk reduction measures for flood prone coastal areas on a global scale. This method was developed as part of Van Oord's sustainability program, which aims to pursue sustainable projects pro-actively all around the world.

The screening method is based on Van Oord's Climate Risk Overview tool, in which global coastal hotspots are indicated that have a predefined risk of flooding in the 21st century. The hotspots consist out of polygons that comprise all land below MSL+10m of approximately 10x10 km^2 and are scattered along the world's coastlines. The tool also provides a large amount of layers that include parameters such as the local sea level rise (SLR), storm surge and population among others, which are assigned to the hotspots.

The method is followed for three adaptation strategies. The adaptation strategies require different magnitudes of interventions to go from the current towards the new situation. The strategies indicate $\boldsymbol{A}$) keeping the coastal protection standard like it currently is and investigate what impact SLR has, $\boldsymbol{B}$) improving the protection standard without taking SLR into account, $\boldsymbol{C}$) improving the protection standard while taking into account SLR.

The method consists of five steps, which means that we perform calculations including three adaptations strategies and two defence approaches for those five steps, resulting in 30 calculations. The steps of the global approach include; 1) determining which NBS can be applied depending on the local physical conditions, 2) determining the costs for both NBS and conventional hard solutions, 3) determining the increase/decrease in flood risk of the different interventions for current and future conditions, 4) monetizing additional benefits that NBS provide, 5) assessing the benefits and costs to determine if NBS are the most optimal solution.

The screening methods designed to find local hotspots, is integrated on a global scale, which allows to draw the following conclusions. Globally 54.6% of the 38,773 coastal hotspots were found suitable for either mangrove and/or coral restoration, which amounts to 21,182 identified potential sites. The global total dike investment costs (not considering NBS) required to improve the protection standard of the current coastal defence for the 38,773 coastal hotspots amounts to \$390-\$2,288 billion, depending on the adaptation strategy used (exclud-

ing/including SLR). If NBS such as mangroves and corals are also considered at the 21,182 identified potential sites, a total reduction in investment costs of \$4.3-\$54.7 billion (1-2% of total) is found for 2,275-5,858 of these sites combined. By improving the protection standard with either dikes or dikes + NBS, a global reduction in flood risk of \$76.5-\$82.6 billion/yr is achieved at the end of the 21st century. In total, carrying out all the NBS solutions identified in this study would create economic benefits of \$270-\$3,925 billion, which would not be generated by only constructing dikes. Depending on the defence approach that is followed, for 7.7-22.0% of the coastal hotspots, the flood risk reduction benefits of improving the protection standard are larger than the corresponding investment costs. Hence, at these locations improving the protection standard is cost-effective. If additional benefits of NBS are also taken into account, the amount of locations increases to 20.3-24.6% of the coastal hotspots. 2.6-3.3% of the hotspots corresponded with locations meeting the requirements for mangrove/coral potential, reduction in investment costs and benefit-cost ratios larger than 1. If the new protection standard is optimized, the number of cost-effective locations increases by 11-17%.

The results of this global method are inherently limited by several simplifying assumptions and by the lack of high resolution local data, which influences the cost/risk estimates and corresponding site identification. A generic sensitivity analysis of the input parameters of the screening method shows that the model was most sensitive to the design water level (DWL) and wave period; a 25% increase of the DWL or wave period increased the median dike investment costs per km of coastline by \$2.2 million. Other limitations include the identification of potential mangrove and/or coral restoration sites due to a lack of global data for local ecosystem requirements and the mangrove and coral wave attenuation magnitudes. This research also involves unexplored uncertainties considering the current protection standards, vegetation widths and additional benefits. However, considering these uncertainties, this work provides an indication of sites with high potential for NBS even if there are currently none present. This can then be investigated in a more detailed assessment in addition to existing assessments. Developing systematic methodologies for identifying potential sites for NBS provides more insight into the economical benefits they yield. Combining the additional benefits of these ecosystems with their flood risk reduction, results in more resilient and sustainable protection methods against SLR.

The global screening method can be improved by developing more accurate data sets involving the physical parameters such as the current protection standard, hydrodynamic parameters, wave attenuation of mangroves and corals and by including land subsidence. More research on the efficacy of NBS must be done in addition to the additional benefits they provide. There is potential for expanding this work by adding sea grasses, salt marshes and oyster reefs as vegetated foreshore systems and by including more thresholds to make the criterion for potential sites to apply NBS stricter.

Table of Contents

V Appendices 86

1 | Introduction

1.1 Motivation for research

1.1.1 Global expected increase in flood risk

Coastal flood risk is expected to increase over the 21st century as a result of climate change and economic growth. Low-lying areas located along the world's coastlines are increasingly populated. As a result, not only are the coastal environment and natural processes impacted significantly due to human-induced changes, also, the exposure to hazards is becoming increasingly higher (Small & Nicholls, 2003). Next to this, there is an increased probability of extreme water levels due to climate change, as sea levels rise and the storminess increases. Land subsidence exacerbates flooding and makes low-lying areas particularly vulnerable.

The worst-case emission scenario, RCP8.5 (Stocker et al., 2013), corresponds to an estimated global mean sea level rise of 0.84m for 2081-2100 (Stocker et al., 2013) and is the result of climate change if no climate mitigation measures are taken. It is expected that 0.2-4.6% of the global population will be flooded annually in 2100 (Hinkel et al., 2014), which results in expected losses of 0.3-9.3% per year of the global gross domestic products (Hinkel et al., 2014). Due to this projected change in global mean sea level (RCP8.5), historically centennial events (local sea levels that occurred $\frac{1}{100}$ years) are predicted to occur at least annually during the 21st century at most locations along the world's coastlines (Pörtner et al., 2019). Low-lying coastal regions account for approximately 600 million people all around the world with a combined revenue of $1,000 billion. Flooding of these regions will have huge environmental and socio-economic consequences (Kirezci et al., 2020). These results highlight the importance of long-term coastal adaptation strategies (Hinkel et al., 2014) and require mitigation measures to keep the flood risk within acceptable levels.

1.1.2 Nature-based solutions as flood risk reduction measures

Globally, hard structures (sea walls, revetments, dikes and breakwaters) are the most common solution for flood risk reduction. However, these solutions have several limitations and are in constant need of maintenance and repair (BA et al., 2001). As the sea level rises and the storminess increases, these types of structures are facing increased cost of maintenance (BA et al., 2001; Morris et al., 2018). Historically the coastal defence approach was focused on optimizing flood safety only. However this is often found to be sub-optimal considering other functions present in the coastal areas such as for example preserving the local ecosystem (Van Slobbe et al., 2013). Next to this, the traditional approach tends to be neither resilient as it cannot keep up with SLR nor sustainable as it can damage the local ecosystems (Van Slobbe et al., 2013). As climate change continues to impact the environment, coastal regions, especially the highly populated ones, require resilient solutions that are robust, sustainable, adaptable and economically feasible (Van Slobbe et al., 2013).

NBS can serve as a resilient solution, as they mitigate flood risk and maintain the ecological values (Van Slobbe et al., 2013). They can also provide co-benefits such as enhancing of fisheries and recreation and tourism (van Wesenbeeck et al., 2017). This type of flood protection can gradually follow the climate-induced changes (Morris et al., 2018; Van Slobbe et al., 2013) if there is enough space available landwards, as ecosystems will retreat if the local sea level rise is high. NBS consist of the integration of existing coastal ecosystems for flood risk reduction while their impact is enhanced to dissipate wave energy and reduce erosion (Pontee et al., 2016). Examples of coastal ecosystems are salt marshes, mangroves, sea grasses and coral & oyster reefs (Pontee et al., 2016). Within this research the definitions in table 1.1 are used (Schoonees et al., 2019).

NBS such as salt marshes, mangrove forests and coral reefs can reduce the flood risk by attenuating waves and storm surge and by reducing erosion (Pontee et al., 2016). Vuik et al. (2018) found that vegetated foreshores reduce the probability of failure due to wave overtopping and wave impact on revetments. Especially for low dikes, the vegetated foreshore can be important for reducing loads from waves (Vuik et al., 2018). Coastal regions that are prone to a highly variable wave climate, could benefit largely from including ecosystems, such as a combination of a vegetation field (mangroves, salt marshes and sea grass beds) with an adaptive dike.

The vegetation field can narrow down the range of incoming wave heights, making the adaptive dike more robust. The dike height can therefore be reduced, which results in a smaller dike base that has less impact on the compaction of soil and hence the surrounding area (van Wesenbeeck et al., 2017).

Type	Classification	Examples
Grey	Hard solutions	Groynes, sea walls, revetments, dikes and breakwaters.
Soft	Nature-based solutions	Salt marshes, mangroves, sea grasses and coral & oyster reefs.
Hybrid	Combination of hard and nature-based solutions	Dikes fronted by vegetated foreshores (mangroves, wetlands).

Table 1.1: *Definitions different marine flood solutions (Schoonees et al., 2019; Pontee et al., 2016).*

NBS are thus important elements in adaptive coastal management, but not yet common practise due to a lack of awareness about the protective role of ecosystems & the complexity and uncertainties surrounding the efficacy of the ecosystems. Next to this, a lack of knowledge concerning financial benefits and stakeholder engagement limits the implementation of NBS. Grey infrastructure is still widely used as there is no full control on how the vegetation will grow. Also, due to the changes in vegetation properties, the exact magnitude of protection is hard to determine. As NBS are tailor-made, it is not possible to copy an exact successful solution from one place to a different location around the world. Note that depending on the local conditions, NBS do not always have to be the best solution.

1.2 Problem description

In order to promote and increase more widespread use of NBS in flood prone coastal regions, global screening techniques are required. Currently, global assessments have been done to evaluate the global costs and/or benefits for dikes (Hinkel et al., 2014; Tiggeloven et al., 2020), mangroves (van Zelst, 2018; Menéndez et al., 2020) and corals (Beck et al., 2018), under several scenarios of SLR. However, these studies did not consider potential sites for mangrove and coral restoration, did not all use the latest information on current protections, and did not investigate the combination of dikes with mangroves and corals. Next to this, the additional benefits that NBS provide were almost always excluded and most flood risk calculations neglected the current coastal protections. As a result there is still a lack of quantitative global knowledge about their contribution to flood risk reduction and their fit to economic considerations.

1.3 Objective

To promote and increase more widespread adaptive decision making in low-lying coastal areas (hotspots as indicated in Van Oord's Climate Risk Overview) that are increasingly at risk due to climate change, this study aims to expand on the current assessments done by developing a **quantitative global method** (see Figure B.6.3). This method combines all relevant local parameters and serves as an advisory function to identify potential NBS sites. Where possible, the aim is to include and hence promote NBS by showing the cost-effectiveness of these solutions. The main objective is the following:

Targeting cost-effective risk reduction measures including NBS for flood prone coastal areas on a global scale.

The possible risk reduction measures include **two defence approaches**; 1) increasing the dike height, 2) a hybrid solution that includes increasing of the dike height in combination with restoring mangroves and/or corals (see Figure 1.3). An important aspect here is to translate the site-specific knowledge of certain NBS to general applicability around the world. This objective was developed as part of Van Oord's sustainability program, which aims to pursue sustainable projects pro-actively all around the world.

The quantitative global screening method is based on Van Oord's Climate Risk Overview tool, in which hotspots are indicated that have a predefined risk of flooding in the 21st century. In order to construct the

hotspots a mathematical space filling algorithm (Voronoi) is used that fills the area from MSL-50 m until MSL+10 m with polygons of 10x10 km^2. These boundaries are chosen, such that the Low Elevation Coastal Zone (LECZ) and the shallow foreshore are taken into account. The polygons are split into wet and dry polygons by the defined coastline, where for flooding calculations only the dry areas are used. With these definitions, globally 61,589 global hotspots are identified (dry polygons), which are located in the LECZ. However, not all these locations are located along the coastline, as there are areas further inland with low elevations such as the Rhine-Meuse estuary, Mekong delta among others. Within this research the quantitative global screening method was applied to the coastal hotspots, which amounts to 38,773 or 63% (Figure 1.1) of the total amount of identified hotspot. The Climate Risk Overview is expanded by developing a systematic methodology for identifying potential sites for NBS to gain more insight in the benefits that they provide.

The tool provides a large amount of layers that include parameters such as the local sea level rise (SLR), storm surge and population among others, which are assigned to the hotspots. The tool was developed to anticipate the hazard of flooding for all coastlines and societies around the world. The polygon size of 10x10 km^2 is chosen, as it amounts to 50,000-100,000 hotspots worldwide, which is a number that is still practically manageable for fast interaction in GIS and BI (Business Intelligence) software. Next to this, it is a practical size for mitigation measures, since it is a typical order of magnitude for local communities and organisations.

(a)

(b)
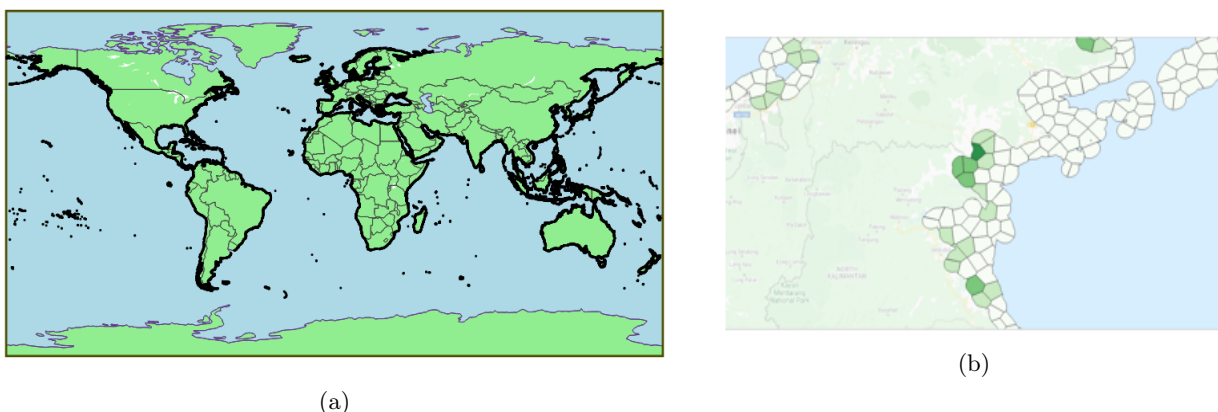
Figure 1.1: *The 38,773 coastal hotspots filtered from the Climate Risk Overview of Van Oord (Figure 1.1a). The hotspots are portrayed by polygons of 10x10 km^2 regions using a space filling algorithm leading to the irregular shapes (Figure 1.1b).*

The quantitative global screening method consists out of five steps and is followed for three adaptation strategies. The adaptation strategies require different interventions to go from the current towards the new situation. Depending on the hotspot, the current situation is assumed to be governed by (Figure 1.3):

- Dike system.
- Dike in combination with mangroves.
- Dike in combination with corals.
- Dike in combination with corals and mangroves.

The protection standard for the current situation is taken from the FLOPROS-database that is based on a hierarchical principle to establish the best possible (i.e. most accurate, closest to hypothetical protection standard) information at different locations (Scussolini et al., 2016). The following adaptation strategies are taken into account in this research (see Figure 1.3):

- $A_{cur,slr}$: Between the current and new situation that includes the local SLR prediction, the protection standard is kept constant in order to investigate the impact that SLR has. To keep the protection standard constant, the coastal defence will have to be improved in locations where local SLR occurs (there are also locations with negative predicted local SLR).

- **B_{new}**: For the new situation, the protection standard is increased towards a new fixed standard, without taking SLR into account. The coastal defence will still need to be improved, as the storm surge component increases for a higher return period. This strategy is taken into account to investigate the impact that SLR has by comparing it to strategy $C_{new,slr}$.

- **$C_{new,slr}$**: For the new situation, the protection standard is increased towards a new fixed standard, while also taking into account SLR.

Recall that the intervention by mitigation measures mentioned in the objective can include either 1) increasing the dike height, 2) a hybrid solution that includes increasing of the dike height in combination with restoring mangroves and/or corals (see Figure 1.3). For the hybrid solutions, mangroves and coral reefs are used depending on whether they can occur at the hotspot. This means that for the three different adaptation strategies each two calculations are performed corresponding to the two different defence approaches mentioned above.

The quantitative global screening method aims to answer the main question: **How can the flood risk reduction potential of various solutions be assessed at a global scale?**

The following sub-questions are connected to each of the fives steps in the method (see Figure 1.3):

1. *Which nature-based solutions can be applied at all global coastal hotspots based on the local environment?*
   In the first step the applicability of corals and mangroves for each location is determined. Coastal ecosystems have specific habitat requirements and can only develop under specific physical conditions. For each hotspot the possibility to apply mangroves and/or corals is determined based on the local conditions such as the morphology, connectivity and climate conditions. This is done by defining thresholds related to the habitat requirements that govern whether a site is suitable for mangrove and/or coral restoration.

2. *What are the global total investment costs for improving the protection standard with or without coral and/or mangrove restoration?*
   The second step determines the costs of the two different defence approaches. The costs are determined for raising of the dikes and for raising the dikes in combination with coral and/or mangrove restoration. The magnitudes are based on the amount of dike heightening and mangrove and/or coral restoration required and on the adaptation strategy that is followed. Different solutions consist of different costs, dike costs are related to the amount of dike heightening required, whereas vegetation costs are related to the amount of hectares of vegetation restored.

3. *What are the global total flood risk reduction benefits of improving the protection standard?*
   The third step determines the benefits through flood risk reduction. Depending on the adaptation strategy, the flood risk can increase or decrease. The difference between the current risk at each location and the new risk is expressed in terms of flood risk reduction. When improving the protection standard, the probability of flooding can be reduced and hence flood risk reduction benefits are provided, expressed in monetary values.

4. *What are the global total additional benefits connected to the restored area of mangroves and corals?*
   The fourth step determines the additional benefits that NBS provide. If NBS can be applied, they will provide additional benefits such as enhancing fisheries and tourism. For mangroves and coral reefs these additional benefits are determined and monetized. Depending on the applicability of mangroves and corals (step 1) and the amount of mangroves and corals restored, the additional benefits per hotspot can be determined.

5. *Based on all the benefits and costs, what are the flood risk reduction potentials of the various solutions?*
   The last step determines the benefit to cost ratios. Here, a benefit-cost comparison is done, based on the investment costs, flood risk reduction benefits and additional benefits. This is done for both defence approaches, dike raising and dike raising in combination with coral and mangrove restoration. The costs involve either solely the costs of raising the dikes or a combination of the costs for raising of the dikes and mangrove/coral restoration costs. The benefits are expressed in flood risk reduction terms and/or by the additional benefits that mangroves and corals provide compared to the current situation.

Summarizing, the local conditions are used to determine for all hotspots whether mangroves and/or corals can be applied. The costs corresponding to the intervention including either dike heightening or dike heightening and coral/mangrove restoration are then determined for the three different adaptation strategies, hence six cases. The costs are determined based on the amount of dike heightening and mangrove and/or coral restoration area. Depending on the adaptation strategy, the flood risk can increase or decrease, where for adaptation strategies B_{new} and $C_{new,slr}$, the benefits of improving the coastal defence can be expressed in terms of flood risk reduction. If NBS can be applied, they will provide additional benefits such as enhancing fisheries and tourism. For the different solutions these additional benefits are determined and monetized. Finally the benefit to cost ratios are used to assess the flood risk reduction potential.

1.4   Reader Guide

The research consists of two main parts, the Global Framework and the Local Framework (Figure 1.2). Firstly the Global Framework is presented (Figure 1.3), that consist out of **chapters 2-6**, which are linked to the steps described in the framework (Figure 1.3). Each of the five sub-questions above corresponds to one step of the global quantitative screening method and consequently to one of the chapters. These chapters explain in detail the established methods and present for each step the corresponding results.

Secondly, the Local Framework is presented that consists out of **chapters 7-8**. **Chapter 7** compares the results obtained for the hotspots on a global scale to different local sites, in order to give more insight towards the errors that can occur when using a global model and to show the corresponding uncertainties that revolve around the results. **Chapter 8** present a generic sensitivity analysis concerning the parameters used for the global screening method. Finally, the results are discussed and recommendations are given in **chapter 9** and the main conclusions are given in **chapter 10**.
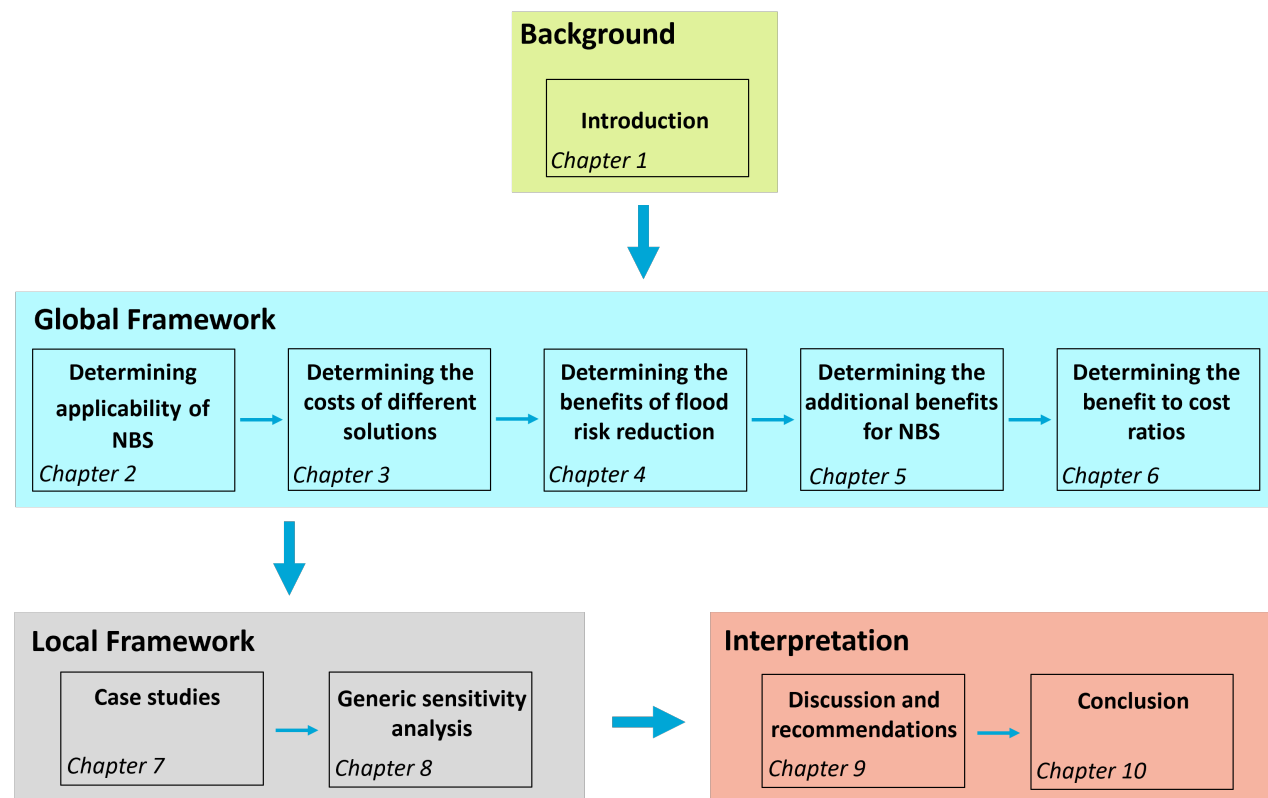
Figure 1.2: *The Global and Local Framework distributed over the chapters. Notice that the five steps within the Global Framework aim to answer each of the five sub-questions listed above separately.*
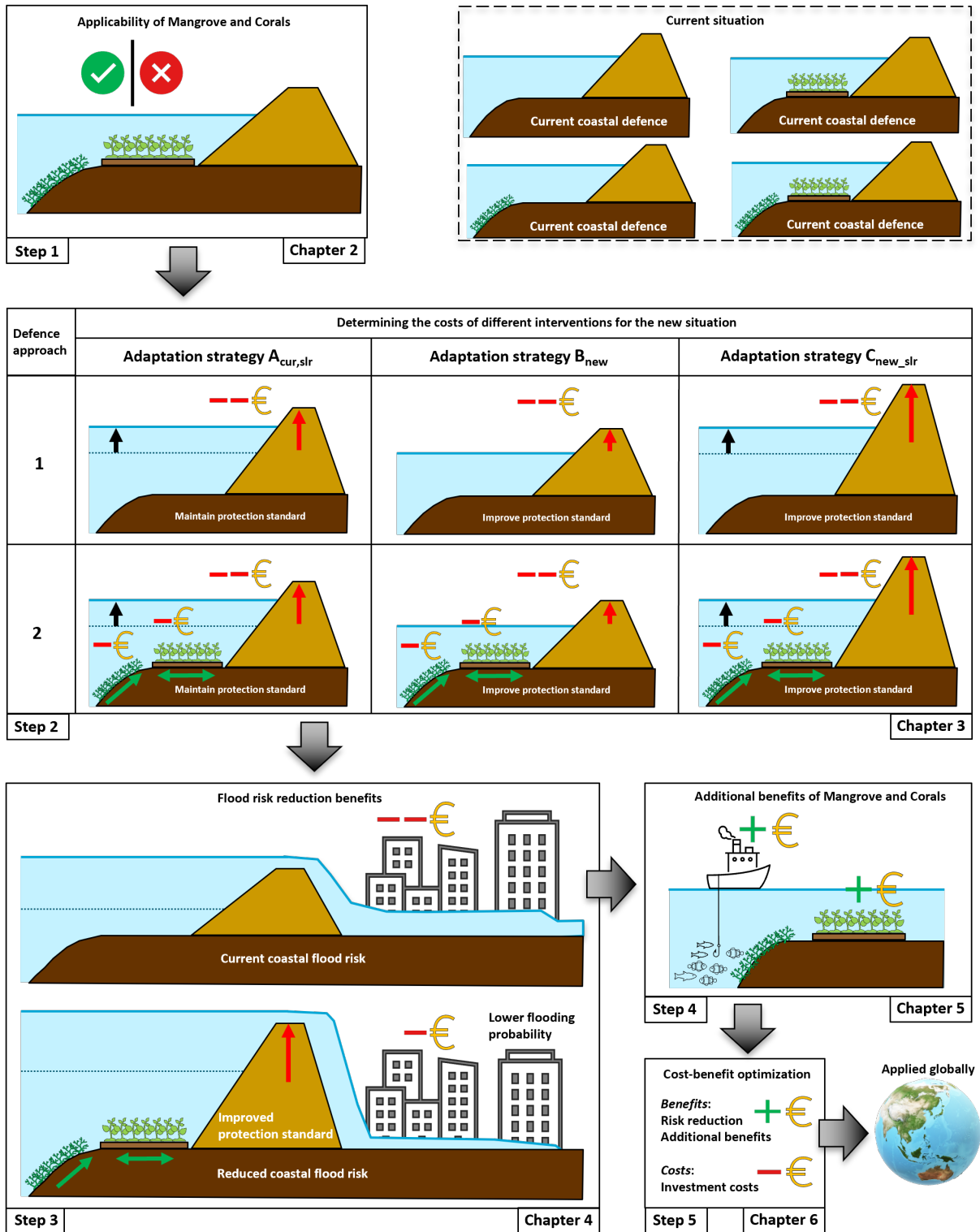
Figure 1.3: *The five research steps followed within this report, targeted at determining the costs and benefits related to interventions including dike heightening or a combination of dike heightening with mangrove/coral restoration.*

Part I

Global Framework

2 | Determining the applicability of nature-based solutions

This chapter aims to answer the sub-question: *"Which nature-based solutions can be applied at all global coastal hotspots based on the local environment?".* The parameters that are used to assess the applicability of mangroves and/or corals are discussed here. For each parameter thresholds are established based on different literature. The origin and information of the different parameters are explained for each threshold below. For each parameter, obtained from global data sets, the data is linked to the hotspots via either linear interpolation or the nearest neighbour principle by using the latitudes and longitudes of the hotspots (see Appendix B.1).

2.1 Thresholds for mangrove applicability

For certain habitat requirements specific to mangroves, global thresholds can be established for which the environmental conditions are suitable. Based on the availability of global data sets, the following thresholds are established:

1. Occurrence of mangroves (Giri et al., 2011).

2. Hotspot should be located between 33°N-39°S (Giri et al., 2011; Worthington & Spalding, 2018).

3. Location should be in the proximity of existing mangrove forests (connectivity) (Mancheño et al., 2021; Clarke, 1993).

The retreating of coastlines is used to assess which hotspots require erosion mitigation measures to enable mangrove restoration, but is not used as an excursion criterion (Luijendijk et al., 2018).

2.1.1 Occurrence of mangroves

For each hotspot, the area of mangroves currently present is based on Giri et al. (2011), which involved mapping of the global mangroves distribution using Global Land Survey data and the Landsat archive. Figure 2.1 shows the hotspots where mangroves are present. If mangroves occur at a location, the environment most likely has local conditions that are appropriate for restoration.

Global distribution of Mangroves
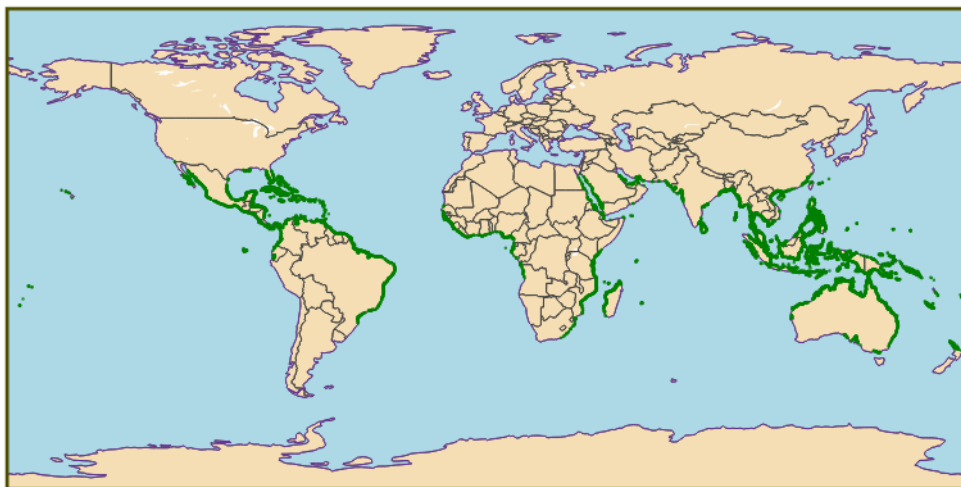
Figure 2.1: *Global distribution of mangroves, green dots denote the hotspots with a certain amount of mangroves (Giri et al., 2011).*

2.1.2 Coastline retreat

Shoreline retreat results in many cases from a decreased sediment supply, caused by for example dam construction upstream (Bidorn et al., 2021). However, sediment deficit is not always the reason why coastlines are eroding. Bidorn et al. (2021) investigated the relation between sediment supply and coastal retreat in the Chao Phraya River and Delta, which has been experiencing high rates of coastline retreat. It was found that the main contributors to coastline retreat are land subsidence and local SLR. The same results were found by Karlsrud et al. (2017) in the Ca Mau Province of Vietnam. In East Asia, land-side mangroves are chopped down for fishponds resulting in narrow mangrove strips. These strips are then not able to maintain themselves, leading to collapse and subsequent erosion. Mangroves require sufficient amount of sedimentation in order to keep up with the local SLR and land subsidence. However, if it is too fast, the roots can be smothered. With coastline retreat, consequently loss of mangroves occurs, which is why for these locations mitigation measures are required.

Luijendijk et al. (2018) researched the state of the world's beaches, resulting in the erosion and accretion rates of the shoreline. The erosion and accretion rates are obtained along coasts, every 300-500m, over the period of 1984 to 2016, with the corresponding yearly averages being available. Figure 2.2a shows eroding hotspots in red and accreting hotspots in green.

(a)

(b)
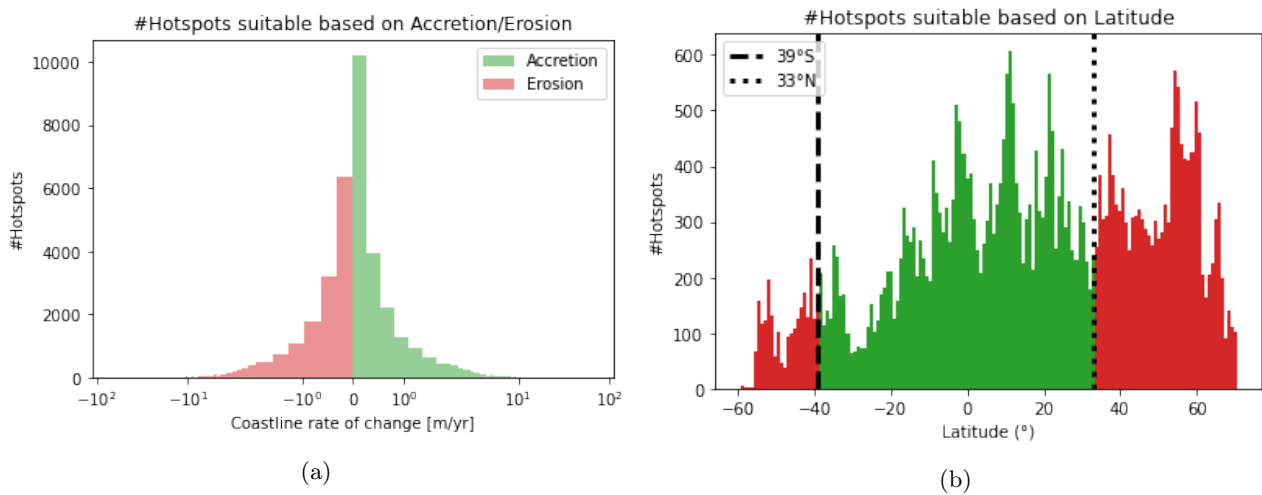
Figure 2.2: *Rate of change of the coastline which is not used as a treshold but as an indication where mitigation measures are required in order to enable mangrove restoration (Luijendijk et al., 2018) (2.2a) and the latitudes of the hotspots (2.2b), y-axis gives the amount of hotspots. The hotspots in red do not meet the requirements whereas the hotspots in green do.*
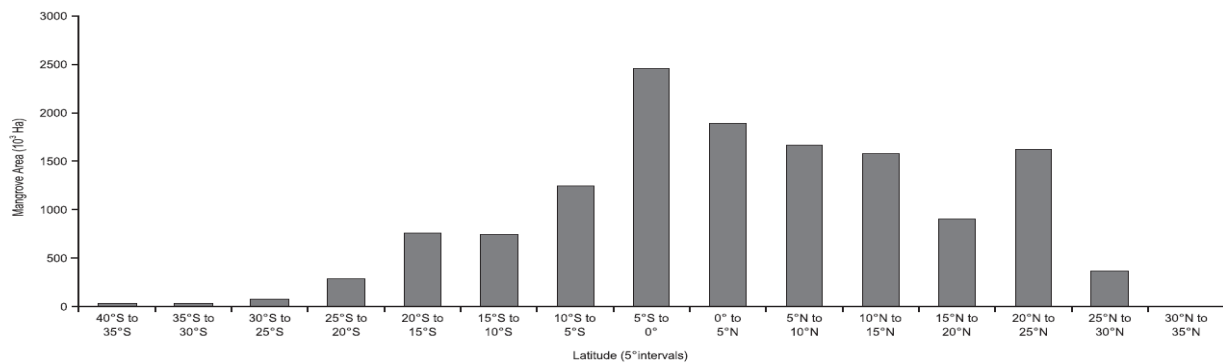
Figure 2.3: *Total mangrove area per latitude (Giri et al., 2011).*

2.1.3 Latitudinal limits

In general mangroves grow in tropical and subtropical coastal areas that are located between 25°N-25°S. However, these latitudinal limits are highly variable depending upon the area of the world and its local climates. Worthington & Spalding (2018) mapped potential locations for mangrove restoration, which resulted in the mangrove Restoration Potential Map (MRP[1]). Within this map, there are location as far as 33°N and 39°S where mangroves can be restored. The same latitudinal limits are found in Giri et al. (2011) (Figures 2.1 & 2.3). Therefore, in this research it is chosen to maintain these latitudinal limits. Figure 2.2b shows the distribution of hotspots with latitude, with the 33°N and 39°S bounds being displayed. The hotspots outside of these bounds are assumed to not be suitable for mangroves restoration and are plotted in red.

2.1.4 Connectivity

If natural establishment of mangroves is not present, artificial planting is necessary. The proximity to other mangroves determines whether natural supply of propagules [2] occurs, which in turn is required for a sustainable ecosystem. For hotspots located within a radius of 10 km of a location with mangroves, the hotspot is assumed to be suitable for (re)colonization (Mancheño et al., 2021). Since the hotspots have average sizes of 10x10 km^2, the question is if there is a neighbouring hotspot with mangroves. This spatial limit is based on dispersal distances that are observed by Clarke (1993) for Avicennia marina seedlings. In reality, these distances will vary between different mangrove species and are dependent on the local hydrodynamic processes. However, as a first assessment this value does provide an indication of the areas where mangroves could recruit naturally.[3] Figure 2.4 shows the coast of Cambodja filled with hotspots. Circles around mangrove hotspots with a radius of 10 km are projected. Within this area hotspots are said to be close enough and hence meet the threshold (green dots), hotspots outside of these circles are not (red dots).

$$d = 2r * arcsin\left(\sqrt{sin^2\left(\frac{\phi_2 - \phi_1}{2}\right) + cos(\phi_1)cos(\phi_2)sin^2\left(\frac{\lambda_2 - \lambda_1}{2}\right)}\right) \ [m] \qquad (2.1)$$
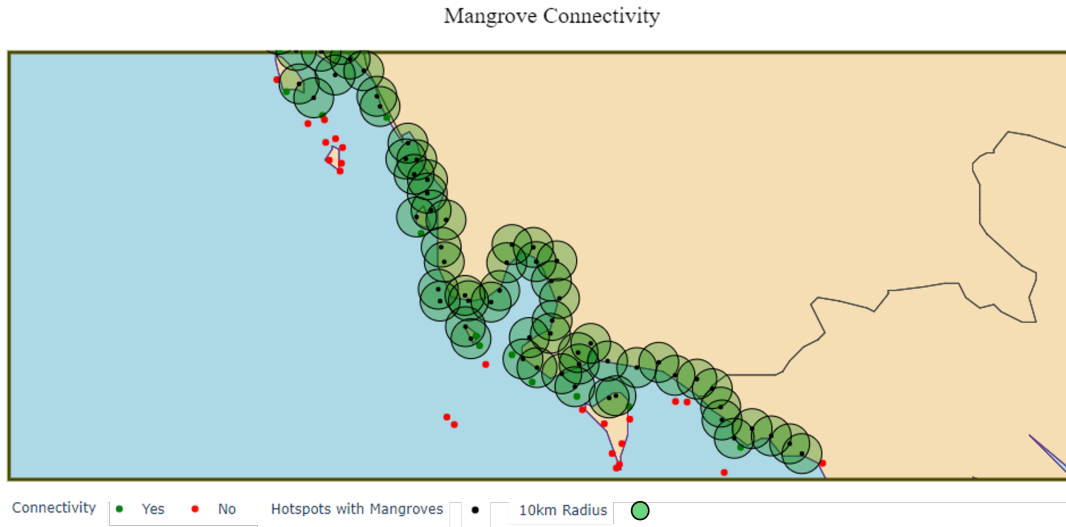
Figure 2.4: *Mangrove connectivity of hotspots based on a maximum haversine distance of 10 km.*

---

[1]http://maps.oceanwealth.org/mangrove-restoration/

[2]Material that functions in propagating an organism to the next stage in its life cycle, such as by dispersal (in the form of seeds and spores for plants).

[3]The haversine distances (d) between the hotspots are calculated based on their longitudes (λ_1 & λ_2) and latitudes (ϕ_1 & ϕ_2). The haversine formula calculates the distance along a great circle between two points (Equation 2.1). It assumes a perfect sphere, however the radius of the Earth (r) varies between the poles and the equator. This makes the formula an approximation rather than returning exact distances between two points. For this research the corresponding error in the order of a few meters can be neglected, especially looking at the applied threshold which is not fixed.

2.2 Thresholds for coral reef applicability

For coral reefs, also not for all habitat requirements data can be obtained on a global scale. Based on the availability of global data sets, the following thresholds are established:

1. Occurrence of corals (IMaRS-USF, 2005; Spalding et al., 2001).

2. Yearly varying sea surface temperature (SST) must be between 18 and 36°C (NOAA, 2021).

3. Salinity is required to be between 15-36 ppt (ecoshape, 2020; Melnichenko et al., 2021).

4. Surface irradiance should be at least 6-8 % (ecoshape, 2020; Balali et al., 2012).

2.2.1 Occurrence of corals

For each hotspot, the area of corals present is determined based on work done by the UNEP World Conservation Monitoring Centre and the WorldFish Centre, who compiled the most detailed global data set currently available of coral reefs. The data set is compiled from multiple different sources, such as the Millennium coral reef Mapping Project (IMaRS-USF, 2005) and the World Atlas of coral reefs (Spalding et al., 2001). Figure 2.5 shows the hotspots where corals are present.
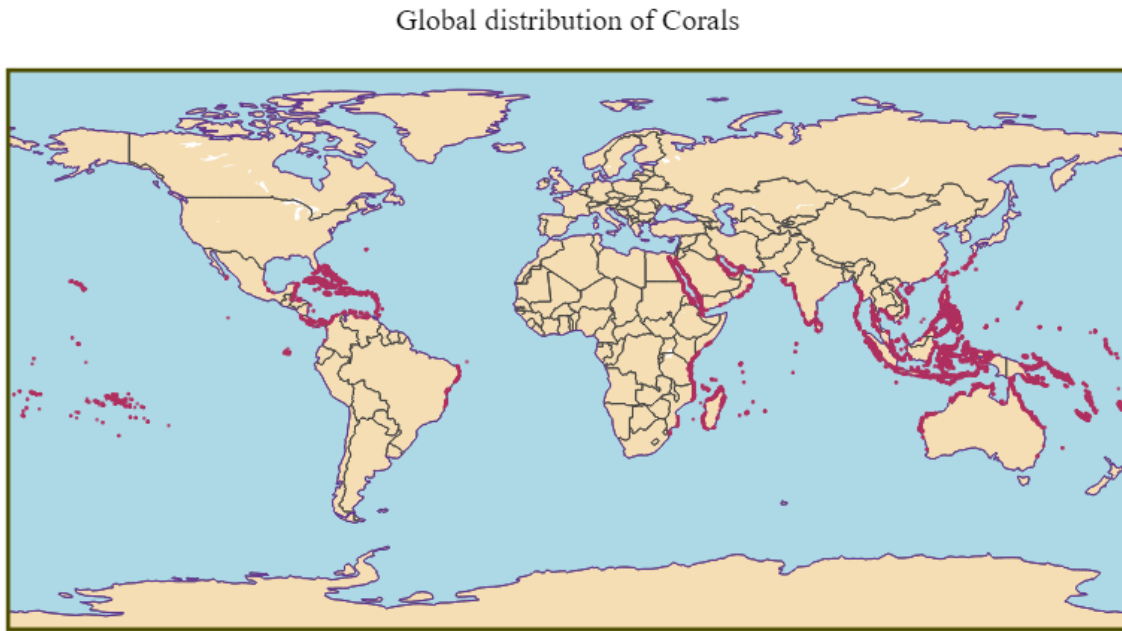
Figure 2.5: *Global distribution of corals, pink dots denote the hotspots with a certain amount of corals (IMaRS-USF, 2005; Spalding et al., 2001).*

2.2.2 Sea surface temperature

For optimal coral growth a water temperature of 18-36 °C is preferred (NOAA, 2021). The SST[4] is taken from global maps that are based on observations made by NASA's Aqua satellite[5], which measures the top millimeter of the ocean surface. Figure 2.6a shows the SST of all hotspots, combined with the threshold that govern the applicability of corals.

---

[4]https://neo.sci.gsfc.nasa.gov/view.php?datasetId=MYD28M
[5]https://aqua.nasa.gov/

2.2.3 Sea surface salinity

Coral reefs require salinity levels to be higher than 15 PSU. For salinity levels higher than 36 PSU the physiology and reproduction capabilities can be negatively affected (ecoshape, 2020). The data set of the sea surface salinity used in this research spans the period from September 2011 until present. It uses data from the Aquarius satellite[6] and is based on a certain interpolation analysis not to be further discussed here (Melnichenko et al., 2021). Figure 2.6b shows the sea surface salinity of all hotspots, combined with the threshold that govern the applicability of corals.

(a)	(b)
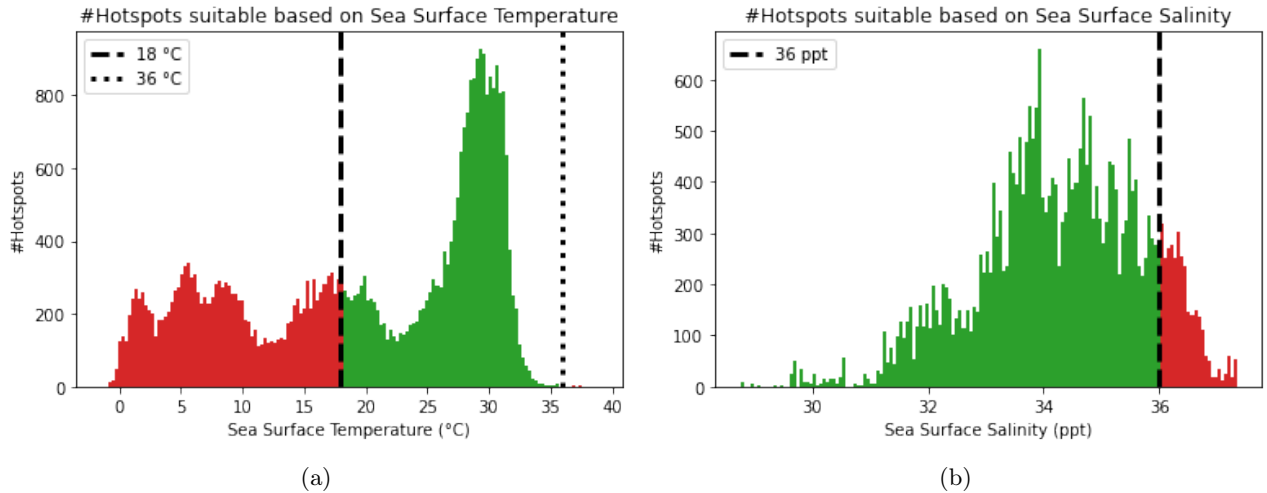
Figure 2.6: *Sea surface temperature (2.6a) and the sea surface salinity (2.6b), y-axis gives the amount of hotspots. The hotspots in red do not meet the requirements whereas the hotspots in green do.*

2.2.4 Surface light irradiance

In order to provide corals with enough food and energy, at least 6-8% of light's surface irradiance is needed, which requires the water column to be clear (ecoshape, 2020). Turbidity is a measurement of the clarity of water. The turbidity is expressed in Nephelometric Turbidity Units (NTU). When high turbidity levels occur, the light penetration through the water is reduced (Balali et al., 2012). Possible causes for turbid water could be a high suspended solids concentration or a bloom of phytoplankton.

Phytoplankton

To determine whether large concentrations of phytoplankton occur, a global map containing Chlorophyll concentrations is used (Hu et al., 2012). Satellites are used to measure the concentrations based on the reflected colors from the upper layers of the water columns. As phytoplankton contains a photosynthetic pigment called Chlorophyll, the water turns green when they appear in large quantities. Demidov et al. (2016) plotted the dependency between the Chlorophyll concentration and the diffuse attenuation coefficient (K_d). It reflects the light intensity at different depths and hence the surface light irradiance. K_d is approximated by a power function including the Chlorophyll concentration at the surface (Chl_0). The data used for the power law has a coefficient of determination (R^2) of 0.64 (Demidov et al., 2016):

$$K_d = 0.162 * Chl_0^{0.398} \; [m^{-1}] \tag{2.2}$$

Using Beers law (Demidov et al., 2016), the irradiation at a given depth can be calculated (I_Z) using K_d. The percentage surface light irradiance reaching a certain depth (Z) then follows from an arbitrary surface irradiation (I_0) (Demidov et al., 2016):

$$\frac{I_Z}{I_0} = e^{-K_d Z} \; [\%] \tag{2.3}$$

---

[6]https://aquarius.nasa.gov/

19

It is not specified for this threshold for which depth this surface light irradiance of at least 6-8% must hold. Coral flats are located in shallow water and can be uncovered during low-tide, which is used to establish the threshold in terms of Chlorophyll concentration. By plugging in a minimum light irradiance of 8% into Equation 2.3 at the maximum low-tide, it is calculated that coefficient K_d must be 0.51 m^{-1} or lower. With Equation 2.2 the threshold for the Chlorophyll concentration at the surface is established at **17.4** mg/m^3. This means that for Chlorophyll concentrations larger than 17.4 mg/m^3 at the surface, the light irradiance at maximum low-tide is lower than the required 8%. These locations are said to be not suitable for corals and are hence denoted in red (Figure 2.7).
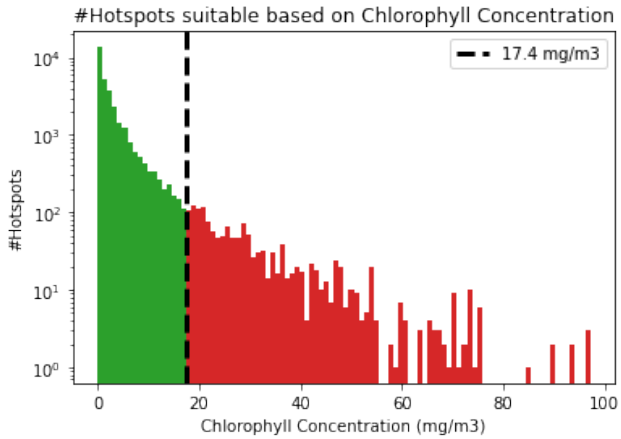
Figure 2.7: *Chlorophyll concentration, y-axis gives the amount of hotspots. The hotspots in red do not meet the requirements whereas the hotspots in green do.*

2.3 Applying thresholds

Using the thresholds established above, the potential to apply mangroves and corals for each hotspot is determined following the order in Figure 2.8. The threshold "mangrove/coral occurrence" is governing over the other thresholds. This means that if the requirements are not met, but there are currently mangroves or corals present, there is still potential found to apply them. Figures 2.10-2.14 show the results.

(a) *Mangrove thresholds.*
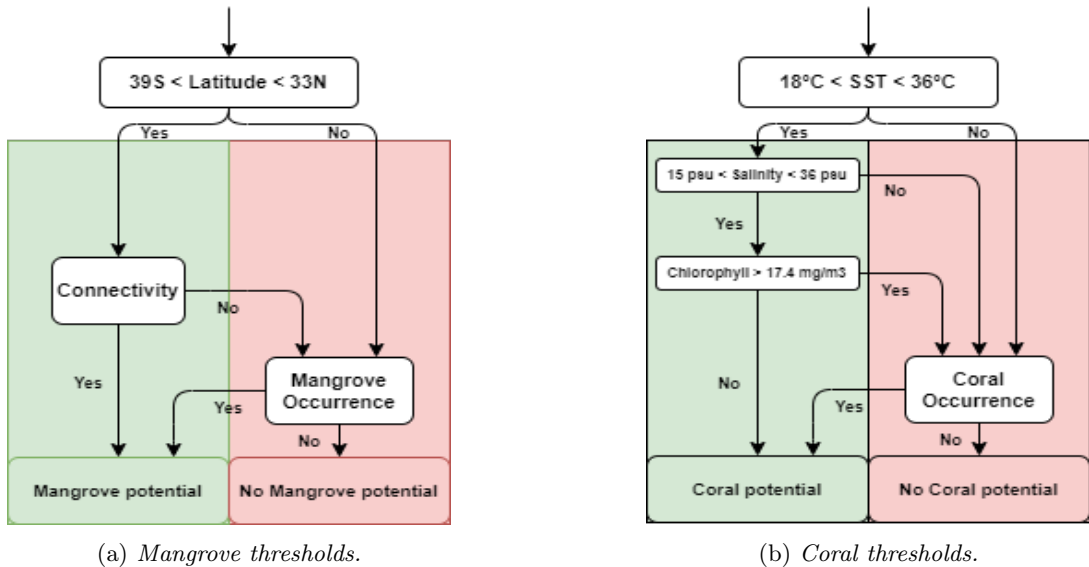
(b) *Coral thresholds.*

Figure 2.8: *Order in which thresholds are applied on the hotspots for mangroves (2.8a) and corals (2.8b).*

2.4 Concluding marks regarding mangrove potential

For each hotspot it is determined whether there is mangrove potential based on the established thresholds (flowchart 2.8a). The results are given in Figures 2.10 and 2.11 for locations with mangrove potential and without respectively. In order to compare the determined mangrove potential with the retreating of coastlines two analyses are performed:

1. Applying flowchart 2.8a while adding the erosion threshold such that retreating coastlines have no potential for mangrove restoration.

2. Flowchart 2.8a (which is without the erosion threshold).

The second analysis is used to generate the results in Figures 2.10 and 2.11. The first analysis can be useful to investigate which hotspots experience coastal erosion. For both analyses cross-tables are made that depict the amount of hotspots for different combinations of mangrove potential and mangroves occurrence.

(a) *With the erosion threshold.*   (b) *Without the erosion threshold.*
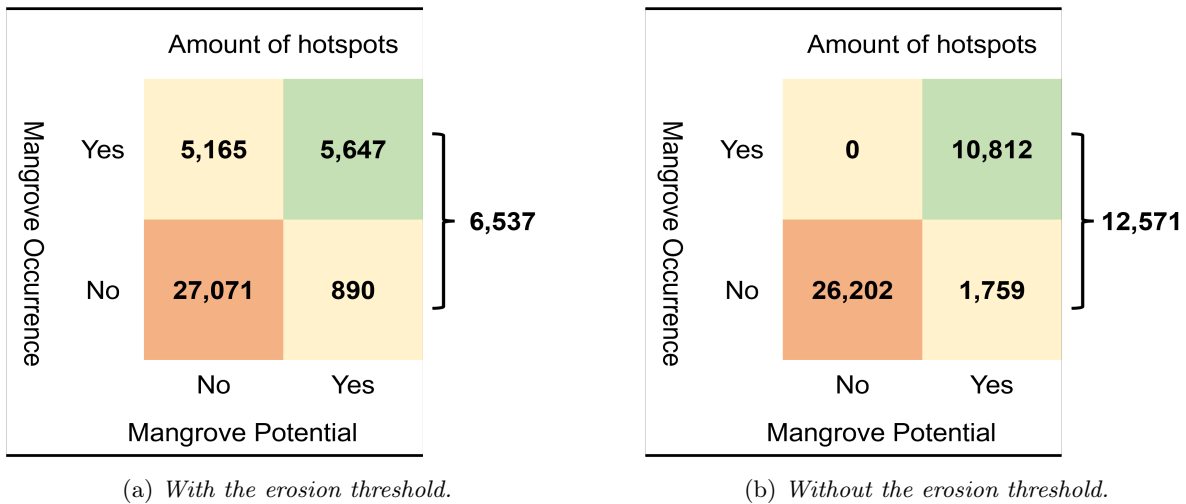
Figure 2.9: *Cross-tables showing the amount of hotspots for different combinations of mangrove potential and mangroves occurrence for analysis 1 (2.9a) and 2 (2.9b). The number of hotspots in each cell add up to the total amount of hotspots investigated in this research, namely 38,773.*

Figure 2.9b shows that if flowchart 2.8a is applied without using the erosion threshold, 12,571 locations are found with mangrove potential. Of these locations, there are 1,759 where currently no mangroves are present (Appendix B.3). There are no locations found that currently have mangroves and are determined to have no mangrove potential as seen by the top left square. It does not mean that for these potential sites for mangrove restoration, in 100% of cases mangroves can always be restored, but as a first indication it does give more insight. Table 2.1, summarizes the main results found in this chapter.

If the retreating of coastlines is added as a threshold, the amount of locations where mangrove potential is found reduces to 6,537. At the locations where previously mangrove potential was found, the coastline is retreating (for example in Indonesia up to 35 m/yr). For 5,165 locations there is now no mangrove potential found, even though there are currently mangroves present. For these locations in the past the coastlines could have been accreting or were stable, making it suitable for mangroves to grow back then. However, at those hotspots, most likely every year mangroves are lost due to the retreating coastline. To enable mangrove restoration, mitigation measures are required to combat the erosion or land subsidence problems (see Appendix C.3). Examples include nourishments or bamboo structures (Mancheño et al., 2021; Spalding et al., 2014) to combat the erosion problems. Regulation of groundwater pumping can reduce the land subsidence rates (Bidorn et al., 2021; Karlsrud et al., 2017).
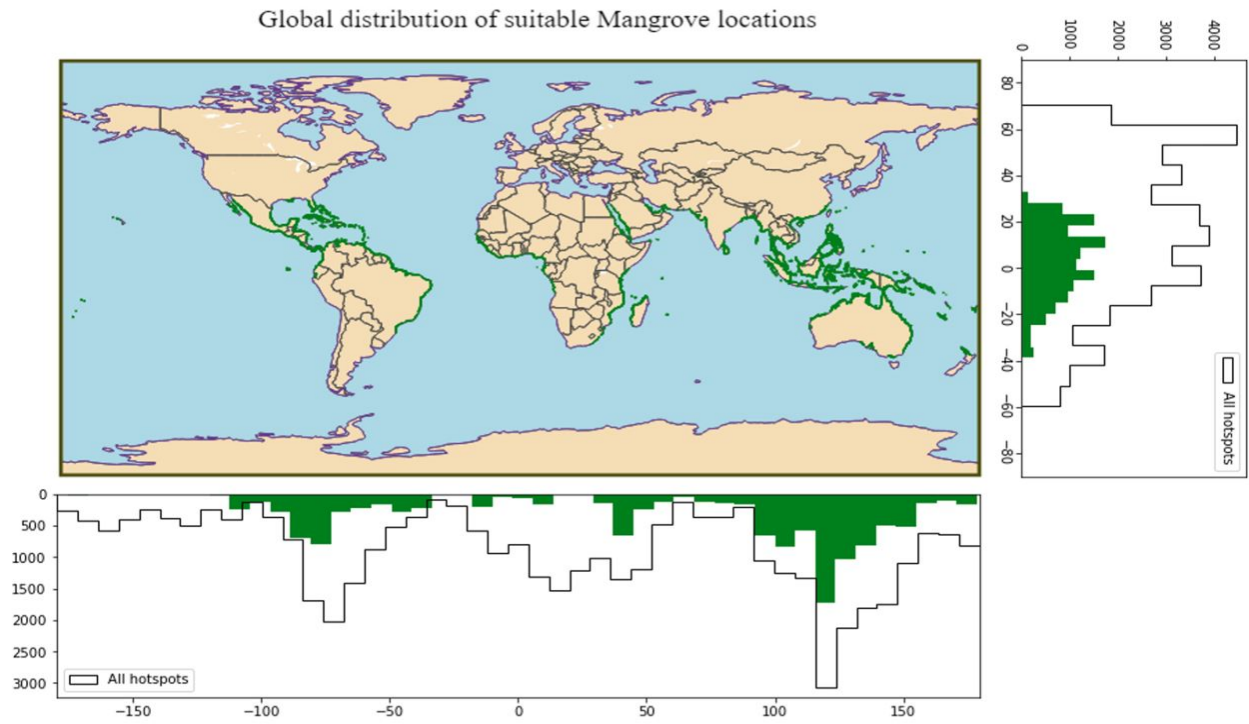
Figure 2.10: *Global distribution of hotspots suitable for mangrove restoration. Histograms shows the amount of hotspots over the longitudes/latitudes.*
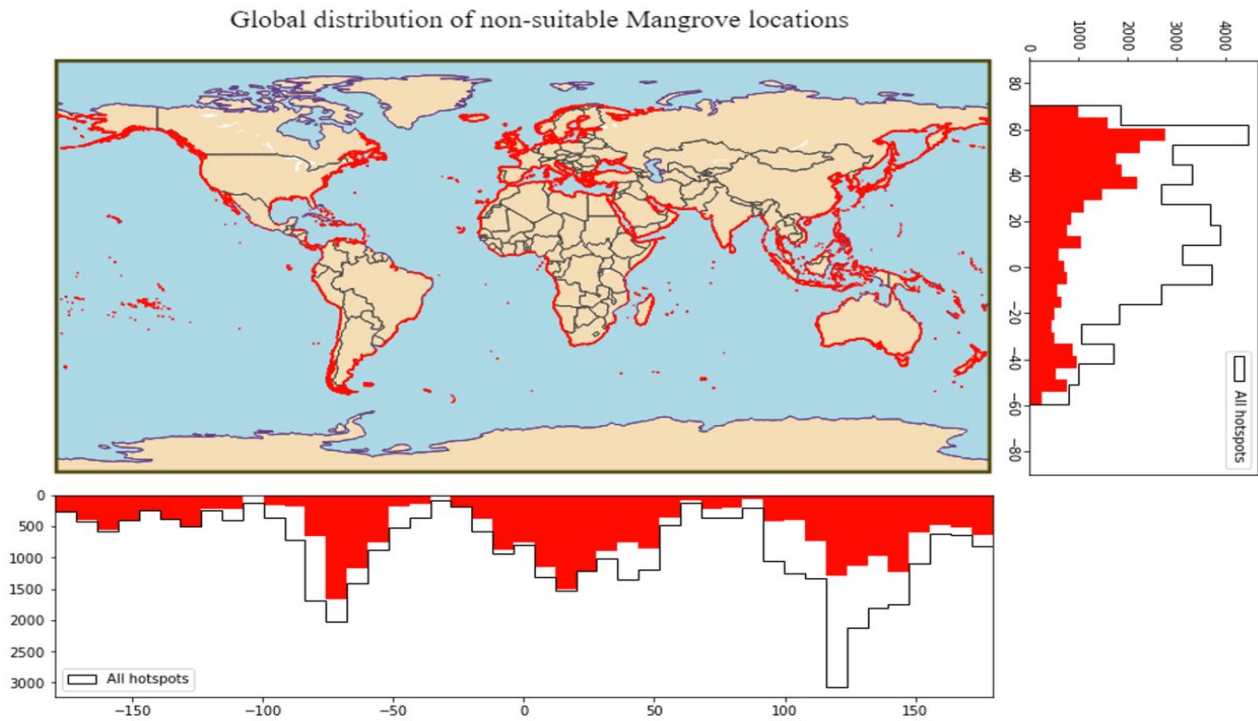
Figure 2.11: *Global distribution of hotspots **not** suitable for mangrove restoration. Histograms shows the amount of hotspots over the longitudes/latitudes.*

2.5 Concluding marks regarding coral potential

It is determined for each hotspot whether there is coral potential based on the established thresholds (flowchart 2.8b). The results are given in Figures 2.13 and 2.14 for locations with coral potential (2.13) and without (2.14). In order to compare the determined coral potential with the occurrence of corals two analyses are performed:

1. Applying thresholds using flowchart 2.8b without coral occurrence.

2. Flowchart 2.8b with coral occurrence.

(a) *Without coral occurrence.*

(b) *With coral occurrence.*
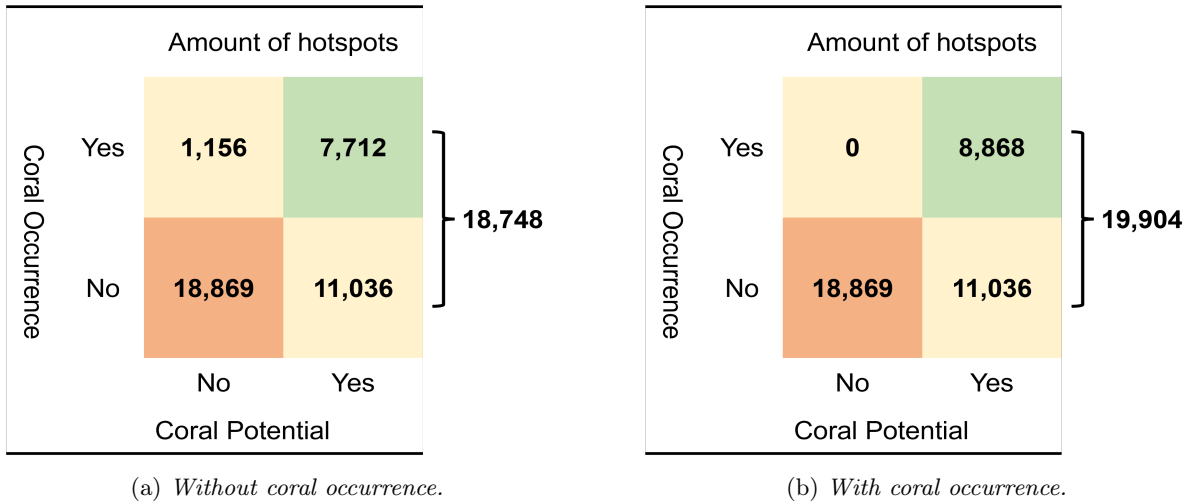
Figure 2.12: *Cross-tables showing the amount of hotspot for different combinations of coral potential and coral occurrence for analysis 1 (2.12a) and 2 (2.12b). The number of hotspots in each cell add up to the total amount of hotspots investigated in this research, namely 38,773.*

Figure 2.12b shows that if flowchart 2.8b is applied including coral occurrence 19,904 locations are found with coral potential. Of these locations, there are 11,036 where currently no corals are present (Appendix B.3). It does not mean that in 100% of the identified potential sites for coral restoration, corals can always be restored, but as a first indication it does give more insight. Table 2.1, summarizes the main results found in this chapter. If the coral occurrence threshold is excluded, there are 1,156 locations with no potential even though there are currently corals present. This is mainly a result of the sea surface salinity threshold, which is not met at 1,125 locations. At those locations there are corals present even though the salinity exceeds the 36 psu threshold. The sea surface salinity data set has a resolution of 0.25° x 0.25° and is taken in the most recent month available, March 2021. As it is a snapshot in time, the salinity may be lower or higher at different times of the year. Hotspots located at the northern coast of Venezuela for example experience salinities in the order of 36 to 37 psu in March of 2021. However, at the same location in September 2020, the salinity was in the order of 35 psu.

NBS	Total restoration potential	Newly identified
Mangroves	12,571 hotspots (32.4%)	1,759 hotspots (4.5%)
Mangroves with erosion	6,034 hotspots (15.6%)	869 hotspots (2.2%)
Corals	19,904 hotspots (51.3%)	11,036 hotspots (28.5%)
Mangroves and/or corals	21,182 hotspots (54.6%)	12,028 hotspots (31.0%)
Total coastal hotspots	38,773 hotspots (100%)	38,773 hotspots (100%)

Table 2.1: *Number of hotspots where potential is found to apply mangroves, corals or one of both. The column newly identified, gives the number of hotspots where currently no mangroves or corals are present, but mangrove or coral potential is found. The percentages are given with respect to the 38,773 coastal hotspots. Mangroves with erosion gives the number of hotspots with potential to apply mangroves where the coastline is retreating.*
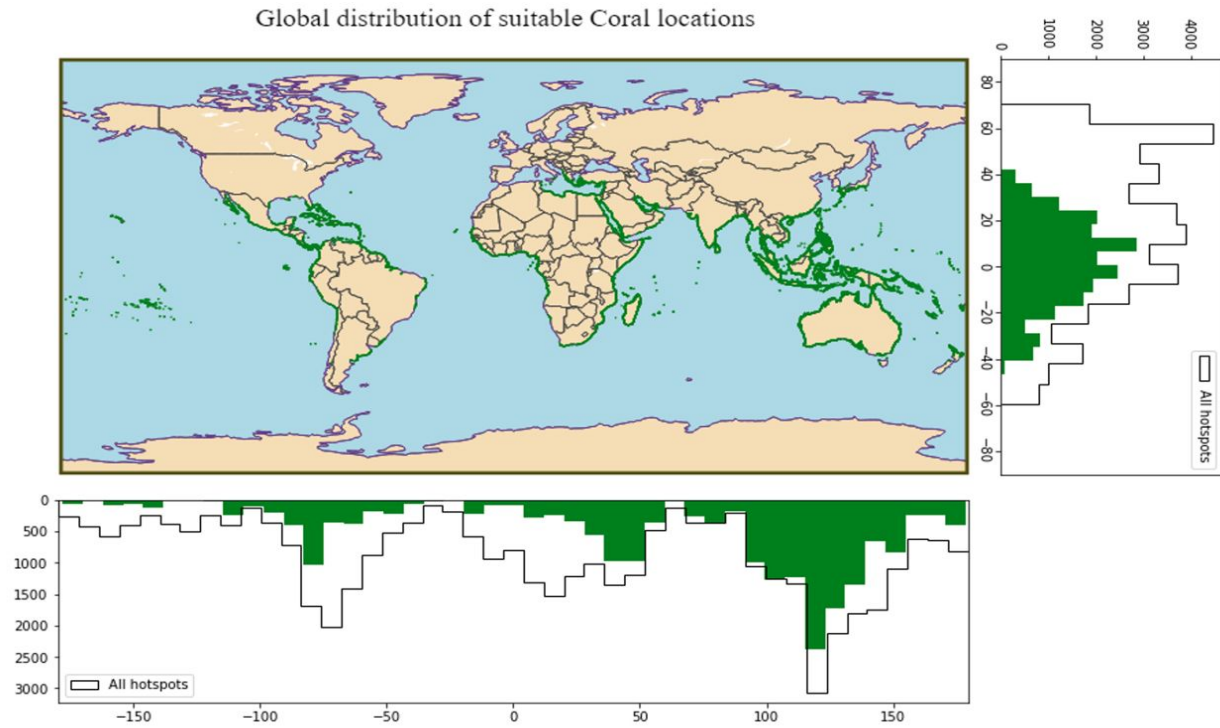
Figure 2.13: *Global distribution of hotspots suitable for coral restoration. Histograms shows the amount of hotspots over the longitudes/latitudes.*
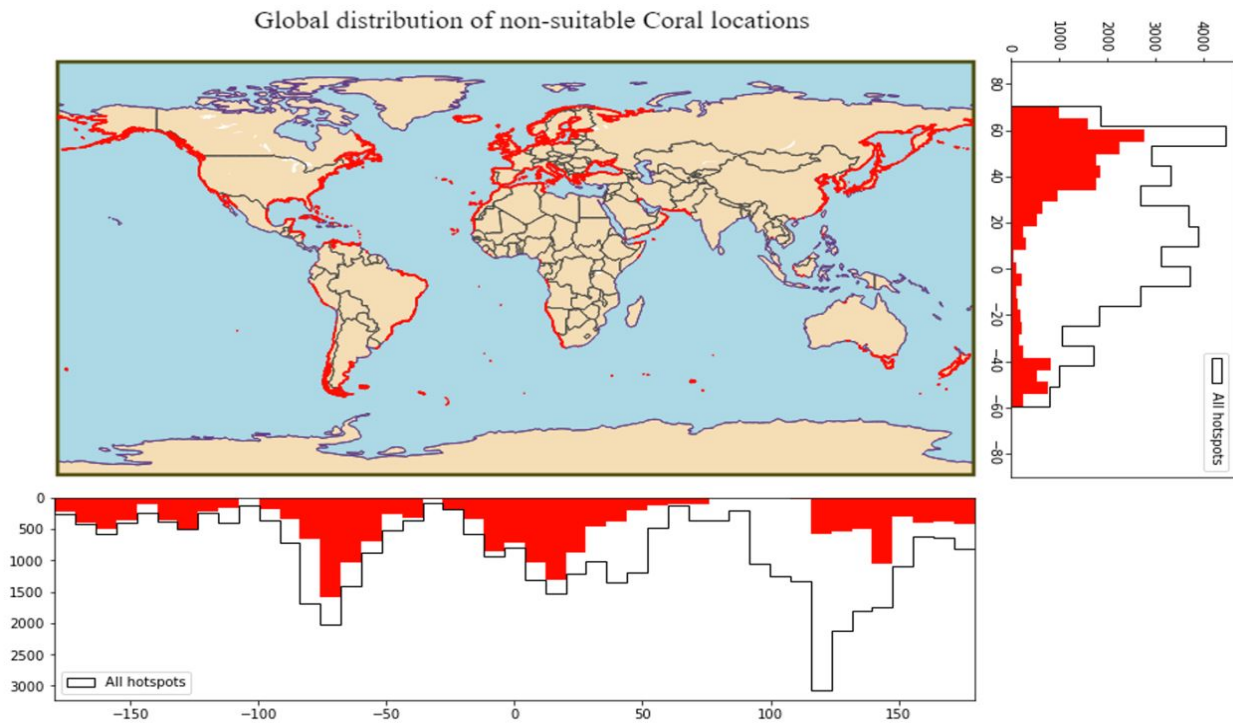
Figure 2.14: *Global distribution of hotspots **not** suitable for coral restoration. Histograms shows the amount of hotspots over the longitudes/latitudes.*

3 | Determining the costs of different solutions

This chapter aims to answer the sub-question: *"What are the global total investment costs for improving the protection standard with or without coral and/or mangrove restoration?".* The total costs are determined for adaptation strategies $A_{cur,slr}$, B_{new} and $C_{new,slr}$. For all hotspots two cost calculations are performed as seen in Figure 3.1 for defence approaches 1 and 2 respectively. To give more insight during this section there are intermezzos that show the calculations/results for one specific hotspot located in the United Arab Emirates at 24.37°N and 54.21°E.

Defence approach 1: Dike raising

The costs are calculated for the first defence approach, which involves solely raising of the dikes (Figure 3.1a). These calculations are explained in sections 3.2 - 3.8 and do not involve restoration of mangroves and/or corals. However, if at the hotspots currently there are mangroves and/or coral reefs present, those are taken into account in the wave attenuation calculation and consequently influence the required amount of dike heightening.

Defence approach 2: Dike raising and mangrove and/or coral restoration

Here the costs are calculated for the second defence approach, which involves a combination of dike raising and mangrove and/or coral restoration (Figure 3.1b). The second calculation depends on the applicability of nature-based solutions as determined in step 1 (section 2). For this cost calculation, the minimum total costs are calculated where the amount of mangrove/coral restoration results in the lowest investment costs. The corresponding calculations are given in section 3.9.
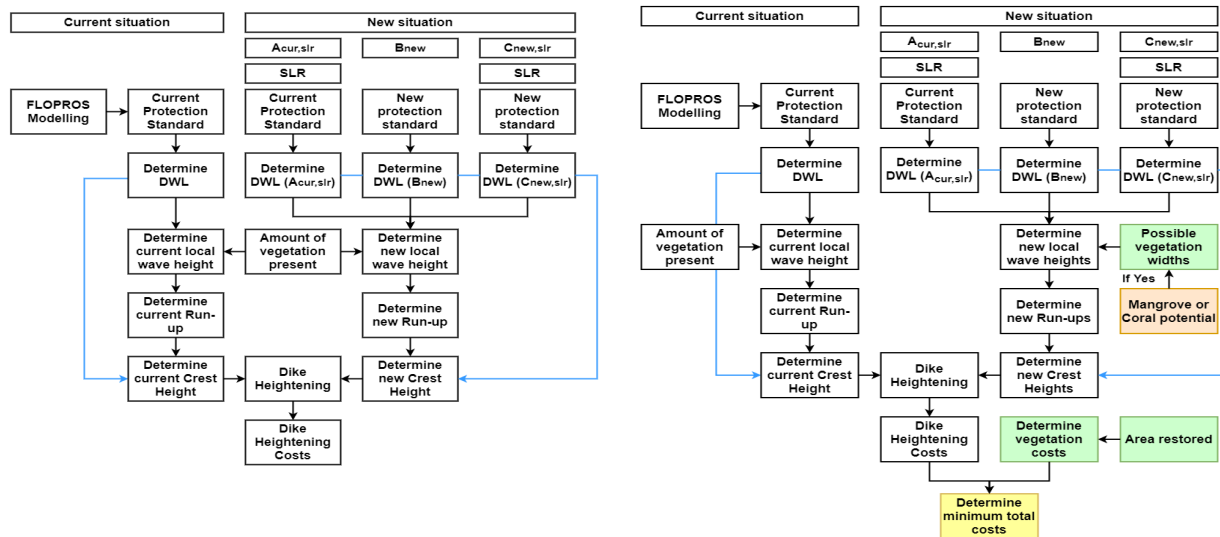
(a) *Defence approach 1.* (b) *Defence approach 2.*

Figure 3.1: *Flowcharts showing the two different costs calculations for defence approaches 1 and 2. The protection standards are based on the FLOPROS modeling approach, for the current and new situation as explained in section 3.2 (Scussolini et al., 2016). $A_{cur,slr}$, B_{new} and $C_{new,slr}$ correspond to the adaptation strategies as explained in Chapter 1. Note that the DWL and the run-up together determine the crest height as explained in section 3.1. For the different adaptation strategies the DWL differs as for $A_{cur,slr}$ SLR is taken into account without upgrading the protection standard. For B_{new}, the protection standard is increased, but no SLR is taken into account and finally for $C_{new,slr}$ both the protection standard is increased, as well as SLR is taken into account. The colored boxes in panel 3.1b are new compared to defence approach 1.*

3.1 Introduction

The required dike height (Figure 3.2) that needs to meet the current and new protection standard (section 3.2) consists of different components listed below. The foot of the dike is assumed to be located at MSL + High Tide (HT) to be able to integrate mangroves in the foreshore as they can grow up to HT.

- The design water level (DWL) is determined (see subsection 3.3) for return periods corresponding to the current protection standard and the new protection standard. The mean dynamic topography of the sea surface (MDOT), wave setup and HT are kept constant for different protection standards, i.e. return periods. In contrast, the storm surge increases for higher return periods, as indicated in Figure 3.2. For the new protection standard, depending on the adaptation strategy, SLR is or is not taken into account for the DWL.

- The run-up (see subsection 3.6) is determined based on the local wave height (see subsection 3.5) at the foot of the dike. This wave height can be of different magnitudes for different return periods, hence the run-up can vary for different return periods as well. If there is already vegetation, i.e. coral reefs or mangroves present at the hotspot, this is taken into account in determining the wave height at the foot. The dike foot is located at HT, hence the depth at the foot is given by DWL - HT.

- For the new protection standard, land subsidence should also be taken into account, however, currently no global data is available for the magnitude of expected land subsidence. Hence, for all hotspots the land subsidence is set at 0 m (see chapter 9).
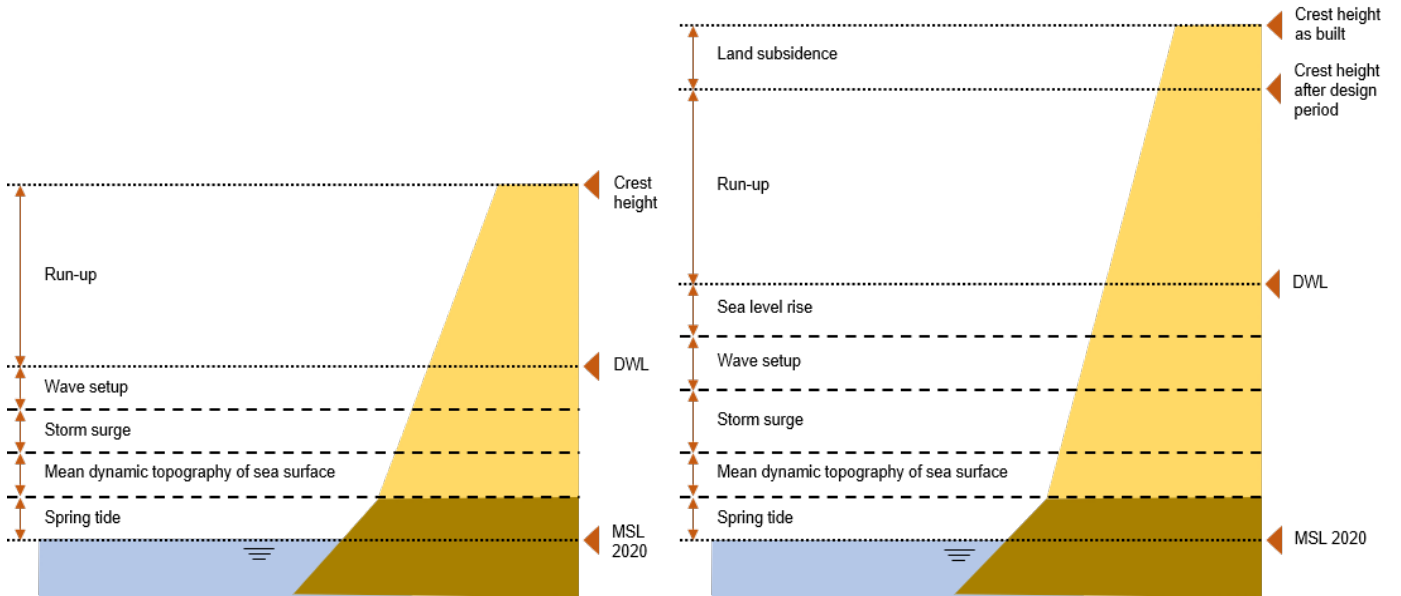
Figure 3.2: *Required dike height to meet the current protection standard (left) and the height required to meet the new protection standard (right). For the new dike height, the local SLR is or is not taken into account depending on the adaptation strategy. The storm surge and run-up can increase in magnitude for the new protection standard as well. The difference in crest height between the current and new protection standard determines the amount of dike heightening required.*

3.2 Globally varying protection standard

Information on the current flood protection standards is important, because if those are neglected and no protection is assumed, flood damage takes place along the whole spectrum of return periods, even though in reality most of this damage does not occur due to the existing coastal defence (Scussolini et al., 2016). The paper Scussolini et al. (2016) presents a database of FLOod PROtection Standards (FLOPROS), that covers

various spatial scales from districts to national levels and is structured into three layers (Scussolini et al., 2016):

- Design layer, based on information from engineers of current infrastructure.

- Policy layer, legislative and required standards from floods.

- Model layer, flood-modelling based on observed relationship between wealth and protection.

The FLOPROS database is based on a hierarchical principle to establish the best possible (i.e. most accurate, closest to hypothetical protection standard) information at different locations. The hierarchy can be seen in Figure 3.3, where the design layer is deemed to be the most reliable layer, and the three layers are merged into one layer. For the merging, subsequent layers (policy or modelled layer) are employed if the design layer does not provide reliable data at a certain location.

Current standard [yr]	New standard [yr]
5	50
10	50
25	50
50	100
100	250
250	500
500	1000
1000	1000
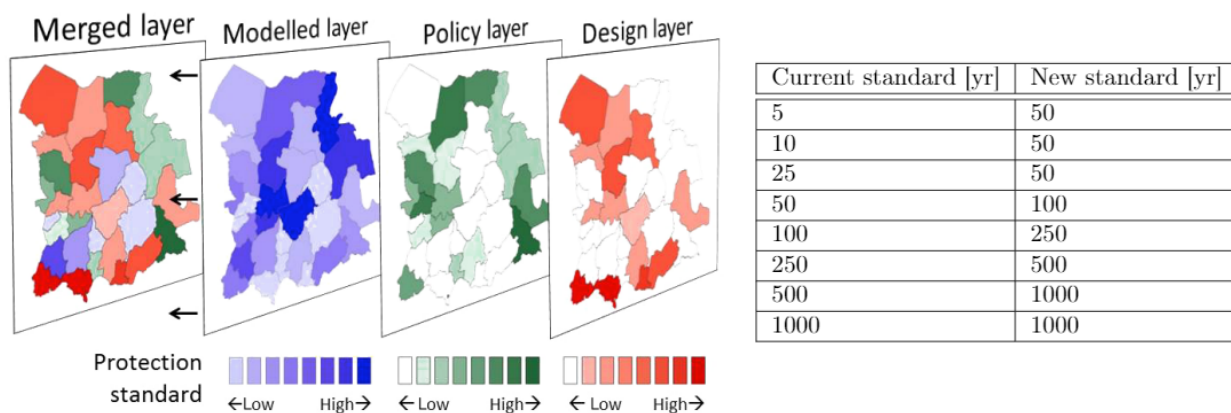
Figure 3.3: *Hierarchical structure of the FLOPROS database (Scussolini et al., 2016). The table shows the current and new protection standards used in this research.*

(a) *Current protection standard.*

(b) *New protection standard.*
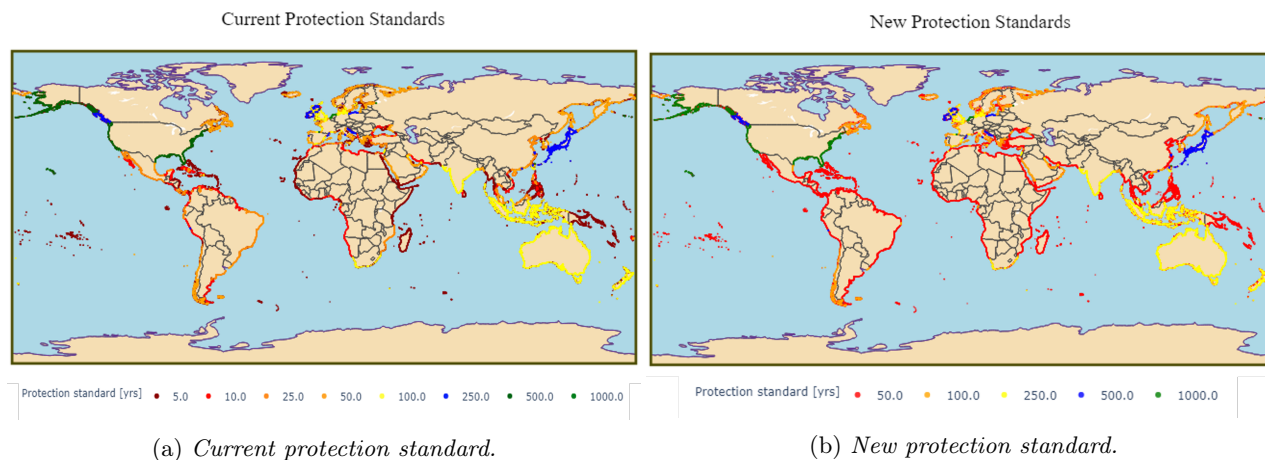
Figure 3.4: *Global protection standards of coastal defences for the current (3.4a) and new (3.4b) situation (Tiggeloven et al., 2020).*

For each hotspot the current and new protection standards are determined by connecting the location of the hotspot to the location of the protection standards from the FLOPROS database. The protection standards correspond to the probability of flooding per year, such that a hotspot with a protection standard of 100

years, has a probability of $\frac{1}{100}$ per year that flooding occurs. As the current protection standards determined with FLOPROS (Scussolini et al., 2016) are very specific, in this research rounded values are used that are closest to the values computed in Scussolini et al. (2016). The values that are used in this research can be seen in Figure 3.3, for the current and new protection standard. For hotspots with a protection standard higher than 1000 (the Netherlands), the protection standard is set at 1000. For the different protection standards different improved protection standards are chosen. The global distribution of the current and new protection standards are given in Figure 3.4a & 3.4b.

3.3 Design water level

The frequency and magnitude of episodic coastal flooding is based on the observed sea levels during extreme storm events, the so-called design water levels (DWLs). Within this research the design water levels are determined for the return periods corresponding to the current and new protection standard including and excluding SLR. This is done via a linear summation of the following components (Kirezci et al., 2020):

- High Tide (HT).

- Mean dynamic ocean topography of sea surface (MDOT).

- Wave setup.

- Sea Level Rise (SLR), depending on the adaptation strategy.

- Storm surge.

The magnitude of these physical processes must be determined in order to make projections of episodic coastal flooding for this century (Kirezci et al., 2020). For each hotspot, the magnitude of these components is determined. For HT, MDOT, wave setup and SLR a single fixed value is used, whereas for the storm surge the magnitude is based on the original and new protection standard of the hotspot from the FLOPROS modelling approach (Scussolini et al., 2016).

3.3.1 High tide
The tidal data is distributed by AVISO+[1] and is taken from the FES2014 model for the solar (S2) and lunar (M2) constituents. The model uses radar altimeter time series to model the ocean's tides. In this research it is assumed that for all hotspots only the S2 and M2 constituents account for the tidal range. The tidal data are displayed in Figure 3.5a.

3.3.2 MDOT
The MDOT is distributed by AVISO+[2], which has determined the MDOT by subtracting the marine geoid from the mean sea surface height measured by satellites. This resulted in that for some areas the water levels are above the geoid and in other areas the water levels are below. The sea level variations across the globe can be up to 150 cm, which makes it important to take this into account for determining the DWL. From the global database, for each hotspot the corresponding value of the MDOT at that location is determined as seen in Figure 3.5b.

3.3.3 Wave setup
A global distribution of the extreme wave setup is determined based on a simple empirical model, for which the Shore Protection Manual (SPM) is used (Jaksic, 2021). The SPM model takes wave steepness and the bed slope as input and returns the wave setup values at the coast. The bed slope is assumed constant for all areas and the wave steepness is retrieved from the global ERA5 wave reanalysis, for which an extreme value analysis is performed, to calculate the wave setup for a return period of $\frac{1}{100}$ years (Jaksic, 2021). Figure 3.5c shows the global distribution of extreme wave setup.

---

[1]https://www.aviso.altimetry.fr/en/data/products/auxiliary-products/global-tide-fes.html
[2]https://www.aviso.altimetry.fr/en/applications/ocean/large-scale-circulation/mean-dynamic-topography.html

3.3.4 Sea Level Rise

According to Stocker et al. (2013) the global mean sea level will continue to rise during the 21st century. As a result historically centennial events (local sea levels that occurred $\frac{1}{100}$ years) are predicted to occur at least annually during the 21st century at most locations along the world's coastlines (Pörtner et al., 2019). Multiple RCP (representative concentration pathways) scenarios are developed to describe the development of greenhouse gases. The different scenarios include, RCP2.6, RCP4.5, RCP6.0 and RCP8.5. The numbers stand for the radiative forcing $[\frac{W}{m^2}]$ expected in the year 2100. Radiative forcing expresses the difference between the incoming solar energy and the reflected energy from the earth. The more extreme scenarios RCP6.0, RCP8.5 correspond to little to no climate measures, whereas RCP2.6 and RCP4.5 require an ambitious climate policy to be achieved in 2100 (Stocker et al., 2013).

	Scenario	Mean	Likely range
Global Mean Sea Level Rise [m]	RCP2.6	0.43	0.29 to 0.59
	RCP8.5	0.84	0.61 to 1.10

Table 3.1: *Projected change in global mean SLR for 2081-2100 (Pörtner et al., 2019).*

With these scenarios different estimates for global mean SLR are made, as seen in table 3.1 (Pörtner et al., 2019). For all the hotspots the local SLR is taken from Pörtner et al. (2019) for the year 2090 based on the RCP8.5 scenario. As the regional SLR is used, the projected SLR varies between the different hotspots as seen in Figure 3.5d.
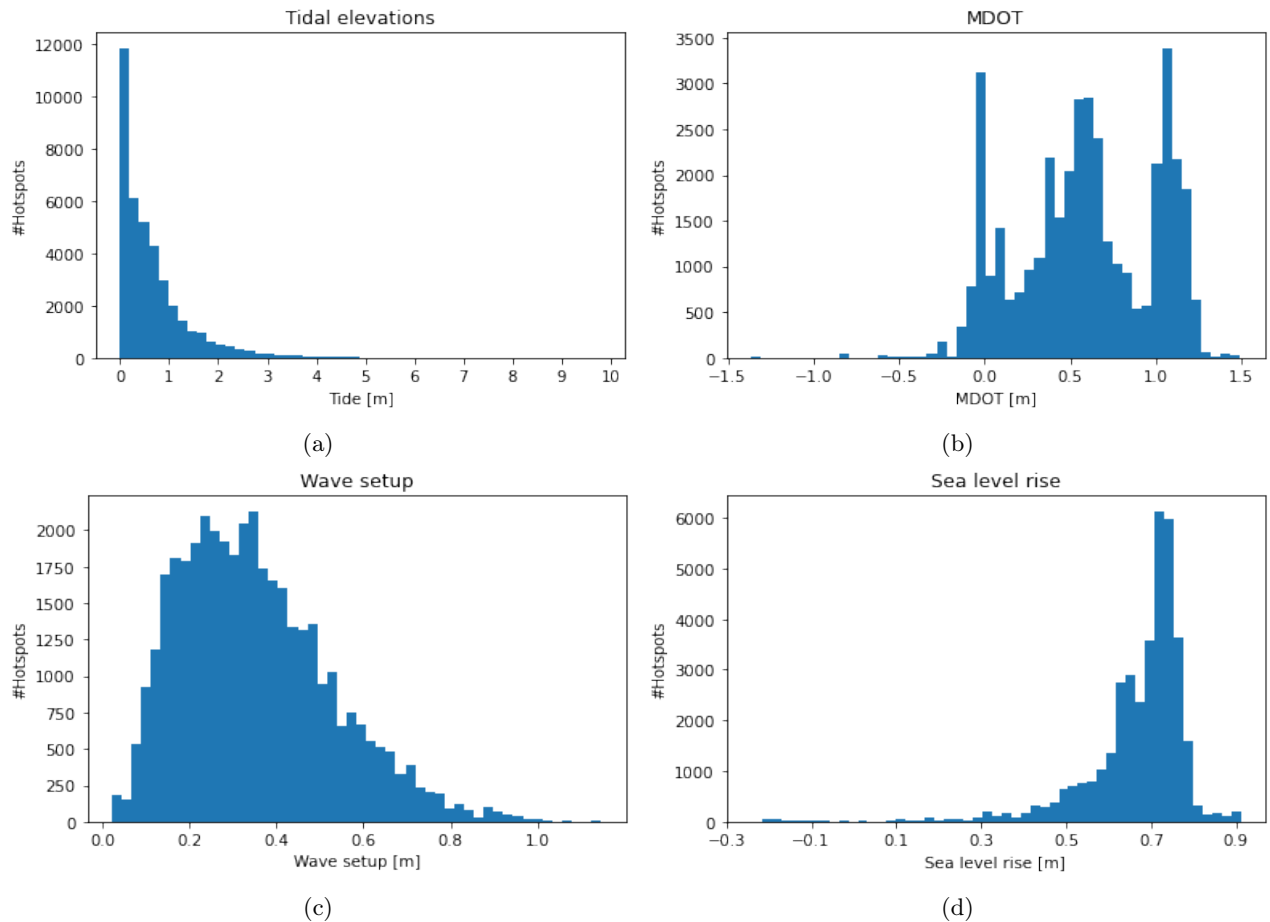
Figure 3.5: *Distribution of high tide (3.5a), MDOT (3.5b), wave setup (3.5c) and SLR (3.5d). Y-axis denotes the amount of hotspots. It can be seen that in some cases the local SLR is negative.*

3.3.5 Storm surge

Muis et al. (2020) presents the GTSR data set which is based on hydrodynamic modelling and consists of a time series containing storm surge and tidal data (see Appendix B.2). This data set covers all coastlines in the world and is validated with field observations (see also section 7.4). From this data set the storm surge data for different return periods (5, 10, 25, 50, 100, 250, 500 and 1000 yrs) is extracted and connected to each hotspot as seen in Figure B.5.

3.3.6 Resulting design water levels

Taking into account the previously mentioned components that form the DWL, the DWLs are calculated according to adaptation strategies $A_{cur,slr}$, B_{new} and $C_{new,slr}$. This means that for each location 4 different DWLs are calculated, namely for the current and new protection standard, including and excluding SLR as seen in Figure 3.6. If SLR is taken into account or the protection standard is increased, it can be seen that the DWL increases correspondingly.
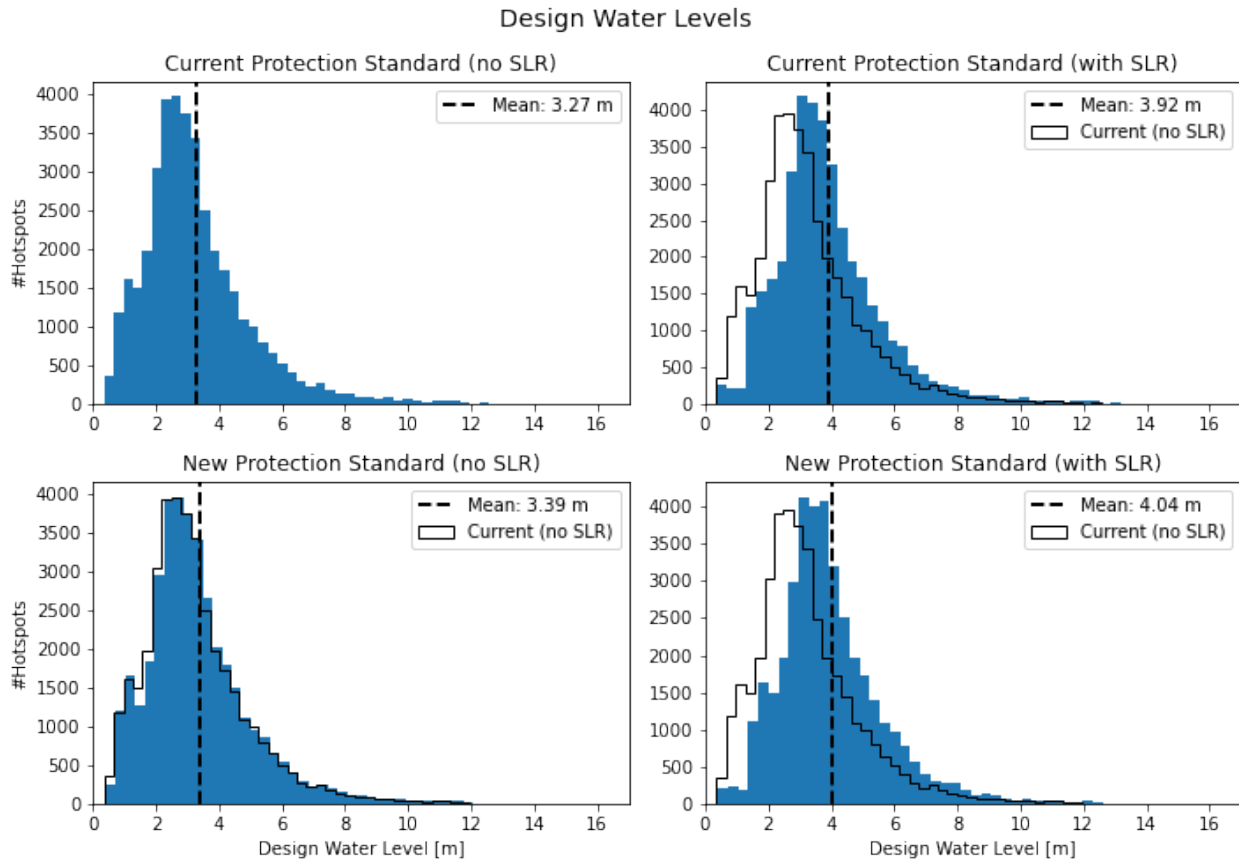
Figure 3.6: *Distribution of design water levels for the current and new protection standard including and excluding SLR for all hotspots. The DWLs are calculated by a linear summation of the components; high tide, MDOT, wave setup, SLR and storm surge.*

Intermezzo 3.2.3: Design water levels (hotspot United Arab Emirates)

- Current protection standard: 5 years, new protection standard: 50 years.

- Current design water level: 2.67 m, current design water level including SLR: 3.25 m.

- New design water level: 2.85 m, new design water level including SLR: 3.43 m.

3.4 Slope of the foreshore

Athanasiou et al. (2019) defines the horizontal length (L) of the nearshore area as the cross-shore distance between the coastline (MSL) and the depth of closure (d_c). For the definition of a coast, the objective and timescale under consideration are important. The most seaward point of interest is defined as the depth of closure, which is the point beyond which repeated field observations of the bed height show no significant changes over a certain period of time. This means that the majority of the bed dynamics take place landward of the depth of closure. This depth is governed by the highest waves that may occur during a certain period of time. For the nearshore bathymetry MERIT, GEBCO and Open Street Map (OSM) data is merged from which transects are formed at 1 km intervals. Using offshore wave data, the depths of closure were estimated, which in combination with the transects resulted in the nearshore slope ($tan(\beta)$) defined as the ratio $\frac{d_c}{L}$ as seen in Figure 3.7 (Athanasiou et al., 2019).
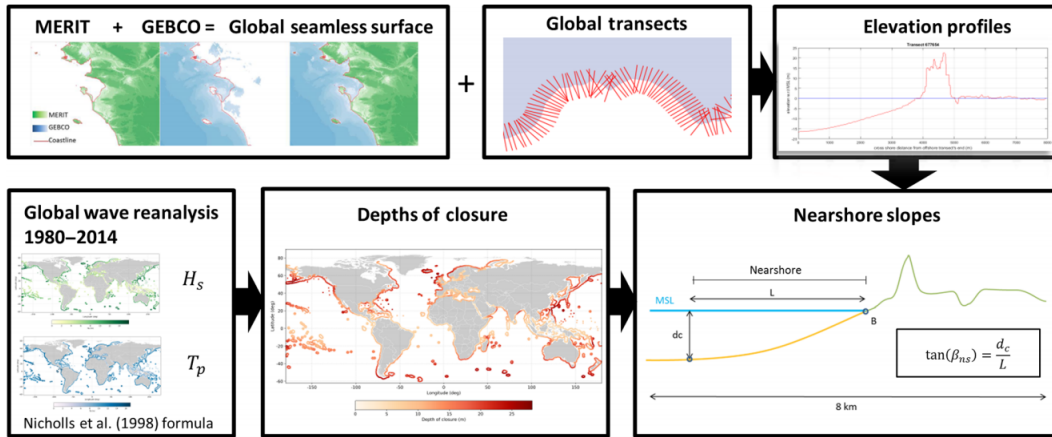
Figure 3.7: *Calculation of nearshore slopes on a global scale (Athanasiou et al., 2019).*
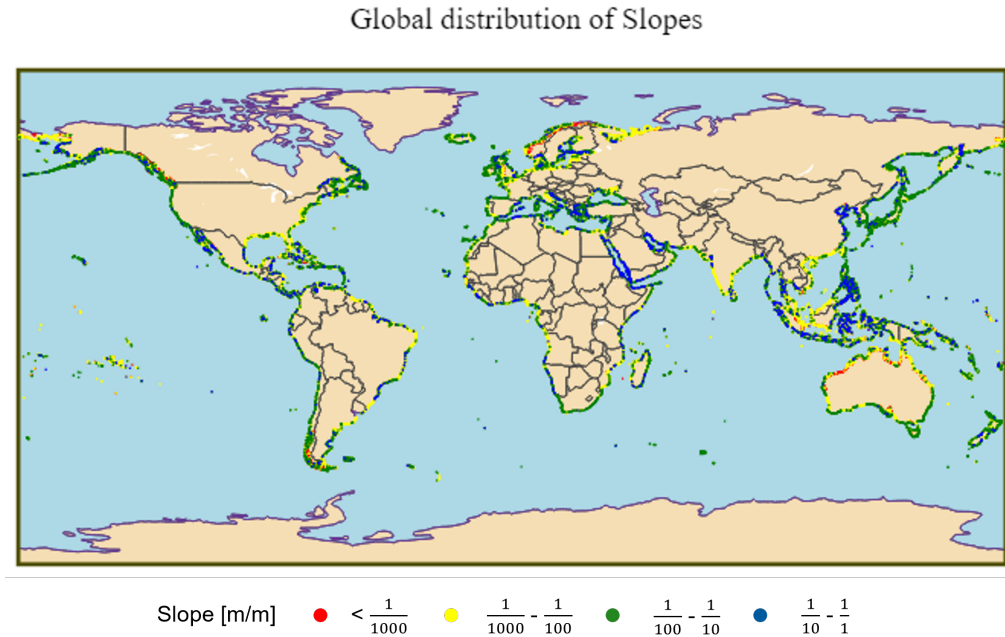
Figure 3.8: *Global distribution of foreshore slopes based on (Athanasiou et al., 2019). Hotspots depicted by red dots are characterized by very shallow foreshores, whereas hotspots depicted by blue dots consist of steep foreshores.*

For all hotspots, the transects that are located within the hotspot's area are determined and the minimum, median and maximum slope of the foreshore is calculated. In this research the median slope of the transects within a hotspot are used, unless there are transects located within the hotspots that produce unrealistic values. Examples are harbours with dredged channels, resulting in very steep slopes. In those cases the minimum transect slope value within a hotspot is used. Figure 3.8 shows the global distribution of slopes across all hotspots.

Intermezzo 3.2.4: Foreshore slope (hotspot United Arab Emirates)

- Slope: $0.02205 = \frac{1}{45} \ \frac{m}{m}$.

3.5   Nearshore wave height

Waves that travel from deep towards shallow water depths experience changes in wave height, length and direction until they break and lose their energy. These changes occur due to interaction with the sea bed and/or vegetated foreshores through processes such as refraction, shoaling, bottom-friction and wave breaking. Within this research, refraction is not considered as waves are assumed to be normally incident (i.e. wave crest parallel to depth contours) and the shoreline is assumed to be alongshore uniform. This subsection explains how the nearshore wave height is determined at the foot of the dike for the different hotspots. The foot of the dike is assumed to be located at HT and the nearshore wave height is required in order to determine the run-up of the dike (see subsection 3.6). Depending on the occurrence and applicability of mangrove and/or corals, there are 4 different configurations possible:

- A bare foreshore, there is no vegetation present.

- A mangrove forest located somewhere between MSL and HT with a certain width.

- A coral reef, located below LT with a certain width.

- A combination of a coral reef and a mangrove forest (see Figure 3.9).
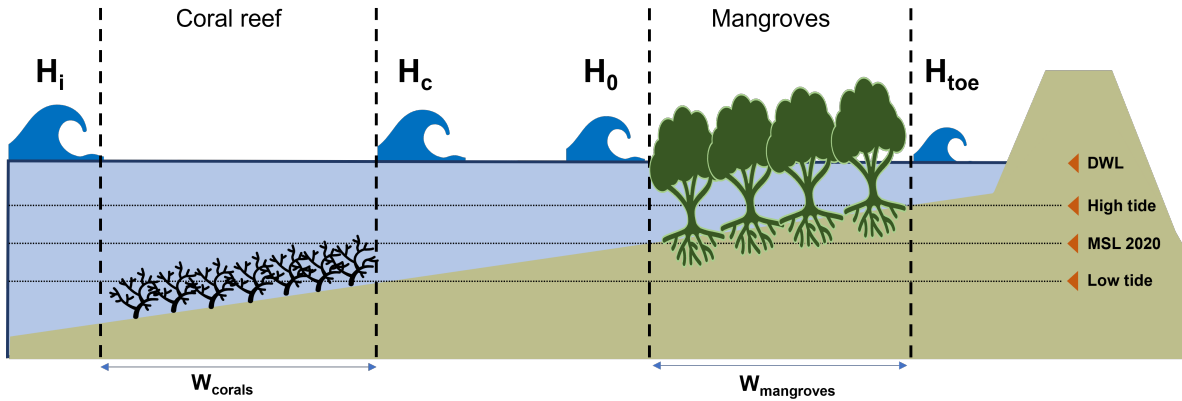
Figure 3.9: *Foreshore including coral reefs and mangroves, the waves are attenuated as they approach the shallow foreshore. Coral reefs are located lower in the foreshore than mangroves.*

Each of these possible foreshore configurations includes a different calculation to determine the wave height at the foot of the dike. For each hotspot, the current width of the mangroves and/or coral reefs is determined based on the area of mangroves/corals located in the hotspot:

$$W_{Mangroves/Corals} = \frac{A_{Mangroves/Corals}}{\sqrt{A_{hotspot}}} \ [m] \tag{3.1}$$

32

This is a simplification as, firstly the hotspots are projected as polygons and not squares (which makes the $\sqrt{}$-approach a simplification) and secondly because the mangrove/coral area is not distributed evenly over the hotspots. It is chosen to apply a maximum extent of the vegetation at the foreshore depending on the type of ecosystem. For mangroves, as they grow between MSL and HT, the maximum width of the mangrove forest is bounded by the tidal range and the slope of the foreshore (Equation 3.2).

$$W_{max,mang} = \sqrt{\left(\frac{HT}{Slope}\right)^2 + HT^2}\ [m] \tag{3.2}$$

Coral reefs appear to have reached their effective limit with reef flats of 1000 m wide as found in Pearson (2016), since the run-up reduction flattened out drastically at this reef size. Therefore this is chosen as the maximum coral reef width. The corresponding calculated coral and mangrove widths distributed over the hotspots can be seen in respectively Figure 3.10a & 3.10b.

(a) *Coral widths.* (b) *Mangrove widths.*
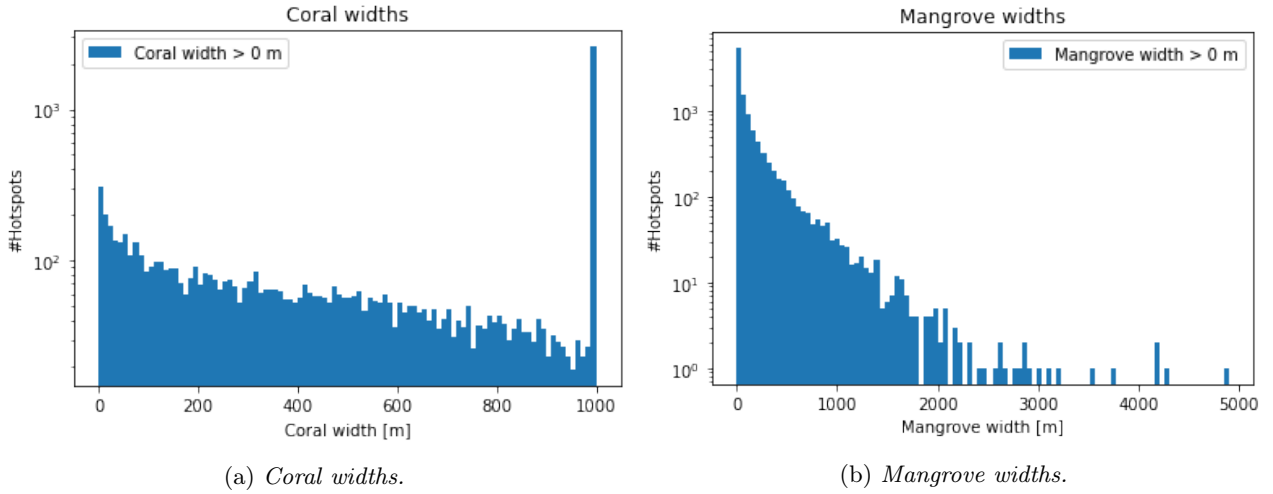
Figure 3.10: *Width of corals and mangroves occurring at the foreshores of the hotspots. The large peek at a coral width of 1000 m is caused by the applied vegetation width boundary explained above.*

3.5.1 Bare foreshore

If there is **no** vegetation currently present at the hotspot, the design wave height at the foot of the dike is limited by the breaking criterion (describing shallow water wave breaking) with respect to the design water depth (h = DWL - HT). The design water depth at the toe of the dike corresponds to the extreme sea level for the different protection standards. This is a conservative approach, as in practise smaller waves could occur during storm events. Especially in estuaries, in sheltered coastal environments the nearshore wave heights will be conservative. For this criterion, the breaker parameter (γ_b) is widely used, which is defined as the ratio of breaker height over breaker depth (Robertson et al., 2013).

The bottom slope influences the breaker index (γ_b) as waves need time to break, which means that at steeper slopes, they will break at smaller water depths, which results in a larger breaker index. The breaking of waves takes place in various different ways depending on the bed slope, offshore wave height and wave length which is guided by the Iribarren parameter:

$$\xi_0 = \frac{tan(\beta)}{\sqrt{\frac{H_i}{L_0}}}\ [-] \tag{3.3}$$

where:

- $tan(\beta)$ the steepness of the foreshore $\frac{m}{m}$.

- L_0 the deep water wave length, estimated with $1.56T_p^2$, that uses the incident peak wave period (T_p). In this research the wave period is assumed to be 10 s for all incident waves [m].

- H_i the offshore wave height, chosen large enough such that wave breaking occurs (conservative approach) [m].

A distinction is made depending on the value of ξ_0 for different types of wave breaking as seen in Figure 3.11. Spilling breakers are usually found on flat beaches as waves begin breaking at a large distance from the shore and gradually break as they enter shallower water. For this type, almost all wave energy is dissipated and little reflection takes place. Plunging breakers are of the curling type, which at breaking dissipates into much turbulence, where some energy is reflected back to the sea. Surging breakers occur at steep shores, where more than half of the wave energy is reflected back to the sea due to the toe of the wave surging on the beach before the crest can curl over and fall. Based on the Iribarren parameter, the surf similarity relationship of Kaminsky & Kraus (1993) is used to determine the wave height at breaking. Equation 3.4 uses the offshore surf similarity parameter (Iribarren, ξ_0) and empirically estimated calibration values to calculate the breaker parameter and consequently the nearshore wave breaker height (H_{toe}).

$$\gamma_b = 1.20 * \xi_0^{0.27} \ [-], \ H_{toe} = \gamma_b * h_b \ [m] \tag{3.4}$$
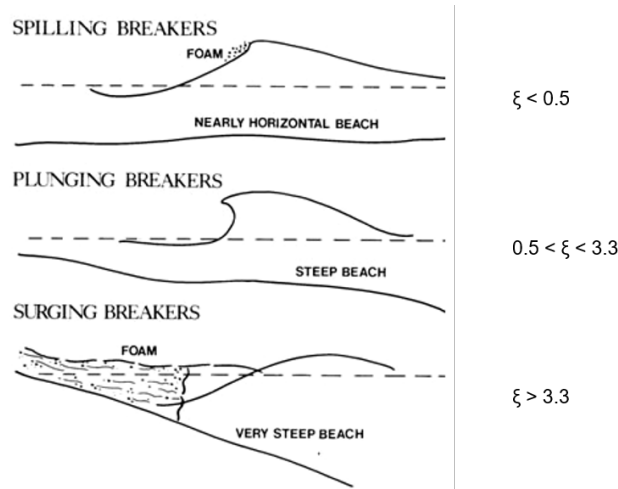
Figure 3.11: *Breaking wave categories (Robertson et al., 2013).*

3.5.2 Vegetated foreshore

If there **is** vegetation currently present at the hotspot, the design wave height at the foot of the dike is governed by either the wave breaking criterion with respect to the design water depth (DWL - HT) or by the attenuated waves over the vegetated foreshore (smallest value is governing).

Reduction of wave energy in the foreshore, occurs due to depth-induced breaking and bottom friction. Depending on the characteristics of the foreshore and the DWL the waves that propagate from offshore to the toe of the dike experience a certain reduction in wave energy. Vegetated foreshores, add additional wave attenuation (Vuik et al., 2018; van Wesenbeeck et al., 2017). Depending on the characteristics of the vegetation, the wave height at the toe of the dike and the corresponding run-up can be reduced, which would result in a lower crest height required to reach the same protection standard.

Different factors influence the effectiveness of coastal protection that nature-based solutions can provide. First of all, the type of habitat, which is controlled by the local conditions such as the wave energy, tidal range, sediment supply and nutrients (Pontee et al., 2016). Secondly, the water depths are an important factor, as the amount of wave dissipation is governed by the water depth relative to the habitats (Pontee et al., 2016). Lastly, the characteristics of habitats determine the effectiveness, to for example attenuate waves. As higher

reef crests or denser mangrove forests are likely to dissipate more wave energy (Pontee et al., 2016). For the wave attenuation caused by coral reefs and mangrove Forests, empirical formulas are used as explained in the next sections.

3.5.3   Coral reefs

Corals dissipate wave energy and change the flow near the bed, which influences the sediment transport. Wave attenuation occurs due to wave breaking and friction over the coral reef. Coral reefs are found to be comparable when it comes to wave attenuation with traditional defences such as breakwaters (Ferrario et al., 2014). The upper vertical limit of coral reefs is determined by the tidal range. It is, however, difficult to define a unique tidal limit due to many different factors influencing the upper limit of coral growth. In this research Low Tide is used which is defined as MSL - LT (Dixon, 2011). Equation 3.5 derived in Ferrario et al. (2014) is used to determine the wave height at the end of the coral reef (H_c).

$$H_c = H_i - H_i * \left(\frac{62.2 * (1 - \exp^{-(W_{coral}/213.3)})}{100} \right) \ [m] \tag{3.5}$$

This Equation originates from a set of experiments that were conducted on coral reefs with variable reef flat widths. The wave height reduction over the flat was measured for a multitude of locations. By fitting a line between the points, Equation 3.5 was constructed.

3.5.4   Mangroves

Mangrove forests attenuate waves and storm surge, through bottom friction. Important parameters include, the cross-shore width of the mangrove forest and the density & shape of the forest (Menéndez et al., 2020). It is found that mangroves can reduce wave energy significantly, in some cases up to 66% in the first 100 m of cross-shore forest width (Menéndez et al., 2020). According to Menéndez et al. (2020), the benefits of mangrove forests as a coastal defence increase with increasing return periods for storms.

Mangroves typically grow between MSL and HT (McIvor et al., 2013). Ecosystems such as mangroves that occur high in the intertidal zone are more effective in attenuating waves than ecosystems that occur lower in the intertidal zone as the maximum depth is lower (Bouma et al., 2014). The maximum depth and hence the maximum wave height increases with increasing tidal range (Bouma et al., 2014). The effectiveness of wave attenuation thus decreases with depth, which means that the size of ecosystems needed to attenuate waves significantly increases with tidal range (Bouma et al., 2014).

Depending on whether at the hotspot coral reefs are also present, the wave height at the start of the mangrove forest (H_0) is governed by either the wave breaking criterion (Kaminsky & Kraus, 1993) or by the attenuated waves over the coral reefs located lower in foreshore. The propagation and hence attenuation of waves through the mangrove forest can then be approximated with Equation 3.6 (Mendez & Losada, 2004) to obtain the wave height at the toe of the dike (H_{toe}) as the end of the mangrove forest is assumed to be located at the toe of the dike. The mangrove width is included implicitly in the water depth (h_0).

$$H_{toe} = H_0 * K_v * K_s \ [m] \tag{3.6}$$

where:

- H_0 the incident wave height at the start of the mangrove forest, governed by either the wave breaking criterion or the attenuated waves over the coral reef (if present) [m].

- K_v damping coefficient (Equation 3.7) [-].

- K_s shoaling coefficient governed by Green's law (Equation 3.9) [-].

$$K_v = \frac{1}{1 + 2\frac{A_1}{m} * H_0 * (K_s - 1)} \ [-] \tag{3.7}$$

where:

- A_1 factor including multiple parameters (Equation 3.8) $[m^{-1}]$.

- m slope of the foreshore $[\frac{m}{m}]$.

$$A_1 = \frac{2C_d b_v N \alpha}{3\pi} \ [m^{-1}] \tag{3.8}$$

where:

- C_d drag coefficient [-].

- b_v plant area per unit height of each vegetation stand normal to u [m].

- N number of vegetation stands per unit horizontal area $[m^{-2}]$

- α relative vegetation height (ratio of vegetation height over average water depth) [-].

$$K_s = \frac{h_0^{0.25}}{h^{0.25}} \ [-] \tag{3.9}$$

where:

- h_0, h the water depth at the start of the mangrove forest and toe respectively [m].

Depending on the location of the hotspot, the type of mangrove species vary. The coefficients (C_d, b_v, N, α) corresponding to the physical characteristics of these mangrove species also vary accordingly (Pinsky et al., 2013). Janssen (2016) listed the average values of these parameters based on different literature studies, which led to the values, seen in Table 3.2. However, when comparing these values to local case studies they seem to under predict the nearshore wave height (Section 7.1). For this global study therefore it is chosen to slightly alter these parameters as explained in section 7.1. The results are given in Table 3.2.

	C_d	b_v	N	h_v
Janssen (2016)	1.77	0.27 m	0.64 stems/m^2	4.2 m
Global study	1.77	0.27 m	0.40 stems/m^2	2.0 m

Table 3.2: *Average physical parameters of mangroves stems (Janssen, 2016) and values used within this research (global study).*

3.5.5 Calculated nearshore wave height

The wave heights at the toe of the dike are determined depending on the different foreshore configurations present at the hotspots (Figure 3.12) as explained in the previous sections. The calculations are performed for the current and the new protection standards, including and excluding SLR, according to adaptation strategies $A_{cur,slr}$, B_{new} and $C_{new,slr}$. The results that are shown include the wave attenuation caused by the mangroves and corals that are currently present at the hotspot. Section 3.9 will go into the calculations involving increased amounts of wave attenuation due to mangrove and/or coral restoration where possible.

Intermezzo 3.2.5: Nearshore wave heights (hotspot United Arab Emirates)

- Mangrove width = 26 m, coral width = 0 m.

- Current design water depth excluding SLR: 2.1 m, including SLR: 2.7 m.

- New design water depth excluding SLR: 2.3 m, including SLR: 2.9 m.

- Current nearshore wave height excluding SLR: 1.43 m, including SLR: 1.82 m.

- New nearshore wave height excluding SLR: 1.55 m, including SLR: 1.94 m.
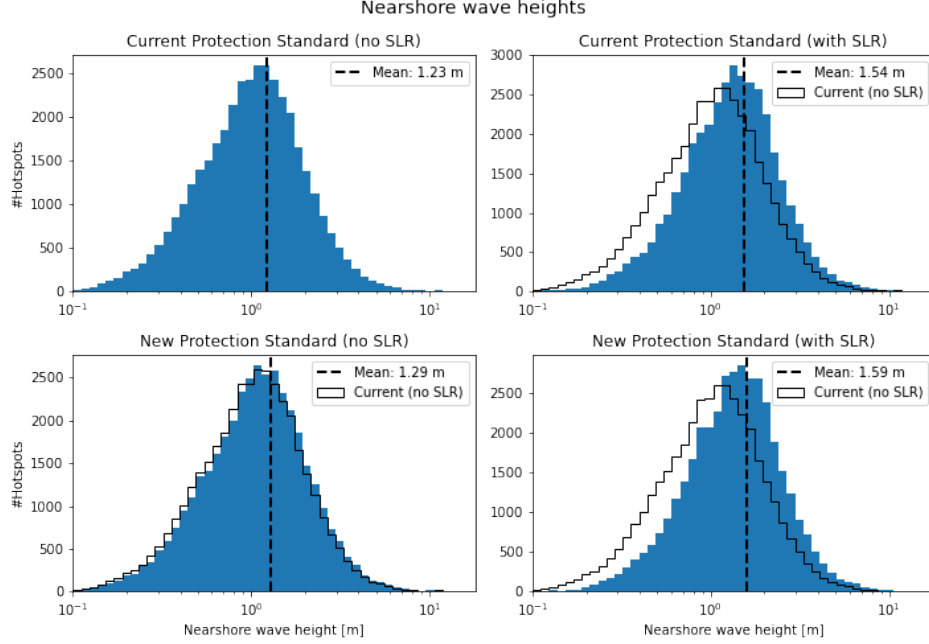
Figure 3.12: *Distribution of nearshore wave heights for the current and new protection standard including and excluding SLR for all hotspots. If the protection standard is improved and/or SLR is taken into account, it can be seen that the nearshore wave heights increase.*

3.6 Run-up

An exact description of the run-up due to waves on the dike front is not possible as wave breaking is a stochastic process. Therefore, empirical formulas are derived to describe the wave run-up based on experiments. The roughness, oblique wave attack and berms are taken into account via influence factors, however, in this research it is assumed that there is no berm present in the dike system and that waves propagate normal to the dike. The run-up height is defined as the vertical difference between the still water level and the highest point of the wave run-up. Due to the stochastic nature of the waves, each wave will give a unique run-up height. In this research the run-up height $R_{u2\%}$ will be used for the design crest height. This is the run-up height that is exceeded by 2% of the waves that are coming in from the toe of the dike (Equation 3.10).

$$R_{u2\%} = H_{m0} * 1.75 * \gamma_f * \xi_{m-1,0} \; [m] \tag{3.10}$$

where:

- $\xi_{m-1,0}$ relates the slope steepness of the dike to the wave steepness (Equation 3.11) [-].

- H_{m0} describes the incident wave height at the toe of the dike [m].

- γ_f is an influence factor for roughness taken as 0.9 in this research [-].

$$\xi_{m-1,0} = \frac{tan(\alpha)}{\sqrt{\frac{H_{m0}}{L_{m-1,0}}}} \; [-] \tag{3.11}$$

where:

- $tan(\alpha)$ is the slope of the dike, taken as $\frac{1}{3}$ in this research [$\frac{m}{m}$].

- $L_{m-1,0}$ denotes the deep water wave length, estimated with $1.56T_{m-1,0}^2$, which uses the wave period at the toe of the structure. In this research the spectral wave period ($T_{m-1,0}$) is assumed to be 10 s for all nearshore waves [m].

The wave heights at the toe (H_{toe}) are determined in previous section 3.5, based on different empirical formulas, that take waves in the form of H_{m0} as input. Therefore, those wave heights can directly be used into equation 3.10 and 3.11. The resulting run-ups for adaptation strategies $\boldsymbol{A_{cur,slr}}$, $\boldsymbol{B_{new}}$ and $\boldsymbol{C_{new,slr}}$ are given in Figure B.6.

Intermezzo 3.2.6: Run-ups (hotspot United Arab Emirates)

- Current run-up: 7.83 m, current run-up including SLR: 8.84 m.

- New run-up: 8.16 m, new run-up including SLR: 9.14 m.

3.7   Crest height

The required crest height of the dike is calculated by summing the DWL and run-up and by subtracting HT, as the foot of the dike is located at HT. For the new protection standard the expected land subsidence during the design period should also be taken into account, however, currently no global data is available for the magnitude of expected land subsidence. Hence, for all hotspots the land subsidence is set at 0 m. The results for adaptation strategies $\boldsymbol{A_{cur,slr}}$, $\boldsymbol{B_{new}}$ and $\boldsymbol{C_{new,slr}}$ are given in Figure B.7.

Intermezzo 3.2.7: Crest heights (hotspot United Arab Emirates)

- Current crest height: 9.92 m, current crest height including SLR: 11.51 m.

- New crest height: 10.43 m, new crest height including SLR: 11.98 m.

3.8   Dike heightening and related costs

For adaptation strategies $\boldsymbol{A_{cur,slr}}$, $\boldsymbol{B_{new}}$ and $\boldsymbol{C_{new,slr}}$ the difference in crest height and hence the required dike heightening (Δz) can be calculated. For adaptation strategy $\boldsymbol{A_{cur,slr}}$, this is the dike heightening that is required to maintain the same protection standard while SLR is taken into account. For adaptation strategy $\boldsymbol{B_{new}}$ this is the dike heightening that is required to increase the protection standard without taken into account SLR. And finally, for adaptation strategy $\boldsymbol{C_{new,slr}}$ this is the dike heightening that is required to increase the protection standard with SLR being taken into account. Figure 3.13 shows the results for the three adaptation strategies.

(a) *Adaptation strategy $\boldsymbol{A_{cur,slr}}$.*   (b) *Adaptation strategy $\boldsymbol{B_{new}}$.*   (c) *Adaptation strategy $\boldsymbol{C_{new,slr}}$.*
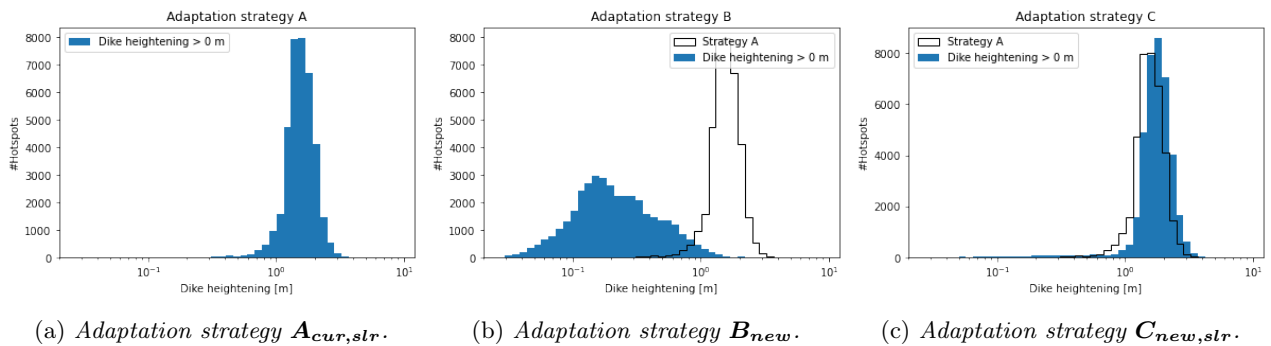
Figure 3.13: *If the protection standard is kept constant and SLR is taken into account (Figure 3.13a), on average 1-2 m of dike heightening is required. If the protection standard is improved and SLR is not taken into account (Figure 3.13b), on average 0.1-1 m of dike heightening (Δz) is required. If the protection standard is improved and SLR is taken into account (Figure 3.13c), on average 1-2 m of dike heightening is required. At the end of the 21st century the SLR contributes more to the required dike heightening than the increased storminess does.*

As the design water depths increase, due to increased extreme sea levels (SLR/increased storm surge), the design wave heights increase accordingly (Figure 3.13). The dike costs are determined per km stretch of coastline depending on the price per m dike raised. Depending on the location of the hotspot, different prices ($\$_{dike}$) are connected to the operation costs as seen in Table 3.3 given in \$/km/m (Aerts, 2018). Maintenance costs are not taken into account here as they only contribute to a small amount. A distinction is made here based on the GDP per capita of the hotspots (WorldBank, 2020), where a line is fitted between the dike costs obtained from Aerts (2018) for different countries with different GDP per capita. For countries where no data is available for the dike costs, the costs are determined by linear interpolation between the obtained values. Here, the minimum and maximum construction costs are given by Vietnam and the United States, meaning that countries with lower and higher GDP per capita will be given those values respectively. The dike investment costs for the three adaptation strategies $A_{cur,slr}$, B_{new} and $C_{new,slr}$ are given in Figure 3.14 and are calculated with Equation 3.12.

$$I_{dike} = \Delta z * \$_{dike} \ [\$/km] \tag{3.12}$$

When taking into account the dike length of each location, the dike investment costs for each hotspot can be calculated. The global total dike investment costs for all 38,773 locations combined amounts to (see Table 3.5):

- $A_{cur,slr}$: $\sum_1^{38773} I_{dike} = \$1,927$ billion.

- B_{new}: $\sum_1^{38773} I_{dike} = \$ \ 390$ billion.

- $C_{new,slr}$: $\sum_1^{38773} I_{dike} = \$2,288$ billion.

Classification	Construction costs [\$/km/m]	Mean value [\$/km/m]	GDP per capita [\$/yr]
The Netherlands	18.7 M - 22.4 M	20.55 M	52,304
United States	25.6 M	25.6 M	63,543
Vietnam	0.7 M - 1.25 M	0.95 M	2,786

Table 3.3: *Construction costs for raising sea dikes by 1 meter based on the country's qualification on GDP per capita (Aerts, 2018; WorldBank, 2020).*

(a) $A_{cur,slr}$ (b) B_{new} (c) $C_{new,slr}$
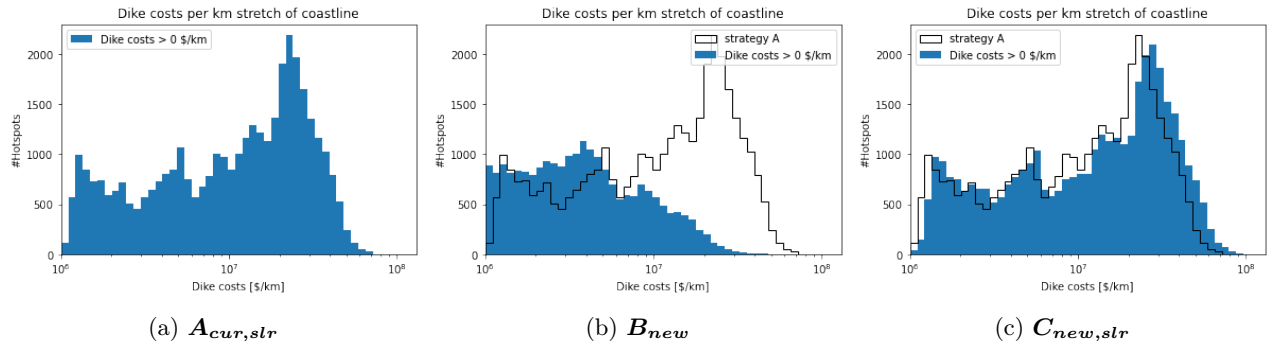
Figure 3.14: *Dike raising costs per kilometer of coastline required to follow the adaptation strategies $A_{cur,slr}$, B_{new} and $C_{new,slr}$. The x-axis makes uses of scientific notation, meaning that values of up to 100 Million \$/km are found for Figure 3.14c.*

Intermezzo 3.2.8: Dike investment costs (hotspot United Arab Emirates)
The dike length is calculated to be 2.45 km for this specific hotspot. By multiplying the dike costs/km with the dike length, the dike investment costs are calculated for the whole hotspot.

- $\$_{dike} = 25,600,000$ \$/km/m.

- $\boldsymbol{A_{cur,slr}}$: $\Delta z = 1.59$ m, $I_{dike} = 40.8$ M\$/km, $I_{dike} = 99.8$ M\$.

- $\boldsymbol{B_{new}}$: $\Delta z = 0.51$ m, $I_{dike} = 13.0$ M\$/km, $I_{dike} = 31.7$ M\$.

- $\boldsymbol{C_{new,slr}}$: $\Delta z = 2.06$ m, $I_{dike} = 52.9$ M\$/km, $I_{dike} = 129.2$ M\$.

3.9 Including vegetation where possible

In chapter 2 the hotspots with potential for coral and/or mangrove restoration are determined (Figures 2.10 and 2.13). Based on this classification, calculations involving the second defence approach can be performed, which includes applying vegetation on the foreshore next to raising the dikes (for all three adaptation strategies $\boldsymbol{A_{cur,slr}}$, $\boldsymbol{B_{new}}$ and $\boldsymbol{C_{new,slr}}$). By applying vegetation at the foreshore the corresponding wave attenuation can result in a reduction of the wave run-up, which in turn reduces the dike costs as well. The run-up calculations are re-done for different coral and/or mangrove widths. An optimal configuration can then be found for which the total costs are lowest.

Based on the amount of vegetation that is currently present at the hotspot different vegetation widths are taken for which the run-up calculations are re-done. The minimum extent of vegetation is hence given by either 0 m if there is no vegetation present in the hotspot, or a certain width if there is already vegetation in the hotspot. The maximum extent, as explained in section 3.5 is is bounded by the tidal range and the slope of the foreshore for mangroves and is found to be 1000 m for corals (Pearson, 2016).

3.9.1 Vegetation costs
Next to the dike costs also the vegetation costs vary across the world. The hotspots are divided into developed and developing countries based on their GDP. Countries with a GDP per capita below \$12,000 /yr are labeled as developing countries, where as countries with a GDP per capita above \$12,000 /yr are labeled as developed countries (WorldBank, 2020). The corresponding costs for restoration of corals and/or mangroves ($\$_{coral}$ & $\$_{mang}$) are taken from Aerts (2018) and can be seen in Table 3.4.

Classification	Type	Construction Costs [\$/ha]
Developing	mangrove restoration	1,191
Developing	coral restoration	89,269
Developed	mangrove restoration	38,982
Developed	coral restoration	1,826,651

Table 3.4: *Restoration costs for mangroves and corals based on the country's GDP per capita (Aerts, 2018).*

3.9.2 Cost optimization
The total investment costs (I_{tot}) are calculated by summing the cost of raising the dikes plus the costs of coral and/or mangrove restoration for different vegetation widths as shown in Equation 3.13. Where ΔW_{coral} and ΔW_{mang} are the restored coral and mangrove area relative to what is already present at the hotspot.

$$I_{tot} = \Delta z * \$_{dike} + \Delta W_{coral} * \$_{coral} + \Delta W_{mang} * \$_{mang} \ [\$/km] \tag{3.13}$$

The optimal vegetation width and corresponding crest height is determined for which the total costs are the lowest. By computing these costs for different widths of vegetated foreshore (ΔW), at some point the total costs reaches a minimum value where the addition of corals and/or mangroves is most cost-effective as seen in Figure 3.15. Here, the results are shown for for all three adaptation strategies $\boldsymbol{A_{cur,slr}}$, $\boldsymbol{B_{new}}$ and $\boldsymbol{C_{new,slr}}$,

for one specific location with only potential to apply mangroves (Figure 3.15). More examples are given in appendix B.4.

(a) *Adaptation strategy $A_{cur,slr}$.*

(b) *Adaptation strategy B_{new}.*

(c) *Adaptation strategy $C_{new,slr}$.*
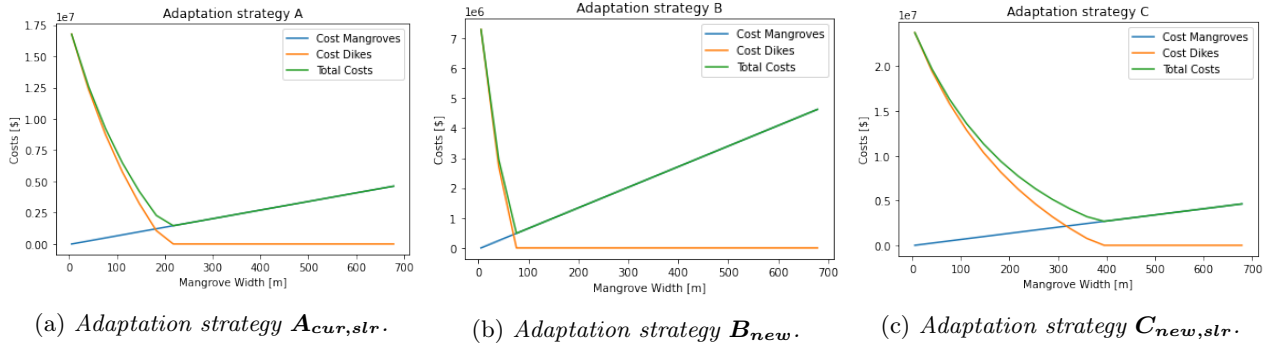
Figure 3.15: *Y-axis showing the total costs consisting of dike costs and vegetation costs for all three adaptation strategies $A_{cur,slr}$, B_{new} and $C_{new,slr}$. The results are given for a hotspot located in China (26.67°N 119.77°E) with only potential to apply mangroves, hence the x-axis denotes mangrove width.*

On the x-axis, the widths are denoted starting with the amount of mangroves currently present in the hotspot. For the hotspot seen in Figure 3.15 located in China, the current width of the mangrove forest is 5 m. From the current width up to the maximum width possible at the hotspot (679 m) which is governed by HT (3.42 m) and the slope (0.00504), the costs are calculated. The optimal vegetation widths (ΔW) where the total costs are minimum are 213 m, 71 m and 390 m for the three strategies respectively relative to the 5 m of mangroves already present.

If the width of the mangrove forest or the coral reef increases, more wave attenuation could be induced. This can result in smaller waves occurring at the toe of the dike, which in turn can result in smaller run-up values and hence, smaller required crest heights. This explains the decrease in dike costs when more vegetation is added (Figure 3.15). For this hotspot, the dike costs even become 0, as for the corresponding vegetation widths the run-up becomes so small that the calculated required crest height for the new protection standard becomes equal to the current crest height.

Intermezzo 3.2.9c: Total investment costs (hotspot China)

- Coral potential = No, mangrove potential = Yes.

- $\$_{coral}$ = 1,826,651 \$/ha, $\$_{mang}$ = 38,982 \$/ha.

- $A_{cur,slr}$: ΔW_{mang} = 213 m, I_{dike} = 9.52 M\$/km, I_{tot} = 0.83 M\$/km, reduction = 8.7 M\$/km.

- B_{new}: ΔW_{mang} = 71 m, I_{dike} = 4.14 M\$/km, I_{tot} = 0.28 M\$/km, reduction = 3.9 M\$/km.

- $C_{new,slr}$: ΔW_{mang} = 390 m, I_{dike} = 13.49 M\$/km, I_{tot} = 1.52 M\$/km, reduction = 12.0 M\$/km.

For this location, the maximum amount of mangroves possible at the foreshore is 679 m. Here, there is only potential for mangrove restoration, which is why only optimal mangrove widths are found that vary for the different adaptation strategies.

The costs for raising of the dikes (defence approach 1) are shown in Figure 3.14, which vary depending on the adaptation strategy used. For each hotspot, for defence approach 2, the optimal cost calculations are performed as explained above. The minimum total costs following this defence approach, considering all hotspots are shown in Figures 3.16a-3.16c. By comparing the costs of defence approach 2 to the cost of solely raising the dikes, the reduction in costs is obtained (see Figures 3.16d-3.16f).

(a)

(b)

(c)

(d) *Adaptation strategy $A_{cur,slr}$.*

(e) *Adaptation strategy B_{new}.*

(f) *Adaptation strategy $C_{new,slr}$.*
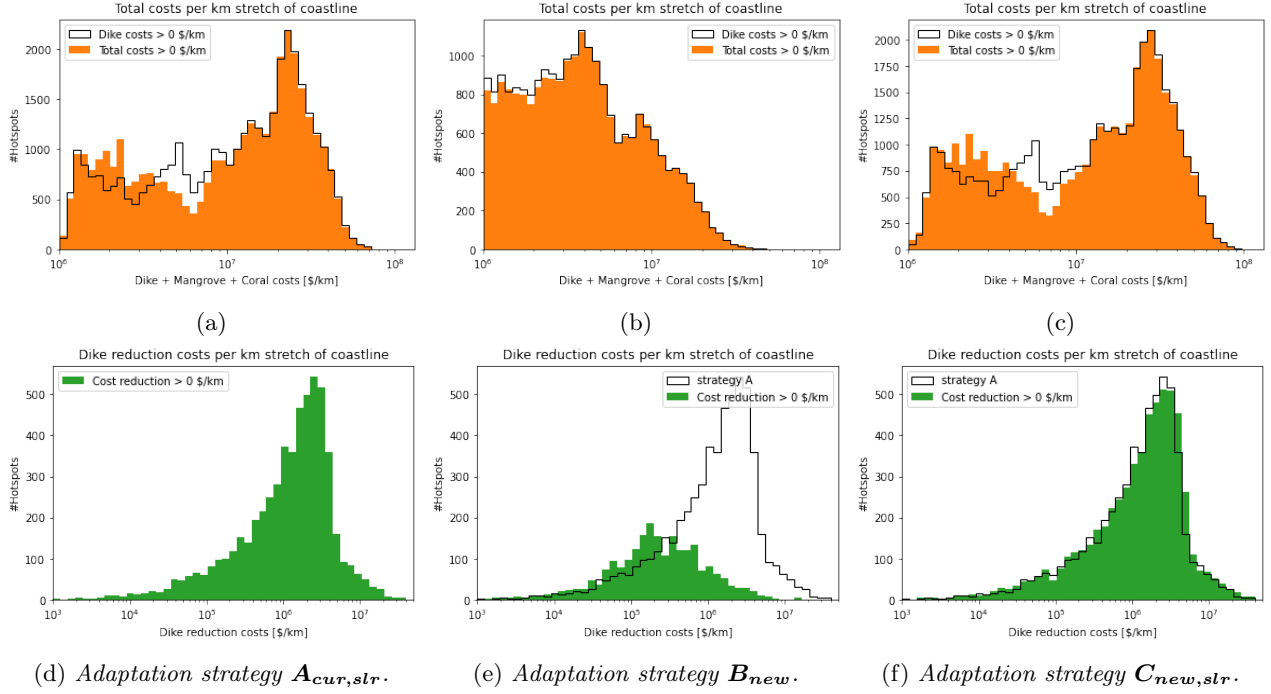
Figure 3.16: *Figures 3.16a-3.16c give the optimal total costs for which the combination of raising dikes and applying corals and/or mangroves result in the lowest investment costs. These panels can be compared to investment costs of solely raising dikes (denoted by black lines, see also Figure 3.14). By making this comparison, the reduction in costs can be obtained for the possibility of using nature-based solutions compared to solely raising of the dikes. This reduction in costs is given in the lower panels, where the results for the different strategies are compared to strategy $A_{cur,slr}$.*

The global total investment costs for the whole hotspot for a combination of dike raising and mangrove/coral restoration where possible for all 38,773 locations combined amounts to (see Table 3.5):

- $A_{cur,slr}$: $\sum_1^{38773} I_{tot} = \$1,877$ billion.

- B_{new}: $\sum_1^{38773} I_{tot} = \$ \ 385$ billion.

- $C_{new,slr}$: $\sum_1^{38773} I_{tot} = \$2,233$ billion.

Table 3.5 compares the total costs for defence approach 1 to defence approach 2. Depending on the adaptation strategy 2,275-5,858 hotspots are found where the investment costs are reduced. These locations can potentially be interesting business cases, as the nature-based solutions can be applied in a cost-effective manner.

Strategy	Global total dike investment costs	Global total dike investment costs including NBS	Total reduction	Locations	Mean reduction
$A_{cur,slr}$	\$1,927 billion	\$1,877 billion	\$50.0 billion	5,722 hotspots	\$2.18 M/km
B_{new}	\$ \ 390 billion	\$ \ 385 billion	\$ \ 4.3 billion	2,275 hotspots	\$0.56 M/km
$C_{new,slr}$	\$2,288 billion	\$2,233 billion	\$54.7 billion	5,858 hotspots	\$2.34 M/km

Table 3.5: *Global total dike investment costs, global total investment costs including dike heightening and mangrove/coral restoration and global total reduction in investment costs due to mangrove/coral restoration. The column with locations shows the number of hotspots where a reduction in costs is achieved and the corresponding global mean reduction in cost per kilometer of coastline is given in the last column.*

4 | Determining the benefits of flood risk reduction

This chapter aims to answer the sub-question: *"What are the global total flood risk reduction benefits of improving the protection standard?"*. The flood risk is analyzed for each hotspot. Flood risk is considered as an expected value defined as *'the probability of a flood event multiplied by the consequences'* (Jonkman, 2018). In this research the consequences are expressed by means of a monetary value. The risk is expressed in \$/yr and consists of a set of scenarios each with a certain probability and consequence (see Equation 4.1).

$$E(d) = \sum_{s_i=1}^{n} = p_i * d_i \ [\$/yr] \tag{4.1}$$

where:

- Scenario s_i, with probability p_i [/yr] and damage d_i [\$]

- $E(d)$, expected value of the damage per year (risk) [\$/yr]

In order to assess the possible damages (d_i), first the flood hazards that can occur must be determined at a given hotspot. For different scenarios (s_i), corresponding to storms with different return periods, the extreme sea levels are of different magnitudes. Depending on the protection at the hotspot, these extreme sea levels can cause flooding. If flooding occurs, damage estimates are made, that increase for more intense floods. The probability (p_i) for which these scenarios occur correspond to the inverse of their return period.

4.1 Flood hazards

In order to make a quantitative flood risk analysis, the hydraulic terms must be expressed in probabilistic terms. Hence, the extreme sea levels (DWLs) that occur for different return periods must be determined. In this case there are 16 different scenarios for which the flood hazards are determined, with return periods of 5, 10, 25, 50, 100, 250, 500 and 1000 years including and excluding SLR. The extreme sea levels consist of the components mentioned in subsection 3.3. Figures B.8 and B.9 show for all hotspots the resulting design water levels for the 16 different scenarios.

4.2 Failure probability

As it is assumed that the hotspots have a flood defence in place, the probability of failure/overflow must be determined. In this simplified analysis, the probability of flooding is taken equal to the likelihood of overflow of the defences, which is equal to the protection standard of the dikes (current and new situation). Here different dike failure mechanisms are not taken into account. The different flood hazard scenarios have a certain probability of exceedance of the corresponding loading conditions. If a certain hotspot has a dike with a protection standard of 250 years, the dike should be designed to safely withstand a load which on average is exceeded once every 250 year. This means that the dike should resist the design water level and the run-up of the waves combined. In this assessment, it is assumed that dike failure only occurs if the DWL corresponds to a return period that is larger than the protection standard of the dike.

4.3 Flood scenarios

The simplest and most conservative flood simulation type is the geometrical approach, where water levels are imposed on elevation models and an assumption is made that all areas lower than a certain water level are flooded. These calculations are done considering that there is no flood defence in place anywhere in the world. In this case, as there are dikes present, only the flooded areas are taken into account if failure of the dike

has occurred. Flood calculations (Google Earth Engine) are performed following this geometrical approach for various extreme sea levels with steps of 1 m (z = -5 m to z = 12 m). Using linear interpolation between these different elevations, the area flooded for the 16 extreme sea level scenarios is calculated. Based on the depth-population curves specific to each hotspot the amount of people being flooded is determined. Figures B.10 and B.11 show for all hotspots the resulting amount of people being flooded if dike failure would occur.

Intermezzo 3.3.3: Depth-population curve (hotspot United Arab Emirates)

For three different hotspots, the depth-population curves are displayed to show that they differ between locations. Based on the flood calculation performed via the geometrical approach, for different water depths different amounts of people are flooded. It can be seen that the flooded population increases with larger flood depths. For this hotspot located in the United Arab Emirates, the linear interpolated values are plotted. The dots align well with the dotted line representing the 'true' values. The dots represent the extreme sea levels for return periods of 5, 10, 25, 50, 100, 250, 500, 1000 excluding SLR.
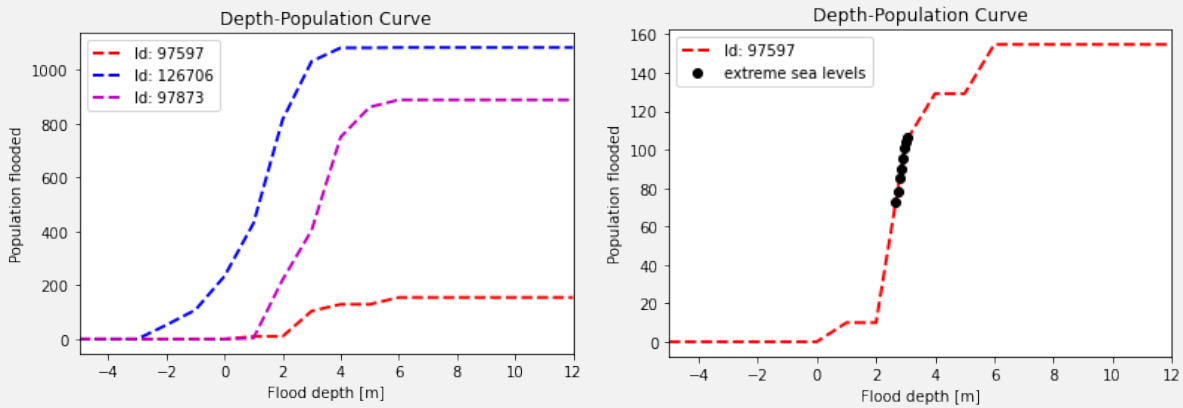
4.4 Damage estimates

To quantify the consequences in terms of financial damage, the hazard component and vulnerability of exposed assets must be combined (Duo et al., 2020). If failure of the dike occurs, the total land area that is located below the extreme sea level causing dike failure is considered to be flooded. For this area the Expected Annual number of People (EAP) being flooded is calculated (see intermezzo 4.5). The amount of people flooded is subsequently converted to the asset damages with the approach used by Hinkel et al. (2014), which uses the sub-national GDP per capita rates and an empirically estimated $\frac{assets}{GDP}$ ratio of 2.8, to estimate damages:

$$E(d) = 2.8 * GDP * EAP \ [\$/yr] \tag{4.2}$$

4.5 Risk calculations

In order to calculate the risk, first the EAP is determined for the extreme sea level scenarios with and without SLR. The EAP are then converted to assets at risk as explained in subsection 4.4. Intermezzo 4.5 explains how these calculations are performed by showing an example calculation for one hotspot. For the three different adaptation strategies mentioned above the change in risk between the current and new situation is calculated for all hotspots (Figure 4.6):

$$\Delta E(d) = E(d)_{initial} - E(d)_{new} \ [\$/yr] \tag{4.3}$$

Where $E(d)_{initial}$ corresponds to the yearly expected damage for the current coastal defence and $E(d)_{new}$ corresponds to the yearly expected damage for the new situation that depends on the adaptation approach $\boldsymbol{A_{cur,slr}}$, $\boldsymbol{B_{new}}$ or $\boldsymbol{C_{new,slr}}$.

Intermezzo 3.3.5: Risk calculation $\Delta E(d)$ **(hotspot United Arab Emirates)**

For this hotspots located in the United Arab Emirates, the current protection standard is 5 years, which means that the area is assumed to be flooded only if extreme sea levels occur with a return period larger than 5 years. Hence, the damage is assumed to be 0 for floods with a height lower than for which the dike is designed. This means that the current people at risk consists of the green area starting with the return period of 5 years (Figure 4.2a). For the new protection standard with a return period of 50 years, this area is reduced (Figure 4.2b). In Figure 4.2c & 4.2d, the areas are also bounded by the protection standard, however, SLR is taken into account here. It can be seen that the amount of people at risk increases with SLR being taken into account. The left bound is given by a return period of 1000 years, as these are the flood events with the smallest probability of occurrence for which the consequences are calculated.

(a)

(b)

(c)

(d)
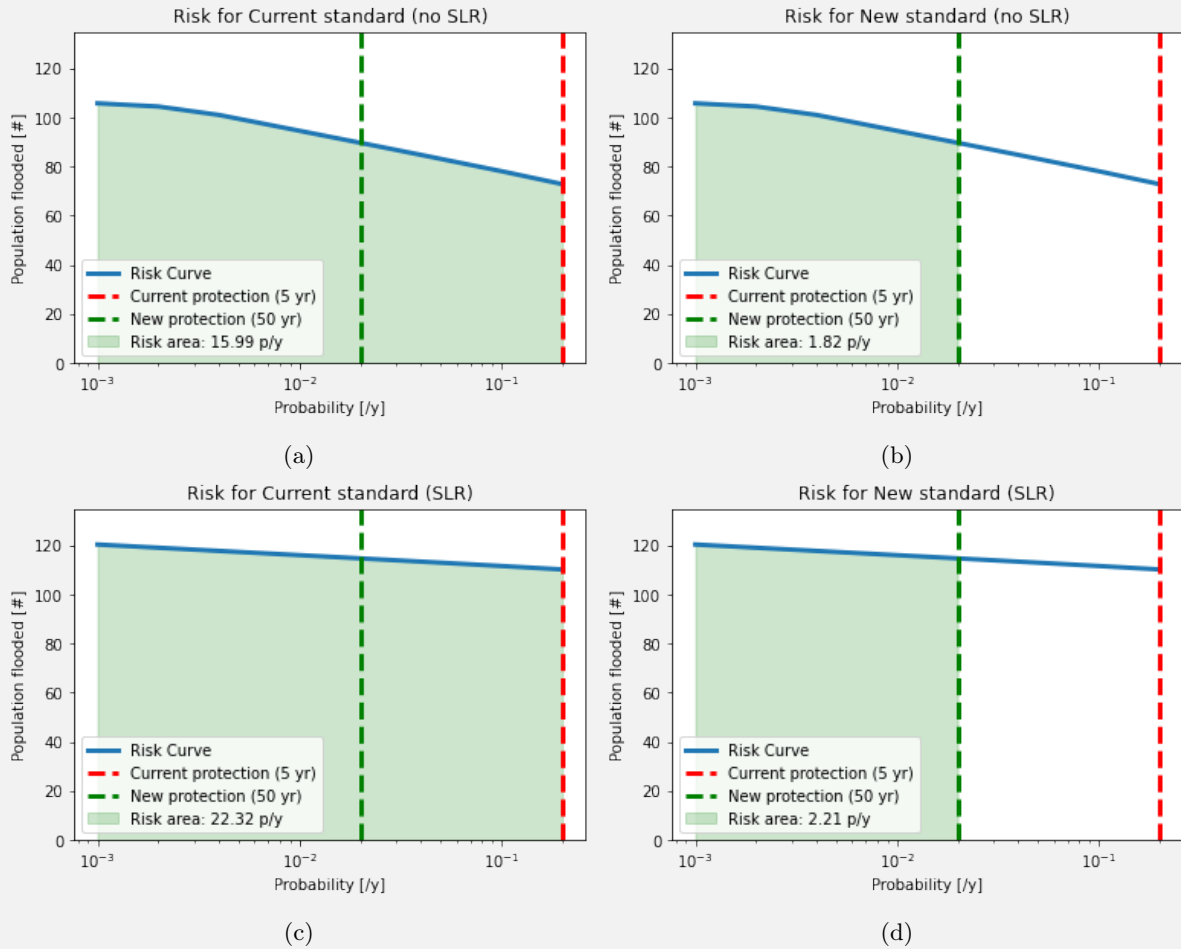
With these risk curves the risk reduction/increase for the different adaptation strategies can be calculated. Recall the definitions of the different adaptation strategies:

$A_{cur,slr}$ Protection standard constant, with SLR.

B_{new} Increasing protection standard towards a new fixed standard, without SLR.

$C_{new,slr}$ Increasing protection standard towards a new fixed standard, with SLR.

For adaptation strategy $A_{cur,slr}$, the risk increases as SLR is taken into account, which can be seen in Figure 4.2c as the graph is shifted upwards. This risk is subtracted from the current risk seen in Figure 4.2a, which results in an increased risk of 6 people per year (Figure 4.3). By multiplying the amount of people at risk per year with the local GDP of $118,383 /yr and an empirical constant of 2.8, an increase in risk of $(\Delta E(d))$ $2,098,224 /yr is obtained for this hotspot.
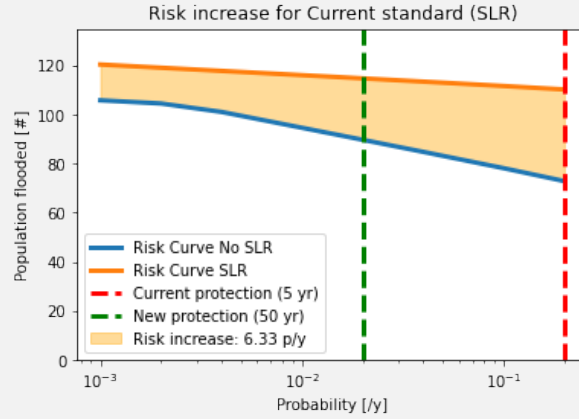
Figure 4.3: *Risk increase* $(A_{cur,slr})$.

For adaptation strategy B_{new}, the risk is reduced since the protection standard is increased. This can be seen in Figure 4.2b as the area under the graph is reduced. This risk is subtracted from the risk area in the Figure 4.2a, which results in a reduced risk of 14 people per year (Figure 4.4). By multiplying the amount of people at risk per year with the local GDP of $118,383 /yr and an empirical constant of 2.8, a reduction in risk $(\Delta E(d))$ of $4,696,973 /yr is obtained for this hotspot.
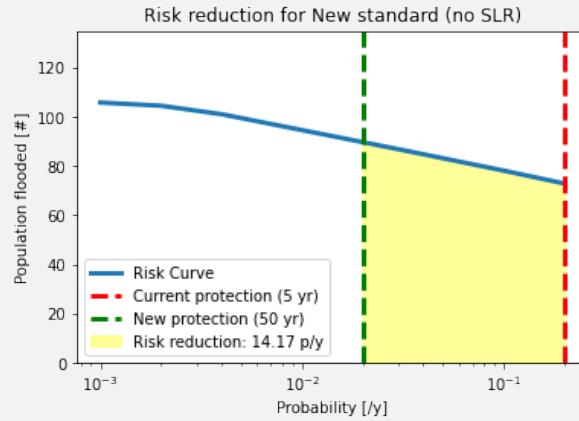
Figure 4.4: *Risk reduction* (B_{new}).

For adaptation strategy $C_{new,slr}$, the risk is reduced (Figure 4.2d) even though SLR is taken into account here. An increase in the protection standard causes a larger reduction in risk than SLR results in an increased risk. The risk is subtracted from the risk area in Figure 4.2a, which results in a reduced risk of 14 people per year when summing the reduction and increase in risk (yellow and orange areas Figure 4.5). The grey area is the increase in risk that is prevented, which is excluded from the results, as the current risk does not include it. By multiplying the amount of people at risk per year with the local GDP of $118,383 /yr and an empirical constant of 2.8, a reduction in risk $(\Delta E(d))$ of $4,567,698 /yr is obtained for this hotspot.
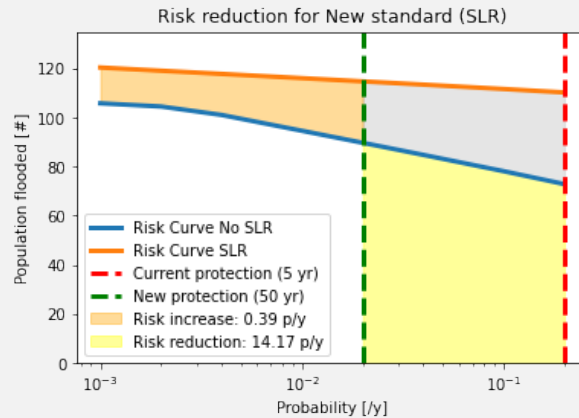
Figure 4.5: *Risk reduction* $(C_{new,slr})$.

- $A_{cur,slr}$: $\Delta E(d) = -\$2,098,224$ /yr.

- B_{new}: $\Delta E(d) = +\$4,696,973$ /yr.

- $C_{new,slr}$: $\Delta E(d) = +\$4,567,698$ /yr.
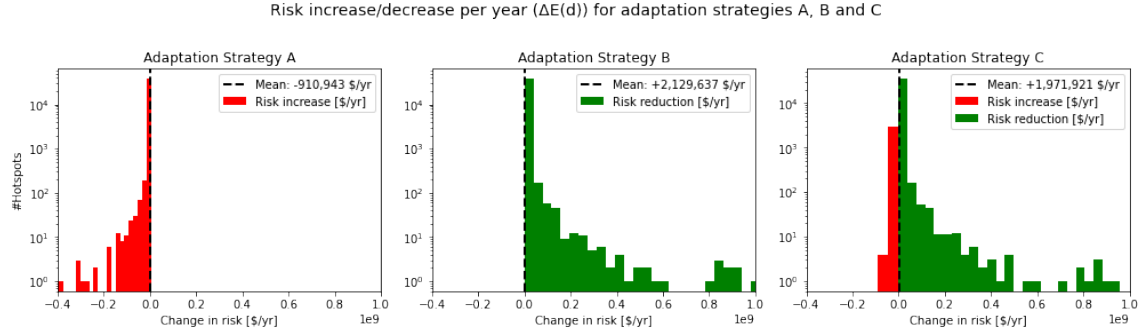
Figure 4.6: *Panel a shows an increase in risk as a result of SLR when the protection standard is kept the same. Panel b shows the amount of risk reduction as a result of increasing the protection standard to a fixed new standard, **without** taking SLR into account. Panel c shows the amount of risk reduction as a result of increasing the protection standard to a fixed new standard, when SLR **is** taken into account.*

It can be seen that for adaptation strategy $A_{cur,slr}$, the risk increases as the protection standard is not improved (Figure 4.6) and SLR is taken into account resulting in more intense extreme sea levels combining to a total risk increase of \$35 billion/yr. For adaptation strategies B_{new} and $C_{new,slr}$, the protection standard is improved, which results in global total risk reduction of \$82.5 billion/yr and \$76.5 billion/yr respectively. Panel c shows that for some hotspots still an increase in risk was found as the local sea level rise contributed more to an increase in risk than the protection standard improvement contributed to a reduction of risk.

4.6 Investment costs

In order to make the coastal defence economically beneficial, the investment (I_{dike} or I_{tot} section 3) should be smaller than the benefits received from flood risk reduction following Equation 4.4.

$$I < \Delta E(d)_{NPV}, \ \Delta E(d)_{NPV} = \frac{\Delta E(d)}{0.05} \ [\$] \tag{4.4}$$

Where $\Delta E(d)$, is transformed towards the Net Present Value (NPV) by dividing with an interest rate of 5%. In case of adaptation strategy $A_{cur,slr}$, by converting the increase in flood risk per year to a NPV, the responsible maximum investment space is obtained as seen in Figure 4.7. This is the investment range that can be used to counter this expected increase in risk in an economically beneficial manner. For strategies B_{new} and $C_{new,slr}$, the NPV can be compared to the investment costs required to upgrade the coastal defence towards the new protection standard. Chapter 6 will present these comparisons. Table 4.1 summarizes the main findings of this chapter.
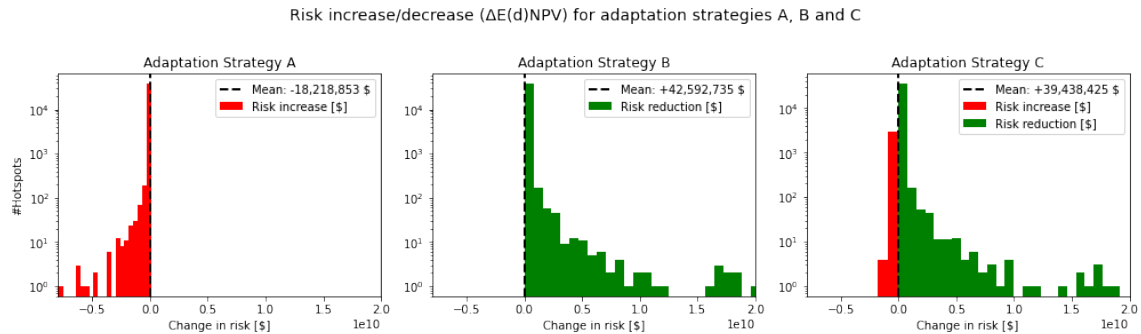
Figure 4.7: $\Delta E(d)$ converted to a Net Present Value with an interest rate of 5% for strategies $A_{cur,slr}$, B_{new} and $C_{new,slr}$ respectively.

47

Strategy	Total yearly change in risk	Total change in risk (NPV)
$A_{cur,slr}$	−$35.3 billion/yr	−$ 706 billion
B_{new}	+$82.6 billion/yr	+$1,651 billion
$C_{new,slr}$	+$76.5 billion/yr	+$1,529 billion

Table 4.1: *Global total risk reduction/increase between the current and new situation ($\mathbf{\Delta E(d)}$) and its corresponding NPV ($\mathbf{\Delta E(d)_{NPV}}$). The definition of the (+) and (-) signs follow from equation 4.3 where (+) denotes a reduction in risk and (-) an increase in risk.*

Intermezzo 3.3.6: Flood risk (hotspot United Arab Emirates)

The dike length is calculated to be 2.45 km for this specific hotspot. The dike costs per km of dike length were calculated in intermezzo 3.8 for strategies $\mathbf{A_{cur,slr}}$, $\mathbf{B_{new}}$ and $\mathbf{C_{new,slr}}$ as respectively 40.8 M$/km, 13.0 M$/km and 52.9 M$/km. To be able to compare the investment costs with the flood risk, the dike costs must be calculated for the whole hotspot as the risk also covers this whole area. Therefore, by multiplying the dike costs/km with the dike length, the dike investment costs are calculated for the whole hotspot. The same can be done for the investment costs including coral and mangrove restoration costs. The corresponding values (I_{dike} and I_{tot}) for this location in the United Arab Emirates are given below.

- $\mathbf{A_{cur,slr}}$: I_{dike} = 99.8 M$, I_{tot} = 99.8 M$, $\Delta E(d)_{NPV}$ = -42.0 M$.

- $\mathbf{B_{new}}$: I_{dike} = 31.7 M$, I_{tot} = 31.7 M$, $\Delta E(d)_{NPV}$ = 94.0 M$.

- $\mathbf{C_{new,slr}}$: I_{dike} = 129.2 M$, I_{tot} = 129.2 M$, $\Delta E(d)_{NPV}$ = 91.4 M$.

For adaptation strategy $\mathbf{A_{cur,slr}}$, there are also costs involved even if the protection standard is kept constant. As SLR is taking into account, the same protection standard will require a more robust coastal defence (see subsection 3.9). Since the protection standard is not improved, there are no flood risk benefits, but rather there is an increase of flood risk (Figure 4.6). From this increase in flood risk the responsible maximum investment space can be obtained to counter this (Figure 4.7).

For this hotspot it can be seen that for adaptation strategy $\mathbf{B_{new}}$ the investment costs are smaller than the corresponding flood risk reduction benefits that the intervention provides. This means that economically speaking, upgrading the protection standard is beneficial, as the benefits outweight the costs. For strategy $\mathbf{A_{cur,slr}}$, an increase in risk and hence investment space of 42M$ is calculated. For strategy $\mathbf{C_{new,slr}}$, the investment costs are higher than the flood risk reduction benefits, which means economically speaking, increasing the protection standard is not a good idea.

5 | Determining the additional benefits for nature-based solutions

This chapter aims to answer the sub-question: *"What are the global total additional benefits connected to the restored area of mangroves and corals?".* Ecosystems contribute to society in different ways (ecological, socio-cultural and economic). By expressing the values that the ecosystems have in terms of monetary values, more awareness about the importance of biodiversity can be conveyed towards the policy makers (De Groot et al., 2012).

Based on local case studies around the world, De Groot et al. (2012) estimated the benefits/values of ecosystem services such as coral reefs and mangroves in $/ha/year (Costanza et al., 2014). Ecosystem services are defined as the benefits that people derive from ecosystems. In total, over 300 case studies were screened and the corresponding data points were stored in the Ecosystem Services Value Database (ESVD). For a selection of these points an analysis was performed, with the following selection criterion:

1. The case study must provide a monetary value of a certain ecosystem service, that can be connected to a specific ecosystem and time period.

2. It must provide information on the area for which the ecosystem provides its value.

3. The valuation method that is used must be known.

4. The location of the case study site must be known.

For each ecosystem within the different biomes categories (open oceans, coastal systems, inland wetlands, lakes, temperate forests, grasslands, woodlands, coastal wetlands, coral reefs and tropical forests) the mean ecosystem service value is calculated. Arguably there is no true average value, as ecosystem services are very site specific. For services such as coral reef tourism, the values of different case studies vary largely between small remote reefs and large heavily visited reefs. However, the average value can still be used as an indication of importance. For both coral reefs and mangroves the monetary values that are obtained from different case studies vary, as seen in Table 5.1 and 5.2. The case studies took place in various countries, with different economic welfare standards. However, in this case no correlation between the degree of welfare and ecosystem value is found. Therefore for this research the average values for the coral reefs and mangroves are used from Davidson et al. (2019) (Table 5.1 and 5.2). Davidson et al. (2019) re-estimated the values as determined in Costanza et al. (2014).

The different ecosystem services that are used to determine the total additional benefits for coral reefs and mangroves are discussed below. The ecosystem classification is based on Kumar (2010) who splits each biome into different services and sub-services. The four main categories include provisioning services (e.g. food, raw materials), regulating services (e.g. climate regulation, erosion prevention), habitat services (e.g. genepool protection) and cultural services (e.g. tourism). Each sub-service provides its own additional value, for each biome, Davidson et al. (2019) sums all the sub-service values to obtain the total ecosystem value.

5.1 Coral reefs

Some of the most important contributors to the ecosystem service value of coral reefs are recreation & tourism and erosion protection.

5.1.1 Recreation & tourism
Burke et al. (2008) calculates the gross revenue of tourism and recreation for the islands Tobago and St. Lucia. The study indicates different recreation and tourism activities related to coral reefs. Firstly, the **accommodation** expenditures, for which it must be known whether hotel guests partly travelled to the specific location

due to the presence of coral reefs. Secondly, **reef recreation** that includes activities such as diving, snorkeling and sport fishing. Next to this **Marine Protected Areas** are important in drawing tourists to a location. In addition, there are **additional expenditures** of visitors in restaurants, shops and transport. Lastly, there are **economy-wide effects**, that are not related to the direct economic impacts mentioned above, but rather are indirect economic impacts for the local communities.

Spalding et al. (2017) bases the tourism value of coral reefs on two components, namely 'reef-adjacent' and 'on-reef' value. Reef-adjacent value includes indirect benefits such as sheltered water and attractive views. On-reef value includes direct benefits such as diving and snorkelling. In Spalding et al. (2017), the benefits were determined as a proportion of the total amount of visitors and their expenses in areas within 30 km of the coral reefs, not including the urban areas. It is found that the total tourism value of coral reefs sums up to almost \$36 billion and accounts for about 9% of the coastal tourism value, in areas where coral reefs are present (Spalding et al., 2017).

5.1.2 Erosion protection

Ruitenbeek et al. (1999) evaluates the value of coral reefs in terms of erosion protection. The value is estimated based on the land that is vulnerable to erosion if no reefs were present. The case study takes place in Montego Bay, Jamaica and estimates \$306,427 /ha/yr from erosion protection.

Coral reefs	Mean [\$/ha/year]	Minimum [\$/ha/year]	Maximum [\$/ha/year]	#
Provisioning services	55 724	33 073	105 106	30
Food	677	0	6175	21
Raw materials	21 528	9	64 328	3
Genetic resources	33 048	33 048	33 048	1
Ornamental resources	427	16	1555	5
Regulating services	172 144	1505	412 838	16
Climate regulation	1118	83	2192	3
Extreme events	16 991	4	104 134	10
Waste treatment	85	85	85	1
Erosion prevention	153 880	1333	306 427	2
Habitat services	16 210	7	92 401	9
Genepool protection	16 210	7	92 401	8
Cultural services	108 837	2208	1 518 777	39
Aesthetic information	11 390	2204	27 351	3
Recreation & tourism	96 302	0	1 484 996	29
Cognitive information	1145	4	6429	6
TOTAL	352 915	36 794	2 129 122	94

Table 5.1: *Monetary values of coral reefs obtained from 94 studies (Davidson et al., 2019).*

5.2 Mangroves

Some of the most important contributors to the ecosystem service value of mangroves are water purification and life-cycle maintenance.

5.2.1 Water purification

Emerton & Kekulandala (2002) calculated the economic value from wastewater purification of mangroves in the Gampaha District in Sri Lanka. As industrial wastewater enters the mangrove forest, the trees and its roots act as a filter for removal of toxic substances and nutrients. If no mangroves were present, the untreated waste water would enter the nearby lagoon, making it unable to use as drinking water. To combat this issue, improved sanitation facilities and latrine pits would need to be constructed. The costs connected to this are used as an estimation of the economic value of mangroves for waste water purification.

5.2.2 Life-cycle maintenance

Edward. & Strand (1997) explored the value of mangroves as a nursery habitat for off-shore fisheries in Mexico, Campeche State. A fishery model is used to account specifically for the effect that mangroves have on the capacity and production of fish. It is found that loss of mangroves result in lower harvest levels and hence revenue. The local prices of fish per kg are used to assess the economic value of mangroves.

Mangroves	Mean [$/ha/year]	Minimum [$/ha/year]	Maximum [$/ha/year]	#
Provisioning services	2998	18	27 845	59
Food	1111	0	18 743	27
Water supply	1217	1	4277	4
Raw materials	358	0	4218	25
Genetic resources	10	10	10	1
Medicinal resources	301	7	596	2
Regulating services	171 515	249	685 696	35
Climate regulation	65	7	184	6
Extreme events	5351	2	32 291	20
Waste treatment	162 125	6	640 099	4
Erosion prevention	3929	188	13 076	4
Nutrient cycling	45	45	45	1
Habitat services	17 138	14	145 940	26
Lifecycle maintenance	10 648	5	123 886	20
Genepool protection	6490	9	22 054	6
Cultural services	2193	20	28 347	19
Recreation & tourism	2193	20	28 347	19
TOTAL	193 845	300	887 828	193

Table 5.2: *Monetary values of mangroves obtained from 193 studies (Davidson et al., 2019).*

5.3 Calculating additional benefits

For the second defence approach there is a possibility to include coral and/or mangrove restoration. As the size of the ecosystem increases, consequently the ecosystem creates additional value and the corresponding benefits increase. For adaptation strategies $A_{cur,slr}$, B_{new} and $C_{new,slr}$, the additional benefits compared to what is already present at the hotspot is calculated with Equation 5.1. The total ecosystem values from Table 5.1 (352,915) and 5.2 Table (193,845) are expressed in \$/ha/yr and the restored area of the coral reef (A_{coral}) and mangrove forest (A_{mang}) are in hectares. In order to convert it into a NPV the benefits are divided by an interest rate of 5%:

$$ben_{NPV} = \frac{A_{coral,rest} * 352,915 + A_{mang,rest} * 193,845}{0.05} \; [\$] \tag{5.1}$$

The additional benefits that the restored areas of mangroves and corals provide per year are given in the panels in Figure 5.1 for coral reefs and mangroves separately for strategies $A_{cur,slr}$, B_{new} and $C_{new,slr}$. Table 5.3 shows the global total areas of mangroves and corals restored and the corresponding total benefits (NPV).

Strategy	Mangrove area	Coral area	Mangrove benefits	Coral benefits	Total benefits
$A_{cur,slr}$	102,054 ha	456,232 ha	\$395.7 billion	\$3,220 billion	\$3,616 billion
B_{new}	17,218 ha	28,807 ha	\$ 66.8 billion	\$ 203 billion	\$ 270 billion
$C_{new,slr}$	110,506 ha	495,395 ha	\$428.4 billion	\$3,497 billion	\$3,925 billion

Table 5.3: *The first two columns show the total amount of restored mangrove and coral area for defence approach 2 following from the optimal cost calculation. The corresponding global total additional benefits due to these restored areas are shown in the subsequent columns.*
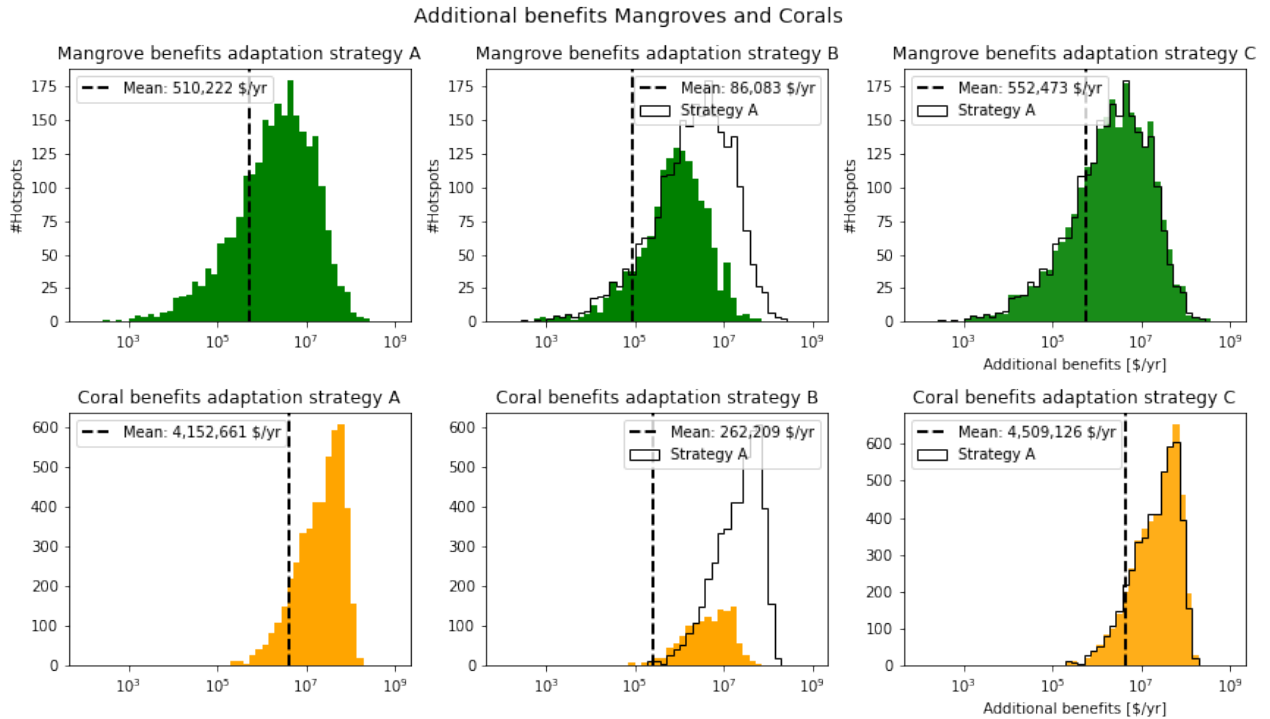
Figure 5.1: *The additional benefits per year calculated for the restored area of mangroves/corals at the hotspots for strategies $A_{cur,slr}$, B_{new} and $C_{new,slr}$. The right panels show that there is a small difference between strategy $A_{cur,slr}$ and $C_{new,slr}$.*

6 | Determining the benefit to cost ratios

This chapter aims to answer the sub-question: *"Based on all the benefits and costs, what are the flood risk reduction potentials of the various solutions?"*. In the previous chapters for each hotspot the investment costs were determined for adaptation strategies $A_{cur,slr}$, B_{new} and $C_{new,slr}$. This was done for two defence approaches, namely dike raising and a combination of dike raising and coral and/or mangrove restoration. Thereafter, the increase in risk for strategy $A_{cur,slr}$ and reduction in risk for strategies B_{new} and $C_{new,slr}$ were calculated. The additional benefits that corals and mangroves provide were also determined for each location. In this final step, for adaptation strategy B_{new} and $C_{new,slr}$ a benefit-cost comparison is done, based on two different methods:

1. The benefit-cost ratios are calculated for the **fixed new protection standards** given in Figure 3.3 by taking into account the results shown in the previous chapters.

2. The benefit-cost ratios are calculated for the **most cost-beneficial protection standard**. Depending on the current protection, the new protection standard is optimized for adaptation strategies B_{new} and $C_{new,slr}$. The costs and benefits are re-calculated for different new protection standards. For the new protection standard where the summation of benefits (+) and costs (-) reaches a maximum, the most cost-beneficial protection standard is found.

For both methods, the benefit-cost ratios are calculated for defence approach 1 and 2 and strategies B_{new} and $C_{new,slr}$ as shown below. Adaptation strategy $A_{cur,slr}$ is excluded from these calculations as it does not involve risk reduction benefits but rather an increase in risk as the protection standard of the coastal defence is kept constant. Since this strategy does not involve raising of the standard, method 2 cannot be performed as well, as an optimization of the protection standard is required here.

(a) **Defence approach 1**.

The costs are related to the amount of dike heightening and the benefits to the flood risk reduction benefits ($\frac{\Delta E(d)_{NPV}}{I_{dike}}$).

(b) **Defence approach 2**.

The costs are related to the amount of dike heightening and mangrove/coral restoration. It chooses the cheapest solution for the new standards, where the investment costs are lowest as explained in section 3.9. The benefits are related to the flood risk reduction benefits ($\frac{\Delta E(d)_{NPV}}{I_{tot}}$).

(c) **Defence approach 2 including additional benefits**.

This also gives the benefit-cost ratio for defence approach 2, but here the benefits also include the additional benefits next to the flood risk reduction benefits ($\frac{\Delta E(d)_{NPV}+ben_{NPV}}{I_{tot}}$).

6.1 Benefit-cost ratios for fixed new protection standard

Figure 6.1 shows the benefit-cost ratios for all coastal hotspots for strategies B_{new} and $C_{new,slr}$ and defence approaches 1 and 2. The benefit-cost ratios for defence approach 1 are shown in Figure 6.1a and 6.1d for strategies B_{new} and $C_{new,slr}$ respectively. For defence approach 2 in Figure 6.1b and 6.1e and for defence approach 2 including additional benefits in Figure 6.1c and 6.1f. If the benefit-cost ratios are larger than 1, the benefits are larger than the investment costs required to obtain these benefits, at these locations improving of the coastal defences is economical. In the Figures these hotspots are shown in green. Appendix B.5 provides more graphs including the benefits and costs separately. The amount of hotspots where the benefits outweigh the costs are determined for the different approaches and shown in Table 6.1.

If SLR is taken into account the number of economical locations reduce by 62-64% if additional benefits are not taken into account. As the sea level rises, the required dike height and/or restoration area of mangroves and

corals increases to achieve the desired protection standard, which means that the investment costs increase. Next to this, the reduction in risk obtained by improving the protection standard is lower for the situation with SLR. Concluding, if SLR is considered, the costs increase and the flood risk reduction benefits decrease, this means that the benefit-costs ratios decrease, which explains the reduction in number of economical locations.

Strategy	Defence approach 1	Defence approach 2	Defence approach 2 + add. benefits
B_{new}	8,199 hotspots	8,549 hotspots	9,527 hotspots
$C_{new,slr}$	2,975 hotspots	3,208 hotspots	7,888 hotspots

Table 6.1: *Amount of hotspots where the flood risk benefits outweigh the dike investment costs (defence approach 1) and where the flood risk benefits outweigh the investment costs including dike heightening and coral/mangrove restoration (defence approach 2). The third column also includes additional benefits for defence approach 2.*

If the additional benefits are taken into account, SLR has less effect in reducing the number of economical locations as the reduction only amounts to 17% of locations. As explained earlier, SLR increases the required dike height and/or restoration area of mangroves and corals to obtain the preferred protection standard. This means that in locations where mangrove/coral restoration is possible, more mangroves/corals can be added. Consequently the additional benefits these ecosystems provide also increase. As a result, the increase in additional benefits counteract the decrease in flood risk reduction benefits. This means that the benefit-cost ratios for those locations increase, which explains the smaller reduction in number of economical locations. If coral and/or mangrove restoration is taken into account, the costs are reduced relative to solely dike raising to obtain the same corresponding flood risk reduction benefits, hence an overall increase in the benefit-cost ratios is observed when comparing Figures 6.1a and 6.1d to 6.1b and 6.1f.
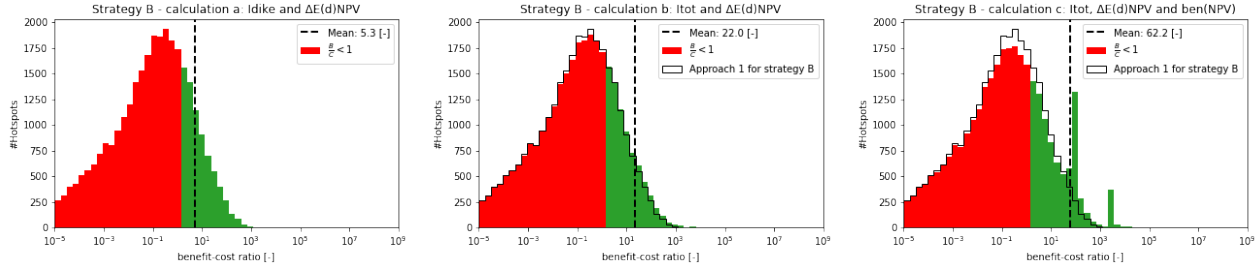
(a) *Defence approach 1 for strategy B_{new}.*

(b) *Defence approach 2 for strategy B_{new}.*

(c) *Defence approach 2 and additional benefits for strategy B_{new}.*
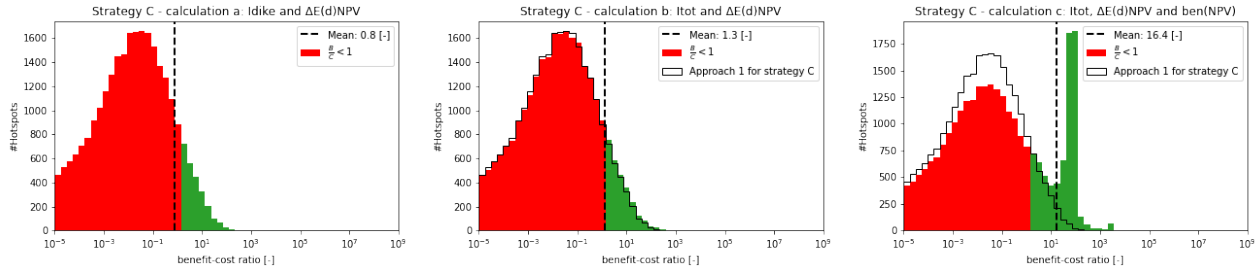
(d) *Defence approach 1 for strategy $C_{new,slr}$.*

(e) *Defence approach 2 for strategy $C_{new,slr}$.*

(f) *Defence approach 2 and additional benefits for strategy $C_{new,slr}$.*

Figure 6.1: *The benefit-cost ratios for defence approach 1 and 2 and strategies B_{new} and $C_{new,slr}$. The black outlines represent the left panels. The hotspots denoted by red have benefit to cost ratios lower than 1, hotspots in green have benefit-cost ratios higher than 1. For the green hotspots the benefits outweigh the costs, such that it is economically beneficial to improve the protection standard of the coastal defence. The green spikes in the right panels are explained by the fixed ecosystem values used in this research, which cause the benefit-cost ratios to fall within the 50-150 range for many locations.*

The locations shown in Table 6.1 can be further investigated as potential business cases. However, depending on the role that stakeholders play, more detailed filtering of these locations can be preferred up front. Two examples are given below from the point of view of an investor or a policy maker.

Investor - Flood risk benefits

The investor looks at the investment cost in relation to the benefits that are obtained via flood risk reduction. Therefore, the investor could look at the first two columns of Table 6.1 as the benefits are larger than the investment costs. However, the number of hotspots shown in Table 6.1 for defence approach 2 can also include locations where mangrove/coral restoration is not possible. Locations where NBS are applicable, reduce investment costs and where the flood risk reduction benefits outweigh the investment costs give more insight towards the cost-effectiveness of NBS. For mangroves these locations are given in Figures 6.2a and 6.2b. For coral reefs, the results are given in Figures 6.2c and 6.2d.

(a) *Strategy B_{new} (mangroves), 863 of 8,549 (10.0%) cost-beneficial locations (see Table 6.1).*

(b) *Strategy $C_{new,slr}$ (mangroves), 446 of 3,208 (13.9%) cost-beneficial locations (see Table 6.1).*

(c) *Strategy B_{new} (corals), 649 of 8,549 (7.6%) cost-beneficial locations (see Table 6.1).*

(d) *Strategy $C_{new,slr}$ (corals), 836 of 3,208 (26.1%) cost-beneficial locations (see Table 6.1)*
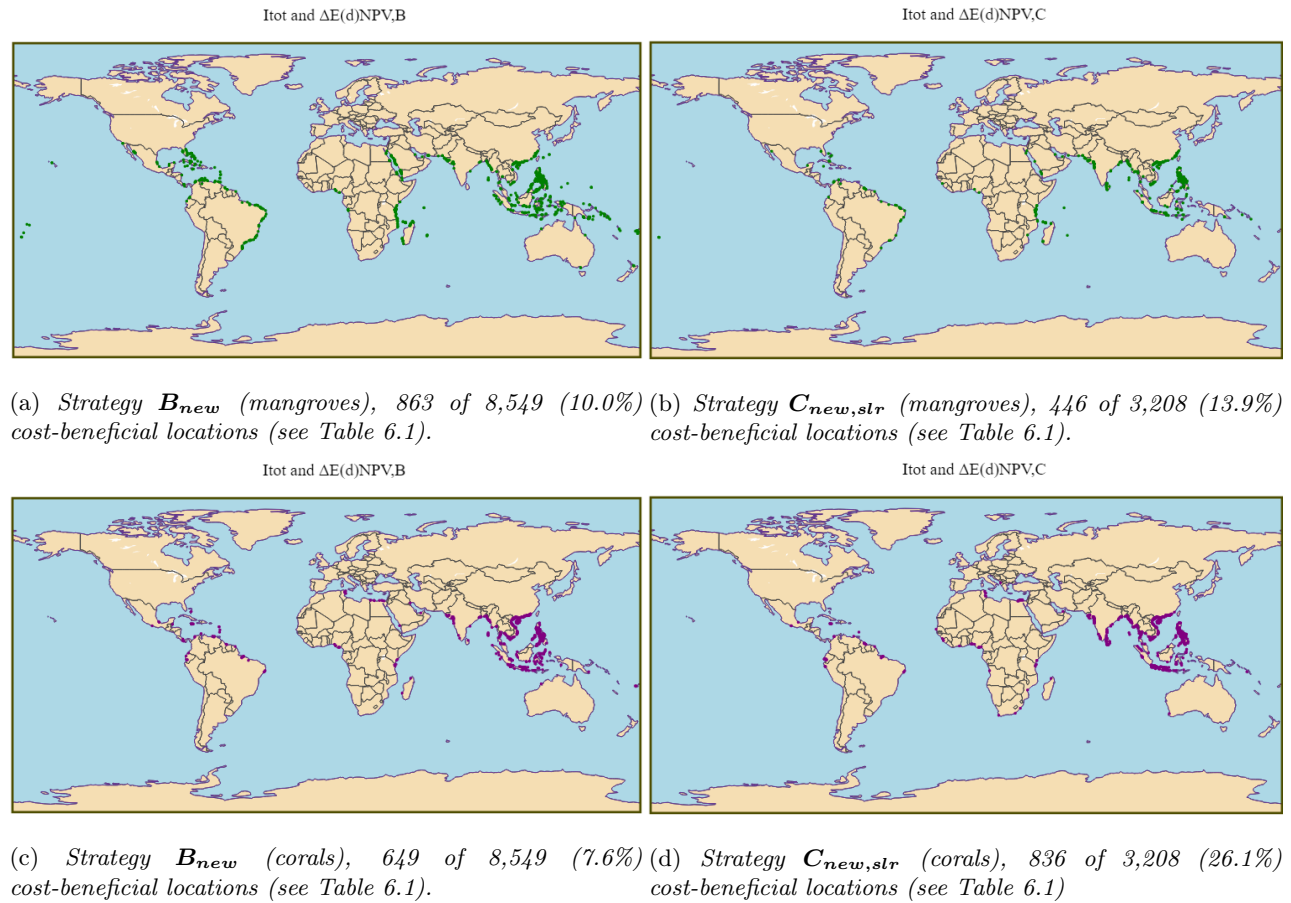
Figure 6.2: *Locations are plotted where the benefits outweigh the costs **and** where mangrove restoration (Figures 6.2a and 6.2b) and coral restoration (Figures 6.2c and 6.2d) reduce the investment costs.*

Policy makers - Flood risk and additional benefits

If additional benefits are taken into account, the corresponding benefit-cost ratios increase. This makes sense as corals and mangrove produce high ecosystem value per hectare as seen in section 5. Those benefits do not directly go into the wallet of the investor as they involve a common good, that have value and the investor is not necessarily the one getting the benefits. The additional benefits can help to raise awareness about the importance of ecosystem services for society. They can serve as a powerful communication tool to conduct more balanced decisions with regards to trade-offs including policies, which enhance the GDP but consequently damage the local ecosystem services (Costanza et al., 2014).

6.2 Benefit-cost ratios for most cost-beneficial protection standard

In order to calculate the most cost-beneficial protection standard for each coastal hotspot, here the costs and benefits (flood risk + additional) are calculated for each new protection standard (5, 10, 25, 50, 100, 250, 500, 1000 yr) instead of only the fixed new protection standard. The costs are denoted by negative values and the additional benefits by positive values. The flood risk reduction benefits are denoted by positive values if it includes a reduction in risk and by negative values if it includes an increase in risk (Equation 4.3). The protection standard for which the sum of these values is largest, corresponds to the most cost-beneficial protection standard. This summation is performed for defence approach 1 and 2 as follows:

(a) **Defence approach 1**.

The costs (dike heightening) are summed with the flood risk reduction benefits $(I_{dike} + \Delta E(d)_{NPV})$.

(b) **Defence approach 2**.

The costs (dike heightening and mangrove/coral restoration) are summed with the flood risk reduction benefits $(I_{tot} + \Delta E(d)_{NPV})$.

(c) **Defence approach 2 including additional benefits**.

The costs (dike heightening and mangrove/coral restoration) are summed with the flood risk reduction benefits and the additional benefits $(I_{tot} + \Delta E(d)_{NPV} + ben_{NPV})$.

6.2.1 Example calculation

As an example, the calculations for a hotspot located in Brazil (26.17°S and 48.50°W) are given below. At this location there are currently no corals or mangroves present and only mangrove potential was found. The calculations to obtain the most cost-beneficial protection standard are shown in Figure 6.3 for strategy B_{new}. More detailed analysis are performed in Appendix B.6.
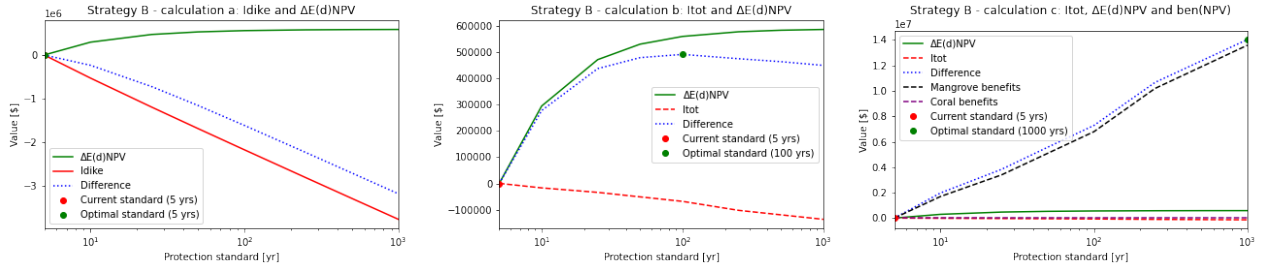
(a) *Defence approach 1 for strategy B_{new}.*

(b) *Defence approach 2 for strategy B_{new}.*

(c) *Defence approach 2 and additional benefits for strategy B_{new}.*

Figure 6.3: *Method to calculate the most cost-beneficial protection standard. The protection standard where the summation of costs (-) and benefits (+) is largest is the most cost-beneficial protection standard. The most cost-beneficial protection standard can also be the same as the current protection standard as seen in Figure 6.3a.*

It can be seen in Figure 6.3a that when the protection standard is increased, the costs (red line) increase (-), while the flood risk reduction benefits also increase (+). The costs however increase more rapidly, hence the model advises to maintain the same protection standard as is currently in place. For the situation where coral/mangrove restoration is taken into account (Figure 6.3b), the investment costs reduce relatively to Figure 6.3a, which means that the flood risk reduction benefits (which remain the same compared to Figure 6.3a[1]) are increasing more rapidly. At the location where the benefits outweigh the costs most, the most cost-beneficial protection standard is now found (100 years). Figure 6.3c also takes into account the additional benefits that increase as more mangroves are restored. As a result the protection standard is found to be 1000 years, since the additional benefits that mangroves provide exceed the local flood risk benefits and costs tremendously for this specific hotspot.

---

[1]The same protection standard for defence approach 1 and 2 provides the same probability of failure.

6.2.2 Most cost-beneficial protection standards

Originally the new protection standard was chosen according to Figure 3.3, where based on the current protection standard a fixed new protection standard was chosen. Following the method above, the most cost-beneficial protection standards are calculated for all hotspots for defence approach 1 and 2 and adaptation strategies B_{new} and $C_{new,slr}$.

Table 6.2 gives the amount of locations where it is economical to improve the current protection standard. It shows for adaptation strategy B_{new} that for all hotspots where it is economical to improve the protection standard, the benefits also outweigh the costs (Table 6.3). Figure 6.4a shows indeed that if it is economical to improve the protection standard, the benefits do outweigh the costs. However, if SLR is taken into account ($C_{new,slr}$), it can be seen in Table 6.3 that the amount of hotspots where the benefit-cost ratios are larger than 1 is smaller than the number of hotspots where it is economical to improve the current protection standard. For these locations there are already investment costs required to keep up with SLR as seen by the starting point of the red line in Figure 6.4b for a specific hotspot. By improving the protection standard, the flood risk reduction benefits increase faster than the costs do such that a maximum is found. At this maximum however, the benefits are still smaller than the costs even though it is economical to improve the protection standard.

Strategy	Defence approach 1	Defence approach 2	Defence approach 2 + add benefits
B_{new}	9,361 hotspots	9,696 hotspots	11,542 hotspots
$C_{new,slr}$	11,200 hotspots	11,578 hotspots	12,753 hotspots

Table 6.2: *Amount of hotspots where it is economical to improve the current protection standard.*

Strategy	Defence approach 1	Defence approach 2	Defence approach 2 + add benefits
B_{new}	9,361 hotspots	9,696 hotspots	11,542 hotspots
$C_{new,slr}$	3,356 hotspots	3,608 hotspots	8,316 hotspots

Table 6.3: *For the most cost-beneficial protection standards, this table gives the amount of hotspots where the flood risk benefits outweigh the dike investment costs (defence approach 1) and where the flood risk benefits outweigh the investment costs including dike heightening and coral/mangrove restoration (defence approach 2). The third column also includes additional benefits for defence approach 2*

(a) Strategy B_{new}. (b) Strategy $C_{new,slr}$.
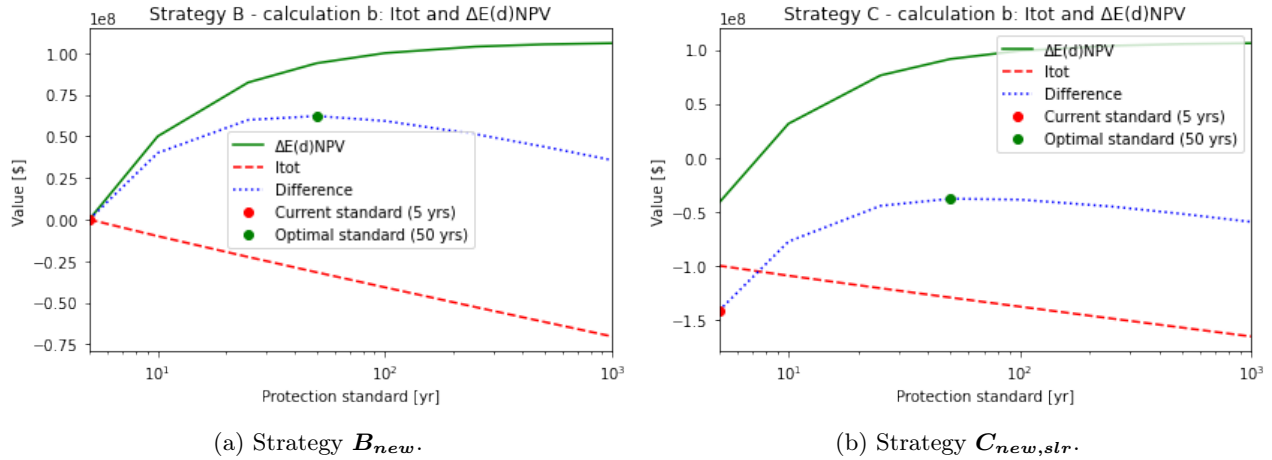
Figure 6.4: *Selected example to explain why improving the protection standard can be economical but does not necessarily have to result in benefit-cost ratios larger than 1. Here, the loss is reduced (economical), but the costs are still larger than the benefits. This example is for a hotspot located in the United Arab Emirates.*

The most cost-beneficial protection standards for all hotspots are given in Appendix B.6. The corresponding benefit-costs ratios for these most cost-beneficial protection standards are plotted in Figure 6.5. If the new protection standard is optimized, the number of cost-effective locations increases by 11-17% compared to the fixed new protection standard. It is found for a large amount of hotspots, that the most cost-beneficial protection standard is equal to the current protection standard. For those locations, the value of the flood-prone area is very low (few to none people living there). As a result, when the protection standard is improved, the corresponding flood risk benefits are negligible. For locations where the value of the hinterland is significant the most cost-beneficial protection standard does provide a more beneficial benefit-cost ratio.

(a) *Defence approach 1 for strategy B_{new}.*

(b) *Defence approach 2 for strategy B_{new}.*

(c) *Defence approach 2 and additional benefits for strategy B_{new}.*

(d) *Defence approach 1 for strategy $C_{new,slr}$.*

(e) *Defence approach 2 for strategy $C_{new,slr}$.*

(f) *Defence approach 2 and additional benefits for strategy $C_{new,slr}$.*
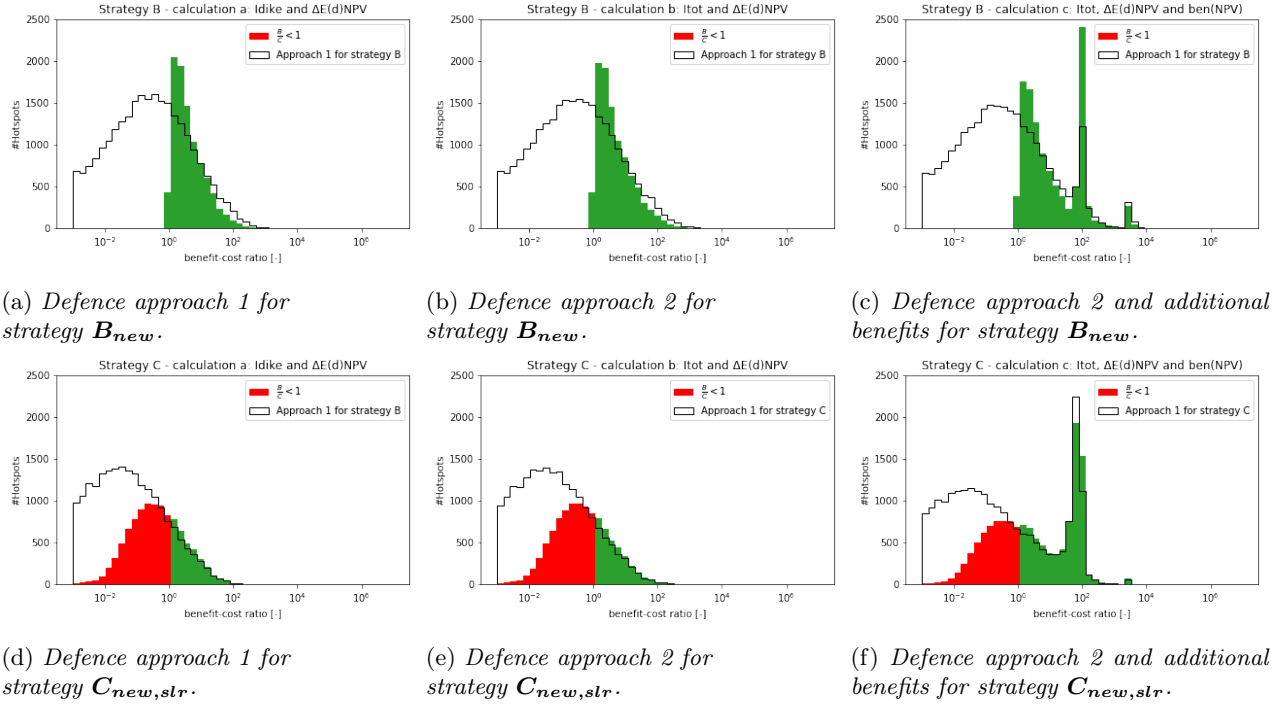
Figure 6.5: *The benefit-cost ratios for defence approach 1 and 2 for strategies B_{new} and $C_{new,slr}$ corresponding to the most cost-beneficial protection standards. The black outlines give the benefit-cost ratios for upgrading towards a fixed new standard. It is seen that for strategy B_{new}, only hotspots remain that have benefit-cost ratios larger than 1. This is the result of the optimization, if upgrading the protection standard is not beneficial, the most cost-beneficial protection standard is found to be equal to the current one. As a result, the investment costs and benefits are 0, resulting in no benefit-cost ratio values. The green spikes in the right panels are explained by the fixed ecosystem values used in this research, which cause the benefit-cost ratios to fall within the 50-150 range for many locations.*

Part II

Local Framework

7 | Case studies

This chapter presents the validation of the calculated nearshore wave height and storm surge against field measurements from literature. The wave attenuation measured in different mangrove field studies are compared to the calculated wave attenuation rates from the empirical model for mangroves (section 7.1). Secondly, in section 7.2 the physical parameters used as input for the mangrove empirical model are chosen such that the resulting wave attenuation rates resemble the observed wave attenuation rates in the field studies as close as possible. Thereafter, section 7.3 shows the wave attenuation comparison for coral reefs. The site characteristics of the mangrove and coral field studies used in this research are given in Appendix C.1 and C.2 respectively. Section 7.4 provides a comparison of the storm surge used in the global model and the predicted storm surge for different field studies. Lastly, the nearshore wave height for bare foreshores computed by the model is compared to the nearshore wave heights obtained from SwanOne.

7.1 Mangrove wave attenuation comparison

The physical parameters of the mangroves present at the field studies are used as input for Equation 3.6 together with the observed offshore wave heights at the field studies. The nearshore wave heights are then computed separately with the bathymetry from the field studies and from the global model (Athanasiou et al., 2019). Figure 7.1 shows the computed nearshore wave heights plotted against the nearshore wave heights observed in the field studies. The left Figure used the bathymetry from the field studies and the right Figure used the global slopes.
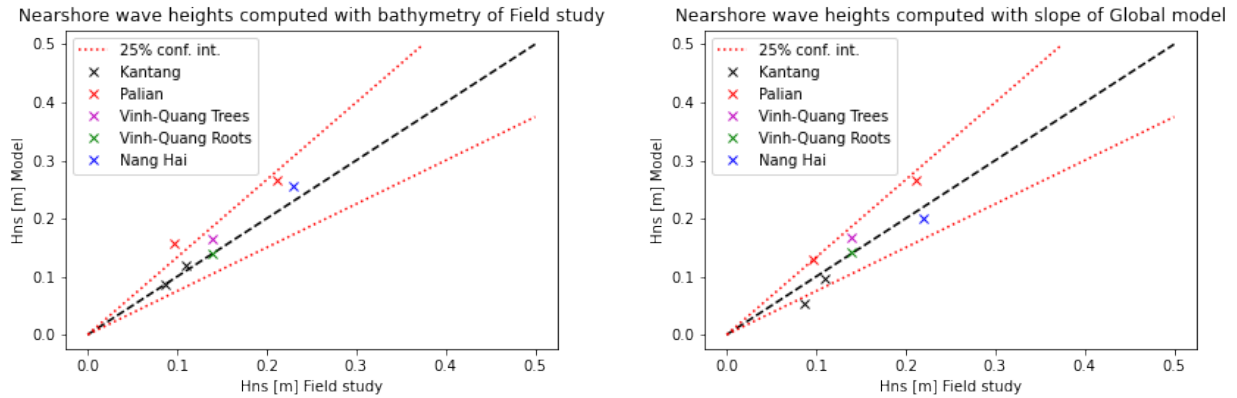
Figure 7.1: *Nearshore wave heights computed with the model plotted against the nearshore wave heights from the field studies. Left Figure uses local bathymetry obtained from field studies, right Figure uses the foreshores slopes as derived in Athanasiou et al. (2019) taken from the location of the field study.*

For the Vinh-Quang field study the nearshore wave heights are computed with the physical parameters corresponding to trees as well as the roots of the trees. As there are little amounts of trees present in the field study, the nearshore wave heights computed with the model are larger when the physical parameters of trees are used in contrast to the roots. Most results lay within the 25% confidence interval, with the results from the Palian transect deviating the most. This can be explained due to the lack of mangrove trees in the transect. There where lots of roots present at the Palian transect, however it is chosen not to use these physical parameters as input as they provide little to no wave attenuation during storm conditions. Concluding, based on the field studies, the empirical approach towards wave attenuation by mangroves produces results within the reasonable range.

7.2 Global average physical mangrove parameters

For the global model, average physical mangrove parameters are used as there is currently no global data set available, including the distribution of mangrove species. Based on the field studies mentioned above, average physical parameters are chosen such that the wave attenuation rates resemble the observed rates most accurately. As a starting point the average global physical mangrove parameters from Janssen (2016) are used as input to the empirical model for the field studies. The field study's local bathymetry and offshore wave heights are taken into account. These parameters are altered until the best fit between observed and computed nearshore wave heights is achieved. The resulting physical parameters are given in Table 7.1 and are used for the global study (see Table 3.2).
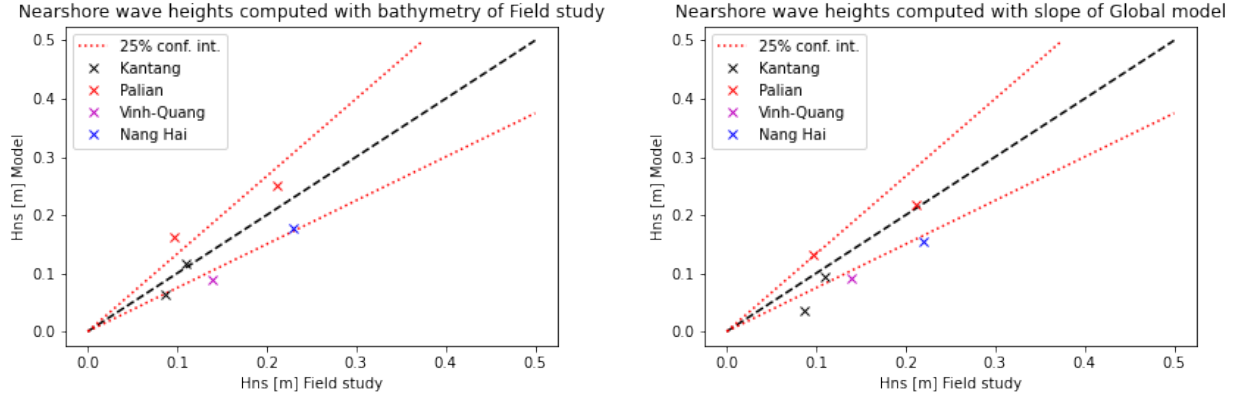
Figure 7.2: *Nearshore wave heights computed with the model plotted against the nearshore wave heights from the field studies. Left Figure uses local bathymetry obtained from field studies, right Figure uses the foreshores slopes as derived in Athanasiou et al. (2019) taken from the location of the field study. For the physical parameters, the values seen in Table 3.2 (global study) are used.*

	C_d	b_v	N	h_v
Janssen (2016)	1.77	0.27 m	0.64 stems/m^2	4.2 m
Global study	1.77	0.27 m	0.40 stems/m^2	2.0 m

Table 7.1: *Average physical parameters of mangroves stems (Janssen, 2016) and values used within this research (global study).*

7.3 Coral reef wave attenuation comparison

Experiments are conducted on five different reef profiles for a range of incident wave heights (see Appendix C.2 for site characteristics). Estimates of the significant wave heights were obtained using the standard deviation of pressure sensor records, where the wave dissipation relative to the offshore wave height is measured during HT. The wave dissipation measured in the field studies are compared to the model calculations. Where for all five coral reefs, the instrument located closest to the coast is chosen. The instruments for the five coral reefs with the corresponding measured wave dissipation at high tide and distance from the reef edge are given in Table 7.2.

Instrument	C3	C6	W1	L3	L5
Wave dissipation [%]	91.1	99.7	85	74	0
Distance from reef edge [m]	480	1080	2713	358	46

Table 7.2: *Wave dissipation measured at the instruments for the different field studies.*

To obtain the wave attenuation rates from the empirical model, the width of the coral reef and the offshore wave heights from the field studies are used as input. Figure 7.3 shows the comparison between the wave dissipation from the field study and the model approach. It is seen that the model underestimates the amount of wave dissipation compared to the field studies.
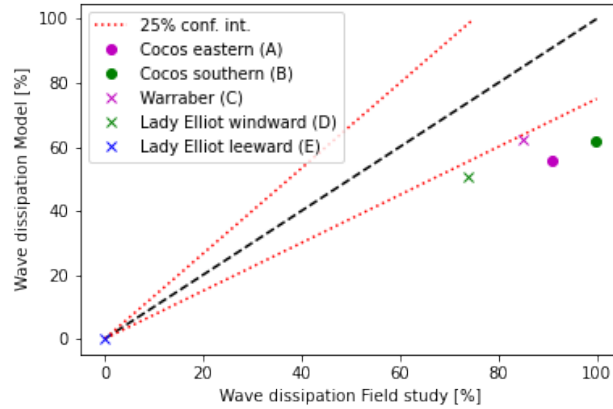
Figure 7.3: *Wave dissipation computed with the model plotted against the wave dissipation from the field studies.*

7.4 Storm surge comparison

For the global storm surge values, the data from Muis et al. (2020) is used for return periods of 5, 10, 25, 50, 100, 250, 500 and 1000 years. The data is available as a series of points along the coasts as seen in Figure 7.4. By using nearest neighbour interpolation the data is connected to the hotspots (polygons in Figure 7.4). In some cases the hotspots are located at a significant distance from the data points, as for example is the case in Lake Borgne. As a result the obtained values might differ from the values expected at the hotspots.

(a) *Lake Borgne (USA).*

(b) *Scheveningen (Netherlands).*

Figure 7.4: *The green polygons denote the hotspots. Lake Borgne located near New Orleans in the USA is shown on the map in Figure 7.4a, the Netherlands (Scheveningen) is shown in Figure 7.4b. The red crosses denote the points from where the data of Muis et al. (2020) is available.*

To find out to what degree the obtained storm surge values differ from local projected values, use is made of six case studies where projections of storm surge levels are done for different return periods. The results are

62

shown in Figure 7.5. The dotted lines are results from the local case studies and the other lines are the values obtained via Muis et al. (2020) for the hotspots located at the location of the case study by using nearest neighbour interpolation.
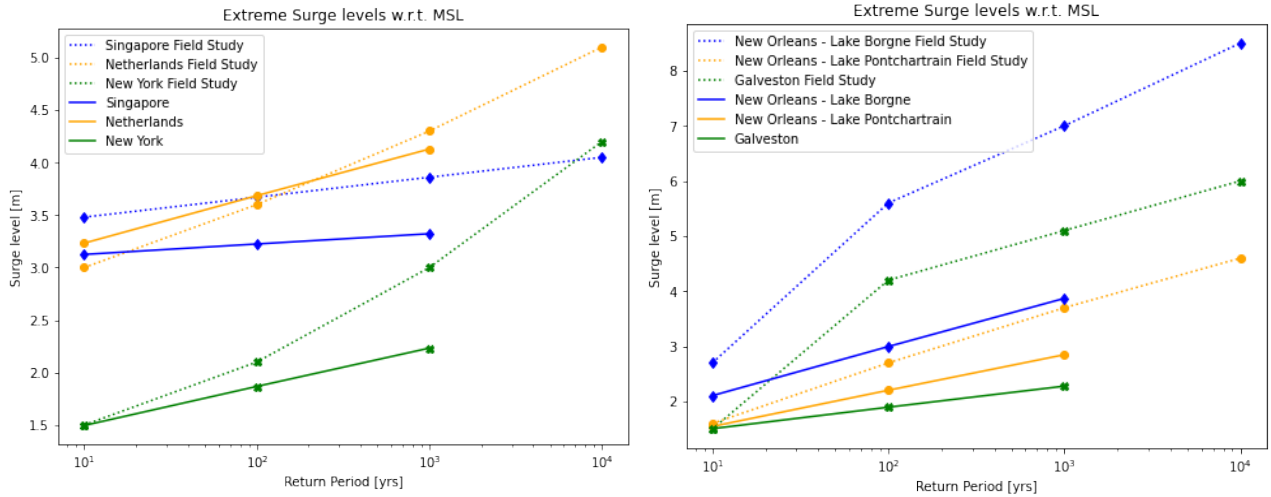
Figure 7.5: *Surge levels obtained from data points and interpolated via the nearest neighbour principle to the hotspots (Muis et al., 2020) compared to the surge levels obtained from several case studies.*

It is seen that for certain locations like New York, Singapore and the Netherlands, the storm surge levels compare relatively well. Whereas in other locations such as New Orleans and Galveston, the predictions differ significantly. A reason could be that in New Orleans, at Lake Borgne and Pontchartrain, the obtained values from the data point (red cross in Figure 7.4a) are located far away from the hotspots in Lake Borgne and Pontchartrain. Next to this, amplifying effects due to the shallow water areas could occur, resulting in local intensified storm surge. For the studies done near Singapore, New York and the Netherlands, the data points are located close to the case study locations, which might be one of the reasons for the better match (Figure 7.4b). Apart from this, the data provided by Muis et al. (2020) is based on a Global Tide and Surge model, whereas the data from the field studies contains more detailed information supplied by for example NOAA[1].

7.5   Nearshore wave height comparison bare foreshore (SwanOne)

In order to check whether the computed nearshore waves in this research are reasonable the program SwanOne is used. SwanOne computes the propagation of waves offshore towards nearshore by using short-crested wind-generated waves. It assumed parallel depth contours and performs a fully 2-D calculation, such that it includes refraction and directional spreading.

For the first check, five SWAN runs are performed for five different foreshore slopes for which all of them are taken as a constant slope extending 10 km offshore (left Figure 7.6). It is seen that for slopes in the order of $\frac{1}{100}$ the nearshore wave heights computed with SwanOne are very similar to the ones computed with the model (Equation 3.4). For more steep slopes in the order of $\frac{1}{10}$ and more gentle slopes in the order of $\frac{1}{1000}$ the deviation is larger but still reasonable as the difference does not exceed 50%.

---

[1]https://www.noaa.gov/
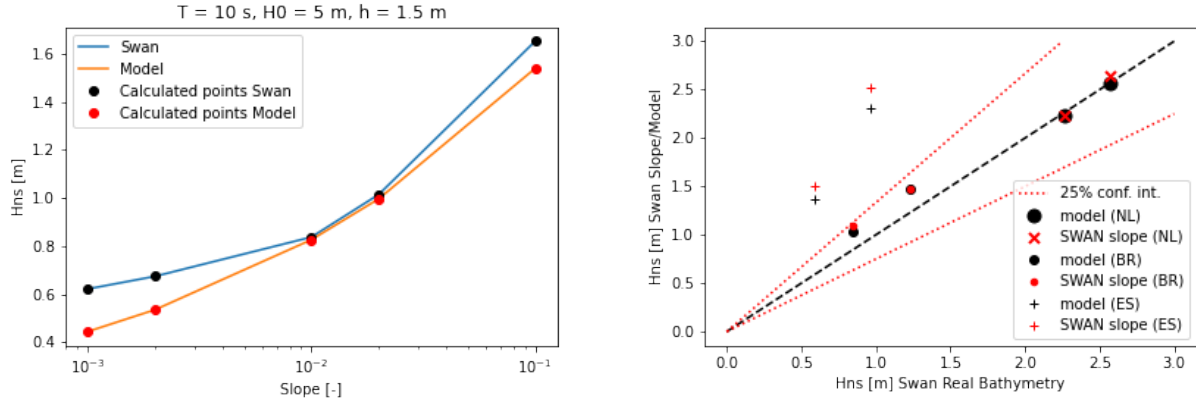
Figure 7.6: *Comparison between nearshore wave heights computed with SwanOne and with the model (left Figure). Comparison between the nearshore wave height computed with the "exact" bathymetry derived from sea maps and the slope approach from Athanasiou et al. (2019).*

For the second check three locations are chosen for which the foreshore slope used in the global study (Athanasiou et al., 2019) deviates slightly, moderately and largely from the "exact" bathymetry measured in these locations (Figure 7.7). The "exact" bathymetry is derived from coastal sea-maps used for ships and is determined for a cross-shore transect extending 10 km from the coastline.
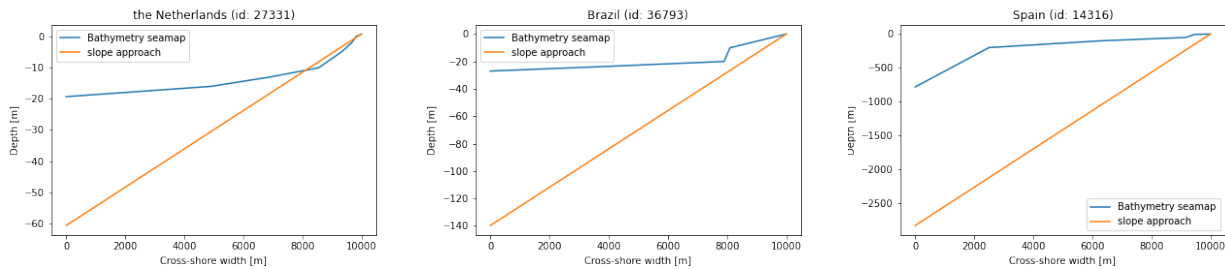
Figure 7.7: *Foreshore profile for the locations in the Netherlands, Brazil and Spain for the "exact" bathymetry (blue line) and the slope approach (orange line).*

For each of these locations in the Netherlands, Brazil and Spain, two SwanOne runs are performed for offshore wave heights of 5 and 7 m, corresponding with wave periods of respectively 10 and 12 s. The same input values are used for the model with a constant slope (Athanasiou et al., 2019) also extending 10 km offshore.

Right Figure 7.6 shows that for the Netherlands the SwanOne as well as the model computes similar nearshore wave heights for the "exact" bathymetry as for the slope approach for the two different wave heights and periods. For Brazil the nearshore wave heights computed with the slope approach are larger than with the "exact" bathymetry. Lastly, for the location in Spain the computed nearshore wave heights show a larger overestimation for the slope approach.

These results can be explained by looking at Figure 7.7. The left Figure shows the "exact" bathymetry and the slope approach for the Netherlands. Since the first 2 km of both approaches show a good match and this is the part of the foreshore where wave breaking takes place the two approaches produce similar results. However, for Brazil (middle Figure 7.7) and especially Spain (right Figure 7.7) the bathymetries deviate much more, thus resulting in different nearshore wave heights. Concluding, the foreshore slope is an important parameter as it influences the nearshore wave heights heavily. If the slope deviates largely from the exact bathymetry in the shallow foreshore the computed wave heights also show a large deviation.

8 | Generic sensitivity analysis

This chapter presents a generic sensitivity analysis of the parameters used in the global approach for all hotspots. Section 8.1 present the sensitivity of the parameters; wave period (T), design water level (DWL), foreshore slope, offshore wave height (H_0) and mangrove and coral width towards the influence on costs. Section 8.2 present the sensitivity of the wave attenuation rates of mangroves.

8.1 Influence on dike investment costs

For all hotspots considered in this research a sensitivity analysis is performed for the parameters that influence the dike raising costs. In this analysis the parameters; wave period (T), design water level (DWL), foreshore slope, offshore wave height (H_0), mangrove and coral width are changed with the same percentages. The cost-calculations of raising dikes are redone for an increase of 10% and 25% and a reduction of 10% and 25% of the aforementioned parameters. In Figure 8.1 the results are given for approach $C_{new,slr}$ (increasing protection standard taking into account SLR), for an increase respectively decrease of 25% of the parameters.
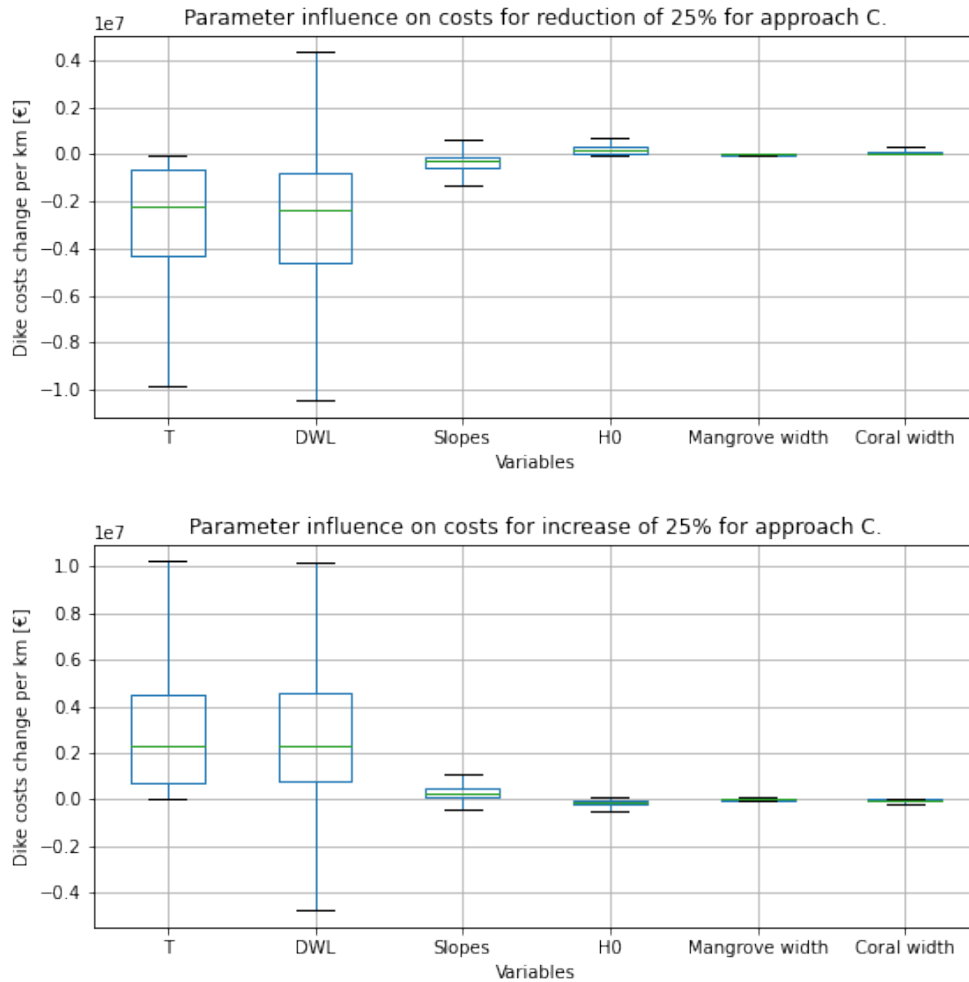
Figure 8.1: *Influence on the dike raising costs per km of coastline for a change of 25% of the parameters for approach $C_{new,slr}$ (green lines denote the median values).*

It is seen that the wave period and the DWL (Intermezzo 8.1) are the most influential parameters. An increase of 25% of the wave period and DWL result in a median dike cost increase per km of coastline of 2.2 Million Euros.

Intermezzo 4.3: Design Water Level data-set

In Figure 8.2a the full spectrum of changes in dike costs per km of coastline are presented for changing the design water level (DWL) by -25%, -10%, 10% and 25% following approach $C_{new,slr}$. By reducing the DWL by 25%, for most hotspots the dike costs reduce by around 15 to 20%. It is observed that there is a larger spread in deviation for a larger change of the DWL, as for an increase of 10% the histogram is more narrow. Figure 8.2b shows the shift of the dike raising cost histogram for all hotspots for an increase of the DWL of 25%. The histograms shifts to the right, meaning that the dike costs increase.
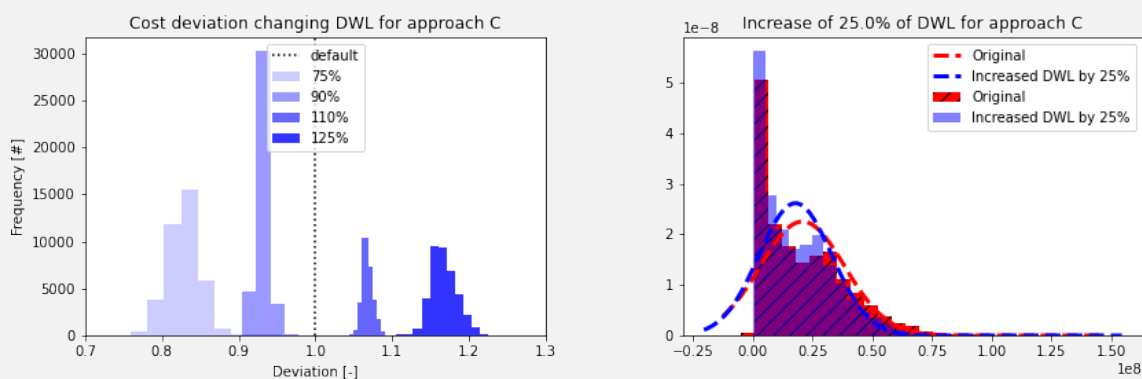
(a) *Deviated divided by the original dike costs.*   (b) *Shift in dike costs.*

For the DWL all the original values are depicted in Figure 8.3a & 8.3b. Depending on the original value, a change of for example 25% has relatively a larger effect on higher values located in the tail of the marginal distribution. Combined with the other variables that differ per hotspot location this results in the variation seen in Figure 8.2a.
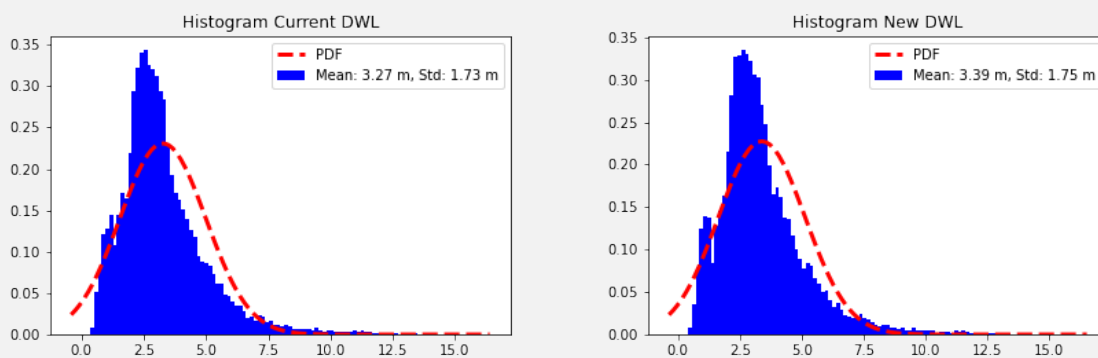
(a) *DWL for current protection standard.*   (b) *DWL for new protection standard (excluding SLR).*

The offshore wave height does not seem to influence the dike costs as the depth-limited breaking is normative in the shallow water regime. This means that higher offshore waves do not necessarily result in higher nearshore waves since these waves have started breaking earlier as they feel the ground earlier. Interestingly changing the width of the mangroves and corals barely influence the results. If the mangrove/coral widths or the

offshore wave heights are reduced, consequently the costs increase in contrast to the other parameters. For the mangrove and coral widths this a logical result as the amount of wave attenuation decreases and hence the run-up increases if less vegetation is present at the foreshore. However, for the offshore wave height, one would expect the costs to reduce if the offshore wave heights are reduced. The answer lies in the wave breaking characteristics, if **only** the offshore wave height is reduced following equation 3.3, the Iribarren parameter increases and as a result the breaker parameter then increases as well (equation 3.4). In practise this means that the wave breaking height increases and thus higher nearshore wave heights are expected to occur. This explains the increase of costs for reducing only the offshore wave heights (assuming the wave length/period remaining the same which in reality they do not).

8.2 Mangrove wave attenuation sensitivity

The wave attenuation can be expressed in a wave reduction per unit length in the direction of the wave propagation denoted by the wave attenuation factor (r). Multiple studies have calculated this factor r based on their field data. The factor r is calculated with Equation 8.1 (Mazda et al., 2006).

$$r = -\frac{\Delta H}{H} * \frac{1}{\Delta x} \ [m^{-1}] \tag{8.1}$$

Where:

- H is the wave height at the start of the mangrove forest [m].

- ΔH is the decrease in wave height between the start and the end of the mangrove forest [m].

- Δx is the width of the mangrove forest [m].

For all hotspots the wave attenuation factors are calculated using Equation 8.1 (Mazda et al., 2006). The results are shown in Figure 8.4 for the current protection standard with and without SLR. The mean value of all calculations are respectively 0.0025 /m and 0.0022 /m. This corresponds reasonably well with the field studies as seen in Table 8.1. Looking at Figure 8.4 no outliers are found, hence for all hotspots the resulting wave attenuation rates include reasonable estimates.
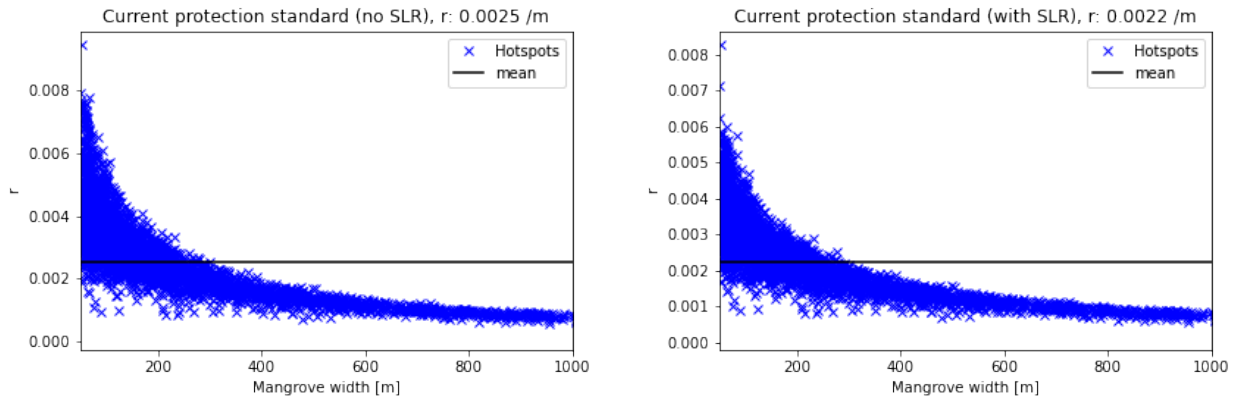
Figure 8.4: *Wave attenuation factors calculated using Equation 8.1 for the current protection standard without SLR (left Figure) and with SLR (right Figure).*

Source	Wave attenuation rate (r) [/m]
Mazda et al. (2006)	0.001 - 0.006
Bao (2011)	0.0055 - 0.01
Horstman et al. (2014)	0.0024 - 0.061
Quartel et al. (2007)	0.0005 - 0.012

Table 8.1: *Wave attenuation rates from field studies.*

It is seen in Figure 8.4 that the wave attenuation rates decrease with increasing mangrove widths. According to the empirical/model approach the mangrove forests are most effective in the first 100s of metres of the mangrove belt. This is also concluded in earlier studies such as Menéndez et al. (2020).

A big limitation for applying the method is choosing the vegetation density and size. It is investigated what influence changing the physical parameters of mangroves have on the resulting wave attenuation rate. To see the influence that the physical parameters have, the parameters C_d, b_v, N and h_v are altered by a factor 1.5 (Figure 8.5) and a factor 0.5 (Figure 8.6). If the physical parameters are increased by 50%, the mangrove characteristics are such that the trees are wider, taller, their drag is larger and more trees occur per square metre. As a result it is seen that the wave attenuation rate increases with approximately a factor of 2. If the parameters are decrease by a factor of 0.5, the resulting wave attenuation rates are found to be reduced by $\frac{2}{3}$. Concluding, the physical characteristics are a important factor in determining the wave attenuation rates via this empirical approach.

Figures 8.4-8.6 also show that when SLR is taken into account the wave attenuation rates decrease. The water depth at the foreshore increases when SLR is taken into account. As a result the relative vegetation height (ratio of vegetation height over average water depth) decreases as well as the shoaling factor governed by Green's law. Which together account for the decrease in wave attenuation that is observed.
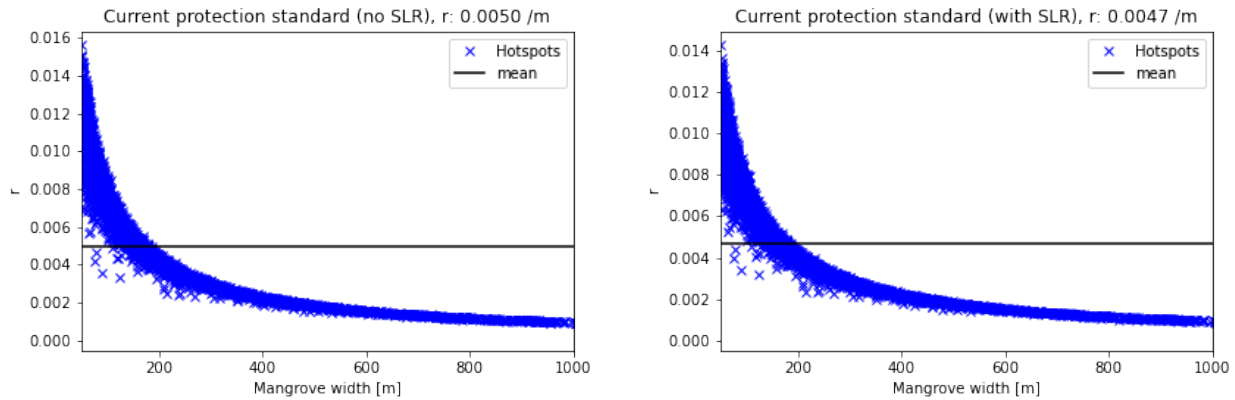
Figure 8.5: *Wave attenuation factors calculated using Equation 8.1 for the current protection standard without SLR (left Figure) and with SLR (right Figure) by increasing the physical parameters by a factor 1.5.*
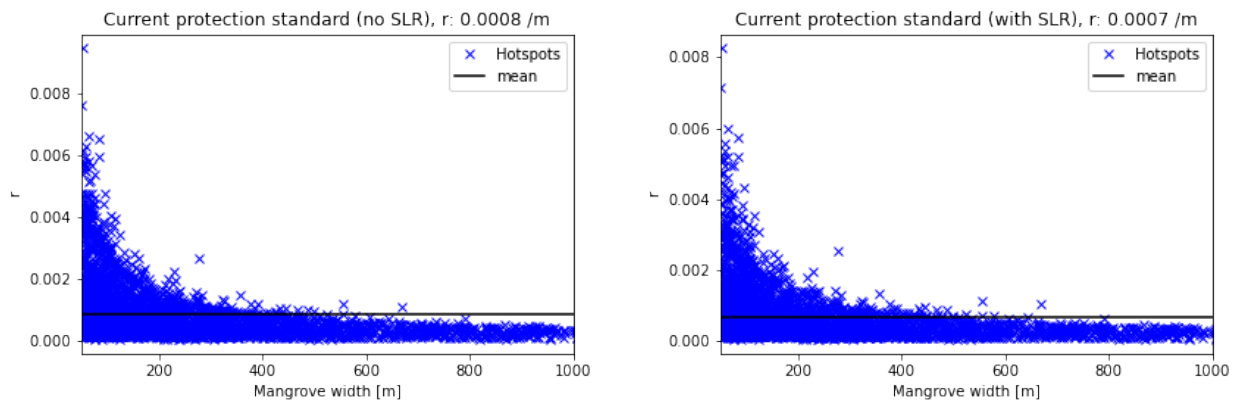
Figure 8.6: *Wave attenuation factors calculated using Equation 8.1 for the current protection standard without SLR (left Figure) and with SLR (right Figure) by decreasing the physical parameters by a factor 0.5.*

Part III

Interpretation

9 | Discussion and recommendations

This thesis presents a global method that identifies potential locations where nature-based solutions (NBS) can be applied in a cost-effective manner. The individual components that are included in this method can be improved further, such that currently the global results should be treated as a first indication of potential sites. This is due to the habitat identification, cost and benefit calculations that are inherently limited by several simplifying assumptions and by the lack of high resolution local data.

Firstly the limitations and recommendations of the most influential data sets are discussed, which involve the design water level, wave period and the slope of the foreshore. Secondly, the limitations and recommendations considering the applied method and formulas are discussed that involve the mangrove and coral reef applicability thresholds and wave attenuation formulas. Thereafter, uncertainties regarding the current protection standards, land subsidence, extent of the vegetation, additional benefits, flood risk, cross-shore configuration and efficacy of NBS are discussed. Lastly, other NBS are mentioned that can also be included within the method during future research.

9.1 Limitations of the screening method

9.1.1 Limitations on the data sets

The data sets used in this work were limited by the global scope of this research, for which it is difficult to precisely predict parameters on a detailed local scale. Therefore, local case studies are investigated to compare the global results with the more detailed local results. The most important limitations surround the most influential parameters. According to our generic sensitivity analysis of the input parameters of the screening method, the model was most sensitive to the design water level (DWL) and wave period; a 25% increase of the DWL or wave period increased the median dike investment costs per km of coastline by \$2.2 million. The potential inaccuracies for these variables are thus discussed below including also the slope of the foreshore.

Design water level

The DWL consists of multiple components such as storm surge, high tide, mean dynamic ocean topography (MDOT), wave setup and sea level rise (SLR). These components are summed by taking into account their respective return periods. However, the combination of these parameters will have a higher return period, since the combination of storm surge, high tide and wave setup occurring at the same time will result in a lower probability of occurrence if they are not fully correlated. By assuming that extreme storm surge occurs together with high tide is therefore conservative. Next to this, the effect of climate change could intensify the hydraulic boundary conditions even more than currently expected, such that the joint probability of occurrence increases.

- **Storm surge:** The global storm surge values from Muis et al. (2020) used in this research deviate between 0-38% from values projected in local case studies, if the location where the global storm surge data is extracted from is located close to the hotspots. If the location is further away however and amplifying effects start playing a role the predicted storm surge of Muis et al. (2020) can differ significantly (27-79%) from the projected values in local case studies.

- **High tide:** The local high tide is now solely based on the tidal constituents M2 and S2, where in reality extra constituents could occur that can also be mainly diurnal as is the case for the eastern coasts of South-East Asia.

- **Wave setup:** The wave setup is determined based on an empirical model that assumes a constant bed slope. As a result, depending on the foreshore characteristics, the actual values might differ significantly. Next to this, in this research the wave setup is only used for a return period of 100 years, even if the protection standard is five years, which leads to conservative wave setups.

- **SLR:** The local SLR is taken from Pörtner et al. (2019) based on RCP8.5 scenario for the year 2090. In practice, a different scenario could be followed over the 21st century or the predictions might have to be altered as more intense observations could be done over time.

For the extreme sea levels (DWLs), a large improvement would be to include the components like storm surge, high tide, mean dynamic ocean topography (MDOT), wave setup and sea level rise (SLR) and perform a combined extreme value analysis. This way a summation of these components with their own respective return periods does not lead to conservative results.

Wave period

The wave period corresponding to the wave at the foot of the dike influences the breaker height and the dike run-up significantly. In this research, the wave periods are not estimated based on an extreme value analysis, but rather one fixed value of 10 s is used for all nearshore waves. This means that at locations where in reality shorter waves occur, the produced results are conservative, whereas in other areas, the calculated run-ups might be too low as in practice longer waves occur. As an example locations on the east coast of Indonesia experience smaller wave periods than on the west coast. The wave periods in the east are in practise around 5-11 s, whereas in the west they are around 13-17 s. For a location on the east coast, the run-up for the new protection standard including SLR was measured to be 6.3 m by using the fixed wave period of 10 s. If a wave period was chosen more in the direction of the actual wave periods occurring at the site such as for example 7.5 s, the design run-up is reduced to 5.2 m. For a location on the west coast, the run-up was measured to be 7.1 m for a period of 10 s. If a wave period of 12.5 s is used, the run-up increases to 9.2 m.

If the wave period is estimated for different return periods, more accurate predictions of the breaker height and dike run-up can be obtained by performing an extreme value analysis on the ERA5 data set, which provides wave periods on a global scale from 1979 until present.

Foreshore slope

The slope of the foreshore is now based on cross-shore transects discussed in Athanasiou et al. (2019). Within the hotspots, multiple cross-shore transects are found, such that it is chosen to use the median slope of all the transects located within a hotspot. In some cases however, the values that are found provide unrealistically high slopes as a result of for example shipping canals that can include 45° slopes. In those cases the minimum value of the slope transects within a hotspots is used. When comparing the determined slopes from this approach with the actual foreshore (extracted from coastal navigation maps used for ships) at the hotspots, it is seen that in some cases there is still a significant difference in the slope values. If the foreshore slopes from the model for the first 2 km measured from the toe of the dike at a certain hotspot are significantly steeper than reality, consequently the computed nearshore wave heights are higher as well. In those cases it is determined that the computed wave height can be overestimated by up to 2.5 times the expected nearshore wave height for the actual foreshore.

9.1.2 Limitations on the formulas/methods

Other limitations include the identification of potential mangrove and/or coral restoration sites due to a lack of global data for local ecosystem requirements and the mangrove and coral wave attenuation magnitudes. Below, the implications are discussed in more detail.

Mangrove and coral reef applicability

For mangroves and corals, a range of biological, chemical and physical parameters must be considered in order to successfully integrate and enable functioning of habitats. Since this research involves a global approach, some of these parameters cannot be included here due to a lack of data availability. As a result there can be locations where according to the thresholds in this research, the potential to apply mangroves or corals is found. But if closer inspection would be performed at these locations, one might find that this is untrue due to for example the local hydrodynamics/morphology that were not able to be captured on a global scale. For

both mangroves and coral reefs, the applied thresholds could be improved by taking into account more requirements. In order to achieve this, extra global layers can be added, which are explained in more detail below.

To sustain mangroves, freshwater input is required that can be provided by precipitation and/or runoff. If the location receives large amounts of precipitation and the coastline's geometry provides for large enough retention times of the fresh water, the site could be suitable for mangroves. By including a global map that produces the sea surface salinity of the nearshore, it can tell us whether freshwater input is provided. Another threshold that can be included is the soil type. Mangroves typically flourish in muddy environments, which in general means that non-muddy coasts experience too high hydrodynamic energy. However, in this research it is chosen to not include this threshold as in practise there are plenty of sites where mangroves are present in sandy foreshores. Other thresholds that could be included in further research involve the redox potential[1] of water, which should be between -400 mV and 150 mV, sedimentation rates, pollution and the wave energy that cannot be too high. It should be considered for the threshold including the latitudinal limits of mangroves that due to climate change, these limits could change, such that mangroves are able to grow further North or South. For future notice, it should be considered that mangrove conservation or restoration is found to be effective up to 1 cm/year of SLR and is limited by the climate-induced ocean warming (max 2°C) and acidification (Pörtner et al., 2019).

For corals, a threshold that can be included is the suspended solids concentration near the coast. If the concentration is too high, consequently the light does not penetrate the water column sufficiently to reach the corals, which would result in coral degradation. Other thresholds include the requirement for a bare hard substratum, sedimentation rates, pollution and the availability of larvea. It should be considered that due to ocean warming, coral reef degradation (bleaching) can occur (Heron et al., 2016). Coral conservation or restoration is found to be effective up to 0.5 cm/year of SLR and is limited by the climate-induced ocean warming (max 2°C) and acidification (Pörtner et al., 2019).

Wave attenuation mangroves

The wave attenuation of mangroves is approximated by an empirical approach discussed in Mendez & Losada (2004). Multiple physical characteristics of mangroves are included, such as the number of trees per square metre, width of the tree trunk and tree height. When the local bathymetry and physical parameters of the field studies are used, the empirical formula produces similar wave attenuation results.

Within this research based on local case studies and Janssen (2016), the parameters are selected such that they produce results that correspond to the obtained wave attenuation observed in field studies. In practice, however, the physical characteristics of mangroves vary over the world as there are many different species. Currently there is no global database that includes which species live where, such that a more detailed approach with the local mangrove characteristics is not possible. As a result the wave attenuation can be over-predicted in locations where the mangrove trees are smaller than the global parameters used, or under-predicted in location with larger trees. Next to this, the physical parameters used in this research assume that the trees are fully grown, such that the tree height is 2 m for example. If mangroves are restored however, the trees still have to grow, thus the first years after restoration the wave attenuation effect is minimal. Next to this, during storm conditions like cyclones, mangroves can break, such that the wave attenuation effect vanishes.

If on a global scale, the distribution of mangrove species and their properties would be mapped, more accurate predictions of the physical characteristics of the trees could be done. As a result, the calculated wave attenuation rates from the empirical approach can be improved. Next to this, a large improvement would be to map the bathymetry of the foreshore in more detail, which companies such as Deltares have started doing. As within this research, the bathymetry of the foreshore in combination with the local tide determines to what extend mangroves can be restored. This way more accurate predictions of the maximum mangrove width can be done, increasing the accuracy of the wave attenuation predictions.

---

[1]A measure of the oxidising or reducing potential of a water body.

Wave attenuation corals

The wave attenuation of corals is based on an empirical approach from Ferrario et al. (2014), who conducted different experiments on coral reef flats, which occur at Fringing reefs. They measured the incident wave height and the wave height at the end of the coral reef and calculated the observed wave attenuation rates. As there is no global database available that gives the types of coral reefs occurring at different locations, it is assumed for the wave attenuation calculation that all reefs are of the Fringing type. In reality however, there are also different types of coral reefs, such as Barrier reefs, Platform reefs and Atolls, for which the wave attenuation rates can differ as their respective geometry varies from each other.

The empirical formula does not include the water depth, such that if high extreme sea levels occur, it could be the case that the actual wave attenuation is lower than determined by the empirical approach. It is seen that if the empirical approach is applied on field studies that the wave attenuation is underestimated by the empirical approach compared to the observed wave attenuation in the field study. Hence, the wave attenuation rates of corals used in this research might be conservative.

Currently there is a lack of approaches available, which can accurately describe the wave attenuation caused by corals. It would be a huge improvement, if the different types of coral reefs, such as Fringing reefs, Platform reefs, Atolls and Barrier reefs are mapped on a global scale, in combination with the depth profiles. One can then start developing approaches specific to the different types of coral reefs and such calculate the wave attenuation in more detail.

9.1.3   Unexplored uncertainties

This research also involves unexplored uncertainties considering the current protection standards, vegetation widths, additional benefits and slope of the foreshore. For these uncertainties the magnitudes by which they influence the results are not determined. However, they are expected to be important, which is why future work should focus on improving these data sets.

Current protection standards

The protection standards for the current situation of the coastal defences are taken from the FLOPROS database (Scussolini et al., 2016) and connected to the different hotspots. This should be seen as a first order estimate as the database involves modelling for locations where there is no local data available of the coastal defence. Moreover, if the infrastructure is damaged, insufficient maintenance is performed or the plans were actually not executed, the level of protection might be lower. Next to this, it is assumed that for each location the protection standard corresponds to a dike system or a dike system in combination with mangroves/corals. In practise, the protection standard might be based on different coastal defence systems such as sea walls, breakwaters or revetments.

If globally more detailed information would be available to map the current flood protections more accurately, the resulting predictions for flood risk and investment costs can be improved significantly. One could improve the database by using Earth Observation based methods to map flood protections globally. This way, a distinction for the different flood protections types can be made, as now it is assumed that all current protections are provided by dike systems, which in reality is not the case.

Land subsidence

Land subsidence is not taken into account in this research as there is no global data set available with predicted land subsidence rates. For future predictions, it is very important that such a data set will be available, as it involves a highly influential parameter that can be an order of magnitude larger (see Appendix C.3) than the local sea level rise at a hotspot. Land subsidence increases the flood risk in coastal areas, as the low-lying areas become even lower. There are multiple anthropogenic causes for land subsidence, but groundwater depletion is one of the main constituents. In the coming decades due to an increase in global population and economic growth the demand for groundwater increases. This will result in more groundwater depletion as periods of prolonged droughts occur, which according to Herrera-García et al. (2021) can increase land subsidence further.

As part of possible solutions, land subsidence policy could/should be included with monitoring and modelling of exposed areas. Measures should be considered, that include groundwater regulation, enhancement of recharging of the aquifers or alternative water supplies.

Extent of the vegetated foreshore

The width of coral reefs and mangrove forests at each location is based on the area of corals/mangroves at the hotspot and the size of the hotspot. This means that, if at a certain hotspot a certain area is found, this does not necessarily mean that they are distributed evenly over the coastline. As a result, the coral/mangrove widths should not be seen as an exact value, but rather an indication of the local extent of these ecosystems.

Additional benefits

The additional benefits that mangroves and corals provide are not scaled on GDP as no correlation is found between the GDP per capita and the additional benefits that corals/mangroves provide at different locations. This seems to be a result of a lack in number of quantitative studies and of different valuation methods that the different case studies use. It is expected that there is a relation between GDP and additional benefits, but for now this relation cannot be used yet. As a result, in developing countries the benefits that are determined could be higher than in practice is expected.

To gain better understanding of the additional benefits that ecosystems provide, more local cases should be investigated, where the aim should be to use similar valuation methods. Currently, there is a big difference between the methods used to determine monetary values that ecosystems provide, which causes partly the large difference in obtained values. Next to this, the number of studies should be increased to produce more accurate estimates.

Flood risk

To calculate the flood risk, the bathtub approach is used, in which all land below a certain flood level is considered to be flooded. This assumption leads to an overestimation as in reality not all the land would instantly be flooded. The flood risk benefits can be improved by considering a different approach to model the amount of land being flooded. Tiggeloven et al. (2020) for example included resistance factors to simulate the reduction of flooding land inwards.

Next to this, the flood risk in terms of monetary values is based on the amount of people being flooded following Hinkel et al. (2014), that uses the sub-national GDP per capita to convert the expected annual number of people (EAP) being flooded to the damage. In reality, the monetary value of assets at risk could differ significantly between areas with similar GDP per capita. By directly calculating the damage to assets instead of a conversion of the expected people being flooded towards assets, these calculations can be improved.

For the Digital Elevation Model that is used, there is no clear distinction between the Digital Terrain Models and Digital Surface Models, such that objects like buildings are included in mapping of elevations, generally leading to an underestimation of flooding. The flood calculations are performed on the hotspots consisting of polygons with sizes of approximately 10x10 km^2. However, in practise for some locations the hinterland behind this polygon could also be flooded if it includes low-lying land. These areas are not considered when calculating the amount of people being flooded, which can lead to an underestimation of the EAP. One can take into account the hinterland behind a hotspot to approximate more accurately the total amount of people being flooded for a storm event for a certain stretch of coastline.

Flooding occurs when the dike fails and here it is assumed that the dike only fails if the extreme sea levels combined with the wave run-up exceed the crest height of the dike. In reality, many failure mechanisms can occur that cause dike failure at an earlier stage, for less intense storms. An improvement would be to include some of the major dike failure mechanisms such as piping or sliding on a global scale.

Cross-shore configuration

The cross-shore configuration is fixed in this model, where the foot of the dike is assumed to be located at high tide, which in reality is not always the case. If in practise the coastal protection is located higher in the foreshore, the water depth at the foot of the dike will be smaller. The maximum wave height and run-up will then be smaller as well, resulting in a lower crest height that is required to meet the protection standard. Hence, depending on the actual location of the coastal protection at the different hotspots, the resulting crest height required to meet the protection standard might be over- or underestimated.

Efficacy of nature-based solutions

It is important to determine the efficacy of nature-based solutions compared to traditional hard coastal structures, in order to successfully promote sustainable solutions on their defensive aspect (Morris et al., 2018). Looking towards an increasingly uncertain future, more research on the efficacy must happen to reduce the vulnerability of low-lying coastal regions.

Including other nature-based solutions

In this research, only mangroves and coral reefs are taken into account. One could also look at other NBS such as salt marshes, sea grasses and oyster reefs. By implementing these NBS, there could also be possible business-cases arising in higher or lower latitudes, as salt marshes for example can sustain in colder climates. This way the screening method can be applied outside of the tropical and sub-tropical regions as well.

10 | Conclusion

10.1 Answering the research questions

The following sub-questions combined provide a framework that answers the main question; "***How can the flood risk reduction potential of various solutions be assessed at a global scale?***".

1. Which nature-based solutions can be applied at all global coastal hotspots based on the local environment?

Globally 54.6% of the 38,773 investigated coastal hotspots were found suitable for either mangrove and/or coral restoration, which amounts to 21,182 identified potential sites (Table 10.1). It must be noted that in this research only the possibilities of applying mangroves and corals is considered. For these sites, it should be further investigated whether in practice restoration could take place, as the local hydrodynamics/morphodynamics are difficult to capture on a global scale.

Out of these potential sites there are 12,571 locations with potential to restore mangroves, however in 48% of these locations the coastline is retreating (15.6% of total). In order to enable mangrove restoration, here mitigation measures such as nourishments or bamboo structures are required to combat the local erosion or land subsidence problems. Retreating coastlines are often caused by local sea level rise (SLR) in combination with land subsidence. Consequently the coastal flood risk at these locations increases rapidly as well. Hence, these can still be potential business cases for companies such as Van Oord to apply NBS for coastal protection. 1,759 of these 12,571 potential mangrove restoration locations are newly identified, meaning that there are currently no mangroves present. Coral potential is found for 19,904 of the 21,182 identified potential sites. For 11,036 of these locations, they are newly identified, such that there are no corals currently present.

NBS	Total restoration potential	Newly identified
Mangroves	12,571 hotspots (32.4%)	1,759 hotspots (4.5%)
Mangroves with erosion	6,034 hotspots (15.6%)	869 hotspots (2.2%)
Corals	19,904 hotspots (51.3%)	11,036 hotspots (28.5%)
Mangroves and/or corals	21,182 hotspots (54.6%)	12,028 hotspots (31.0%)
Total coastal hotspots	38,773 hotspots (100%)	38,773 hotspots (100%)

Table 10.1: *Number of hotspots where potential is found to apply mangroves, corals or both. The column newly identified, gives the number of hotspots where currently no mangroves or corals are present, but mangrove or coral potential is found. The percentages are given with respect to the total amount of investigated hotspots.*

2. What are the global total investment costs for improving the protection standard with or without coral and/or mangrove restoration?

The global total dike investment costs (not considering NBS) required to improve the protection standard of the current coastal defence for the 38,773 coastal hotspots amounts to \$390-\$2,288 billion, depending on the adaptation strategy. Where the calculations for the lower bound do not take into account SLR ($\boldsymbol{B_{new}}$[1]) in contrast to the upper bound ($\boldsymbol{C_{new,slr}}$). The spread in results is thus caused by the predicted local SLR as it contributes heavily to the increased extreme sea levels and run-up (higher waves possible) and consequently the required amount of dike heightening. Hinkel et al. (2014) estimated the global costs of protecting the coast with dikes at \$1,900-\$4,200 billion for SLR scenario RCP8.5 in the 21st century, which are of the same order of magnitude as the upper bound that includes SLR.

---

[1]$\boldsymbol{A_{cur,slr}}$: Keep protection standard constant, take into account SLR. $\boldsymbol{B_{new}}$: Increase protection standard to fixed new standard, not taking into account SLR. $\boldsymbol{C_{new,slr}}$: Increase protection standard to fixed new standard taking into account SLR.

If NBS such as mangroves and corals are also considered at the 21,182 identified potential sites, a total reduction in investment costs of \$4.3-\$54.7 billion (1-2% of total) is found for 2,275-5,858 of these sites combined. NBS add additional wave attenuation (Vuik et al., 2018; van Wesenbeeck et al., 2017). Depending on the characteristics of the vegetation, the wave height at the toe of the dike and the corresponding run-up can be reduced. This can result in a lower crest height required to reach the same protection standard and hence a reduction in investment costs. For the identified potential sites, a more in-depth site investigation may be worth-wile, as it involves a potential reduction in investment costs per kilometer of coastline of \$0.56-\$2.34 million. If SLR is taken into account, the reduction in costs that can be achieved by applying mangroves and/or corals increases with a mean value of \$1.78 million/km (\$2.34-0.56 million/km). With ongoing climate change and the corresponding SLR, the use of nature-based solutions such as mangroves and corals will thus become more cost-effective compared to traditional grey infrastructure such as dikes.

Strategy	Global total dike investment costs	Global total dike investment costs including NBS	Total reduction	Locations	Mean reduction
$A_{cur,slr}$	\$1,927 billion	\$1,877 billion	\$50.0 billion	5,722 hotspots	\$2.18 M/km
B_{new}	\$ 390 billion	\$ 385 billion	\$ 4.3 billion	2,275 hotspots	\$0.56 M/km
$C_{new,slr}$	\$2,288 billion	\$2,233 billion	\$54.7 billion	5,858 hotspots	\$2.34 M/km

Table 10.2: *Global total dike investment costs, global total investment costs including dike heightening and mangrove/coral restoration and global total reduction in investment costs due to mangrove/coral restoration. The column with locations shows the number of hotspots where a reduction in costs is achieved and the corresponding global mean reduction in cost per kilometer of coastline is given in the last column.*

3. What are the global total flood risk reduction benefits of improving the protection standard?

If the protection standard is kept constant with either defence approach 1 (dike heightening) or 2 (dike heightening + restoring mangroves/corals), for the predicted local SLR at the end of the 21st century, there is a global total increase in risk of \$35.3 billion/yr. SLR increases the extreme sea levels and in order to meet the same protection standard, the coastal defence must be improved. Storm events that occur for the same protection standard at the end of the 21st century are more intense. If flooding then occurs, the consequences are larger, which explains the increase in risk even if the protection standard is kept constant.

By improving the protection standard with either defence approach 1 or 2, a global reduction in flood risk of \$76.5-\$82.6 billion/yr is achieved at the end of the 21st century. If the protection standard is improved, the yearly risk is reduced as some events that caused flooding for the original standard do not result in flooding for the improved protection standard. In some locations still an increase in risk was found as the local sea level rise contributed more to an increase in risk than the protection standard improvement contributed to a reduction of risk. This means that if at a certain location the predicted local SLR (and land subsidence) is large, one should consider increasing the protection standard more.

In order to compare the global total investment costs with the global total obtained risk reduction, the yearly change in risk is transformed into a Net Present Value (NPV). It is then seen that on a global scale the dike investment costs (-\$2,288 billion) are larger than the corresponding flood risk reduction benefits (+\$1,529 billion) if SLR is taken into account. This is because, for many of these locations there are no people and consequently assets located in the hinterland, resulting in very few to none flood risk reduction benefits. In the last step (question 10.1), the optimal protection standard is calculated, such that for these locations the model advises to maintain the current protection standard.

Strategy	Total yearly change in risk	Total change in risk (NPV)
$A_{cur,slr}$	−$35.3 billion/yr	−$ 706 billion
B_{new}	+$82.6 billion/yr	+$1,651 billion
$C_{new,slr}$	+$76.5 billion/yr	+$1,529 billion

Table 10.3: *Global total risk reduction/increase between the current and new situation and its corresponding NPV. The symbol (+) denotes a reduction in risk and (-) an increase in risk.*

4. What are the global total additional benefits connected to the restored area of mangroves and corals?

If all the restoration of mangroves and corals identified in this study for defence approach 2 would be carried out, it would create economic benefits of $270-$3,925 billion, which would not be generated by only constructing dikes. On a global scale it is suggested to restore more coral area than mangrove area, which is logical as there are 58% more locations identified with coral potential. Together with the larger ecosystem value for coral reefs from Davidson et al. (2019), the global total additional benefits that the restored area of corals provide are larger than for mangroves.

When comparing the global total additional benefits (+$3,925 billion) to the global total dike investment costs including NBS (-$2,233 billion), it is seen that the additional benefits outweigh the investment costs. However, the additional benefits should be interpreted in a different way than flood risk reduction benefits, as these additional benefits do not directly go into the wallet of an investor as they involve a common good, that have value and the investor is not necessarily the one getting the benefits. The additional benefits can help to raise awareness about the importance of ecosystem services for society. They can thus serve as a powerful communication tool to conduct more balanced decisions with regards to trade-offs including policies, which enhance the GDP but consequently damage the local ecosystem services (Costanza et al., 2014).

Strategy	Mangrove area	Coral area	Mangrove benefits	Coral benefits	Total benefits
$A_{cur,slr}$	102,054 ha	456,232 ha	$395.7 billion	$3,220 billion	$3,616 billion
B_{new}	17,218 ha	28,807 ha	$ 66.8 billion	$ 203 billion	$ 270 billion
$C_{new,slr}$	110,506 ha	495,395 ha	$428.4 billion	$3,497 billion	$3,925 billion

Table 10.4: *The first two columns show the total amount of restored mangrove and coral area for defence approach 2 following from the optimal cost calculation. The corresponding global total additional benefits due to these restored areas are shown in the subsequent columns.*

5. Based on all the benefits and costs, what are the flood risk reduction potentials of the various solutions?

Depending on the defence approach that is followed, for 7.7-22.0% of the coastal hotspots, the flood risk reduction benefits of improving the protection standard towards **a fixed new standard**, are larger than the corresponding investment costs. Hence, at these locations improving the protection standard is cost-effective. The variation in results is governed by the adaptation strategies. If namely SLR is included, the risk reduction benefits of improving the protection standard are relatively smaller and the investment costs are larger, such that the benefit-cost ratios decrease. NBS increase the amount of cost-effective locations as a result of the reduction in investment costs they provide. If next to the flood risk reduction benefits also the additional benefits are taken into account, the amount of locations increases to 20.3-24.6% of the coastal hotspots.

If the **new protection standard** is **optimized**, the number of cost-effective locations increases by 11-17% compared to the fixed new protection standard. It is found for a large amount of hotspots, that the optimal protection standard is equal to the current protection standard. For those locations, the value of the flood-prone area is very low (few to none people living there). As a result, when the protection standard is improved, the corresponding flood risk benefits are negligible. For locations where the value of the hinterland is significant, the optimal protection standard provides a more beneficial benefit-cost ratio.

The cost-effective locations mentioned above can be further investigated as potential business cases. However, defence approach 2 can also include cost-effective locations where mangrove/coral restoration is not possible, since it includes NBS based on the potential to apply them. If there is no potential found to include either mangroves or corals, solely dike heightening is taken into account and the same approach as defence approach 1 is followed for these locations. As climate change continues to impact the environment, coastal regions, especially the highly populated ones, require resilient solutions that are robust, sustainable, adaptable and economically feasible (Van Slobbe et al., 2013). Therefore, it is interesting to find locations where NBS are applicable, result in a reduction in investment costs and where the corresponding flood risk reduction benefits outweigh the investment costs, following these requirements 1,011-1,277 hotspots are found.

	Amount of hotspots where flood risk reduction benefits outweigh the investment costs		
	For fixed new standard		
Strategy	**Defence approach 1**	**Defence approach 2**	**Defence approach 2 + add. benefits**
B_{new}	8,199 hotspots (21.1%)	8,549 hotspots (22.0%)	9,527 hotspots (24.6%)
$C_{new,slr}$	2,975 hotspots (7.7%)	3,208 hotspots (8.3%)	7,888 hotspots (20.3%)
	For optimal protection standard		
B_{new}	9,361 hotspots (24.1%)	9,696 hotspots (25.0%)	11,542 hotspots (29.8%)
$C_{new,slr}$	3,356 hotspots (8.7%)	3,608 hotspots (9.3%)	8,316 hotspots (21.4%)
	Investment costs are reduced due to NBS and benefits outweigh investment costs		
Strategy	**Mangroves**	**Corals**	**Mangroves and/or Corals**
B_{new}	863 hotspots (2.2%)	649 hotspots (1.7%)	1,277 hotspots (3.3%)
$C_{new,slr}$	446 hotspots (1.2%)	836 hotspots (2.2%)	1,011 hotspots (2.6%)
Total	38,773 hotspots (100%)	38,773 hotspots (100%)	38,773 hotspots (100%)

Table 10.5: *The results are shown for improving the protection standard of the coastal defence towards a new fixed standard (first two rows) and improving towards the optimal protection standard (row 3-4). The results include the amount of hotspots where the flood risk benefits outweigh the dike investment costs (defence approach 1). Locations where the flood risk benefits outweigh the investment costs including dike heightening and coral/mangrove restoration (defence approach 2). The third column also includes additional benefits for defence approach 2. Row five and six show the number of locations where NBS reduce the investment costs and where the benefits outweigh the costs.*

Summarizing, the cost-effectiveness of mangroves and corals compared to solely dike raising depends on:

1. The investment costs for restoring mangroves and corals compared to the costs of raising the dikes.

2. The original dike height and how much mangroves and corals can influence the required amount of dike heightening by reducing the run-up for the situation with and without sea-level rise.

3. The value of the low-lying coastal region that is protected.

4. The additional benefits that mangroves and corals provide.

To decide whether nature-based solutions are a viable option compared to grey infrastructure next to these factors, research on local scale must be done whether nature-based solutions are applicable in the physical system and to what degree the ecological impact is considered.

Societal perspective of calculated values

The GDP of the Netherlands is $914 billion as of 2020 (WorldBank, 2020). The investment costs of improving the protection standard while taking into account SLR is estimated at $13.4 billion for the Netherlands, which is only 1.5% of the GDP. This can provide flood risk reduction benefits in the order of $23.3 billion. In comparison, the dutch government have spend more than $76 billion on corona measures so far.

The GDP of Indonesia is \$1,058 billion as of 2020 (WorldBank, 2020). The investment costs of improving the protection standard while taking into account SLR is estimated at \$78.2 billion for Indonesia, which is only 7.4% of the GDP. This can provide flood risk reduction benefits in the order of \$57.8 billion euros. Next to this in Indonesia, the use of NBS provides \$924.1 billion additional benefits combined for the calculated possible restored area of mangroves and corals.

10.2 Comparison with other studies of the literature

Currently global assessments have been done to evaluate different aspects touched upon in this research such as the global costs and/or benefits for dikes (Hinkel et al., 2014; Tiggeloven et al., 2020), mangroves (van Zelst, 2018; Menéndez et al., 2020; de Koning, 2021) and corals (Beck et al., 2018) all over the world, under several scenarios of SLR. Below, the contributions to the current work are discussed and portrayed in Table 10.6. More detailed information concerning the current assessments are given in Appendix A.

Contributions to current work

Increased coastal flood damage and the required adaptation to combat this problem can become one of the most costly aspects of climate change. Only few studies have assessed this impact on a global scale. Many of the studies above investigated certain dimensions of the required global adaptation. However, this study claims to have combined the state-of-the art approaches of the different dimensions conducted on this subject. It expands on the current assessments done by adding/restoring NBS such as mangroves and corals in addition to the additional benefits they provide. Next to this, it is the first study that identifies potential sites for mangrove and/or coral restoration. It also includes two different defence approaches separately and compares the results. The flood risk calculations include the current coastal protections in contrast to many existing studies. This work provides an indication of sites with high potential for NBS even if there are currently none present, which can be then investigated in a more detailed assessment. Developing systematic methodologies for identifying potential sites for NBS provides more insight into the economical benefits they yield. Combining the additional benefits of these ecosystems with their flood risk reduction, results in more resilient and sustainable protection methods against SLR.

Study	Flood risk	Current protection	Mangroves	Corals	Costs	Add. benefits	Pot. sites
Hinkel et al. (2014)	+	+	-	-	++	-	-
Tiggeloven et al. (2020)	++	++	-	-	+	-	-
van Zelst (2018)	-	+	++	-	+	-	-
de Koning (2021)	+/-	-	++	-	++	+	-
Menéndez et al. (2020)	+	-	++	-	-	-	-
Beck et al. (2018)	+	-	-	++	-	-	-
This research	+	++	+	+	++	+	+

Table 10.6: *Comparison to other studies, (-) means that the dimension is not included in the research, (+/-) means that it is included implicitly, (+) means that it is included and (++) means that it is included in more detail.*

10.3 Use of the screening method

By identifying locations where the benefits through flood risk reduction outweigh the investment costs, sites are found that can be a potential location for investing cost-effectively in the coastal defence. One can identify locations where NBS reduce the investment costs, but also locations where in addition to this, the flood risk reduction benefits outweigh the costs. For locations where NBS are a cost-effective solution more detailed assessments can be performed whether NBS can be applied here.

Part IV

Bibiliography

References

Aerts, J. C. (2018). A review of cost estimates for flood adaptation. *Water*, *10*(11), 1646.

Athanasiou, P., Dongeren, A. v., Giardino, A., Vousdoukas, M., Gaytan-Aguilar, S., & Ranasinghe, R. (2019). Global distribution of nearshore slopes with implications for coastal retreat. *Earth system science data*, *11*(4), 1515–1529.

BA, I. M., Spencer, T., French, J., Leggett, D., & Dixon, M. (2001). The sea-defence value of salt marshes: field evidence from north norfolk. *Water and Environment Journal*, *15*(2), 109–116.

Balali, S., Hoseini, S. A., Ghorbani, R., & Balali, S. (2012). Correlation of chlorophyll-a with secchi disk depth and water turbidity in the international alma gol wetland, iran. *World Journal of Fish and Marine Sciences*, *4*(5), 504–508.

Bao, T. Q. (2011). Effect of mangrove forest structures on wave attenuation in coastal vietnam. *Oceanologia*, *53*(3), 807–818.

Beck, M. W., Losada, I. J., Menéndez, P., Reguero, B. G., Díaz-Simal, P., & Fernández, F. (2018). The global flood protection savings provided by coral reefs. *Nature communications*, *9*(1), 1–9.

Bidorn, B., Sok, K., Bidorn, K., & Burnett, W. C. (2021). An analysis of the factors responsible for the shoreline retreat of the chao phraya delta (thailand). *Science of the Total Environment*, *769*, 145253.

Bouma, T. J., Van Belzen, J., Balke, T., Zhu, Z., Airoldi, L., Blight, A. J., ... others (2014). Identifying knowledge gaps hampering application of intertidal habitats in coastal protection: Opportunities & steps to take. *Coastal Engineering*, *87*, 147–157.

Burke, L., Greeenhalgh, S., Prager, D., & Cooper, E. (2008). Economic valuation of coral reefs in tobago and st. lucia. final report. *World Resources Institute, Washington DC*.

Clarke, P. J. (1993). Dispersal of grey mangrove (avicennia marina) propagules in southeastern australia. *Aquatic Botany*, *45*(2-3), 195–204.

Costanza, R., De Groot, R., Sutton, P., Van der Ploeg, S., Anderson, S. J., Kubiszewski, I., ... Turner, R. K. (2014). Changes in the global value of ecosystem services. *Global environmental change*, *26*, 152–158.

Davidson, N., Van Dam, A., Finlayson, C., & McInnes, R. (2019). Worth of wetlands revised global monetary values of coastal and inland wetland ecosystem services. *Marine and Freshwater Research*, *70*(8), 1189–1194.

De Groot, R., Brander, L., Van Der Ploeg, S., Costanza, R., Bernard, F., Braat, L., ... others (2012). Global estimates of the value of ecosystems and their services in monetary units. *Ecosystem services*, *1*(1), 50–61.

de Koning, R. (2021). Effectiveness of mangroves in flood risk reduction.

Demidov, A., Gagarin, V., & Mosharov, S. (2016). Measurement of water column primary production using photosynthesis-irradiance relations for surface phytoplankton, the vertical chlorophyll profile, and underwater light intensity. *Oceanology*, *56*(5), 637–642.

Dixon, D. J. (2011). Tidal effects on coral reefs. In D. Hopley (Ed.), *Encyclopedia of modern coral reefs: Structure, form and process* (pp. 1086–1091). Dordrecht: Springer Netherlands. Retrieved from `https://doi.org/10.1007/978-90-481-2639-2_276` doi: 10.1007/978-90-481-2639-2_276

Duo, E., Fernández-Montblanc, T., & Armaroli, C. (2020). Semi-probabilistic coastal flood impact analysis: From deterministic hazards to multi-damage model impacts. *Environment International*, *143*, 105884.

ecoshape. (2020). Facilitating coral development.

Edward., B., & Strand, I. (1997). *Valuing mangrove-fishery linkages: a case study of campeche, mexico.* University of York.

Emerton, L., & Kekulandala, B. (2002). Assessment of the economic value of muthurajawela wetland. *IUCN—The World Conservation Union, Sri Lanka Country Office and Regional Environmental Economics Programme Asia, Colombo.*

Ferrario, F., Beck, M. W., Storlazzi, C. D., Micheli, F., Shepard, C. C., & Airoldi, L. (2014). The effectiveness of coral reefs for coastal hazard risk reduction and adaptation. *Nature communications*, *5*(1), 1–9.

Giri, C., Ochieng, E., Tieszen, L. L., Zhu, Z., Singh, A., Loveland, T., . . . Duke, N. (2011). Status and distribution of mangrove forests of the world using earth observation satellite data. *Global Ecology and Biogeography*, *20*(1), 154–159.

Hendriks, J. (2014). *Wave dissipation in mangroves: Parameterization of the drag coefficient based on field data.* (Unpublished master's thesis). University of Twente.

Heron, S. F., Maynard, J. A., Van Hooidonk, R., & Eakin, C. M. (2016). Warming trends and bleaching stress of the world's coral reefs 1985–2012. *Scientific reports*, *6*(1), 1–14.

Herrera-García, G., Ezquerro, P., Tomás, R., Béjar-Pizarro, M., López-Vinielles, J., Rossi, M., . . . others (2021). Mapping the global threat of land subsidence. *Science*, *371*(6524), 34–36.

Hinkel, J., Lincke, D., Vafeidis, A. T., Perrette, M., Nicholls, R. J., Tol, R. S., . . . Levermann, A. (2014). Coastal flood damage and adaptation costs under 21st century sea-level rise. *Proceedings of the National Academy of Sciences*, *111*(9), 3292–3297.

Horstman, E. M., Dohmen-Janssen, C. M., Narra, P., Van den Berg, N., Siemerink, M., & Hulscher, S. J. (2014). Wave attenuation in mangroves: A quantitative approach to field observations. *Coastal engineering*, *94*, 47–62.

Hu, C., Lee, Z., & Franz, B. (2012). Chlorophyll aalgorithms for oligotrophic oceans: A novel approach based on three-band reflectance difference. *Journal of Geophysical Research: Oceans*, *117*(C1).

IMaRS-USF, I. (2005). Millennium coral reef mapping project. *Validated maps. Cambridge (UK): UNEP World Conservation Monitoring Centre.*

Jaksic, L. (2021). Van oord coastal assessment database for climate adaptation: preliminary method for the inclusion of wave setup.

Janssen, M. (2016). Flood hazard reduction by mangroves.

Jonkman, S. N. (2018). *Lecture notes flood defences.* Delft University of Technology.

Kaminsky, G. M., & Kraus, N. C. (1993). Evaluation of depth-limited wave breaking criteria. In *Ocean wave measurement and analysis* (pp. 180–193).

Karlsrud, K., Vangelsten, B., & Frauenfelder, R. (2017). Subsidence and shoreline retreat in the ca mau province–vietnam. causes, consequences and mitigation options. *Geotechnical Engineering Journal of the SEAGS & AGSSEA*, *48*(1).

Kench, P. S., & Brander, R. W. (2006). Wave processes on coral reef flats: implications for reef geomorphology using australian case studies. *Journal of Coastal Research*, *22*(1 (221)), 209–223.

Kirezci, E., Young, I. R., Ranasinghe, R., Muis, S., Nicholls, R. J., Lincke, D., & Hinkel, J. (2020). Projections of global-scale extreme sea levels and resulting episodic coastal flooding over the 21st century. *Scientific reports*, *10*(1), 1–12.

Kumar, P. (2010). *The economics of ecosystems and biodiversity: ecological and economic foundations.* UNEP/Earthprint.

Luijendijk, A., Hagenaars, G., Ranasinghe, R., Baart, F., Donchyts, G., & Aarninkhof, S. (2018). The state of the world's beaches. *Scientific reports*, *8*(1), 1–11.

Mancheño, A. G., Herman, P. M., Jonkman, S. N., Kazi, S., Urrutia, I., van Ledden, M., et al. (2021). Mapping mangrove opportunities with open access data: A case study for bangladesh. *Sustainability*, *13*(15), 1–18.

Mazda, Y., Magi, M., Ikeda, Y., Kurokawa, T., & Asano, T. (2006). Wave reduction in a mangrove forest dominated by sonneratia sp. *Wetlands Ecology and Management*, *14*(4), 365–378.

McIvor, A. L., Spencer, T., Möller, I., & Spalding, M. (2013). The response of mangrove soil surface elevation to sea level rise. *Natural Coastal Protection Series: Report 3. Cambridge Coastal Research Unit Working Paper 42. ISSN 2050-7941.*.

Melnichenko, O., Hacker, P., Potemra, J., Meissner, T., & Wentz, F. (2021). Aquarius/smap sea surface salinity optimum interpolation analysis.

Mendez, F. J., & Losada, I. J. (2004). An empirical model to estimate the propagation of random breaking and nonbreaking waves over vegetation fields. *Coastal Engineering*, *51*(2), 103–118.

Menéndez, P., Losada, I. J., Torres-Ortega, S., Narayan, S., & Beck, M. W. (2020). The global flood protection benefits of mangroves. *Scientific reports*, *10*(1), 1–11.

Morris, R. L., Konlechner, T. M., Ghisalberti, M., & Swearer, S. E. (2018). From grey to green: Efficacy of eco-engineering solutions for nature-based coastal defence. *Global change biology*, *24*(5), 1827–1842.

Muis, S., Apecechea, M. I., Dullaart, J., de Lima Rego, J., Madsen, K. S., Su, J., . . . Verlaan, M. (2020). A high-resolution global dataset of extreme sea levels, tides, and storm surges, including future projections. *Frontiers in Marine Science*, *7*, 263.

NOAA. (2021). In what types of water do corals live?

Pearson, S. G. (2016). *Predicting wave-induced flooding on low-lying tropical islands using a bayesian network* (Unpublished master's thesis).

Pinsky, M. L., Guannel, G., & Arkema, K. K. (2013). Quantifying wave attenuation to inform coastal habitat conservation. *Ecosphere*, *4*(8), 1–16.

Pontee, N., Narayan, S., Beck, M. W., & Hosking, A. H. (2016). Nature-based solutions: lessons from around the world. In *Proceedings of the institution of civil engineers-maritime engineering* (Vol. 169, pp. 29–36).

Pörtner, H.-O., Roberts, D. C., Masson-Delmotte, V., Zhai, P., Tignor, M., Poloczanska, E., . . . others (2019). Ipcc special report on the ocean and cryosphere in a changing climate. *IPCC Intergovernmental Panel on Climate Change: Geneva, Switzerland*, *1*(3).

Quartel, S., Kroon, A., Augustinus, P., Van Santen, P., & Tri, N. (2007). Wave attenuation in coastal mangroves in the red river delta, vietnam. *Journal of Asian Earth Sciences*, *29*(4), 576–584.

Robertson, B., Hall, K., Zytner, R., & Nistor, I. (2013). Breaking waves: Review of characteristic relationships. *Coastal Engineering Journal*, *55*(01), 1350002.

Ruitenbeek, J., Cartier, C., Bunce, L., Gustavson, K., Putterman, D., Spash, C., . . . Westmacott, S. (1999). Issues in applied coral reef biodiversity valuation: results for montego bay, jamaica. *World Bank Research Committee Project RPO*, *682*, 22p.

Schoonees, T., Mancheño, A. G., Scheres, B., Bouma, T., Silva, R., Schlurmann, T., & Schüttrumpf, H. (2019). Hard structures for coastal protection, towards greener designs. *Estuaries and Coasts*, *42*(7), 1709–1729.

Scussolini, P., Aerts, J. C., Jongman, B., Bouwer, L. M., Winsemius, H. C., de Moel, H., & Ward, P. J. (2016). Flopros: an evolving global database of flood protection standards. *Natural Hazards and Earth System Sciences*, *16*(5), 1049–1061.

Small, C., & Nicholls, R. J. (2003). A global analysis of human settlement in coastal zones. *Journal of Coastal Research*, *19*(3), 584–599. Retrieved from `http://www.jstor.org/stable/4299200`

Spalding, M., Burke, L., Wood, S. A., Ashpole, J., Hutchison, J., & Zu Ermgassen, P. (2017). Mapping the global value and distribution of coral reef tourism. *Marine Policy*, *82*, 104–113.

Spalding, M., McIvor, A., Tonneijck, F., Tol, S., & Eijk, P. v. (2014). Mangroves for coastal defence.

Spalding, M., Spalding, M. D., Ravilious, C., Green, E. P., et al. (2001). *World atlas of coral reefs*. Univ of California Press.

Stocker, T. F., Qin, D., Plattner, G. ., Tignor, M. M. B., Allen, S. K., Boschung, J., . . . Midgley, P. M. (2013). Climate change 2013 the physical science basis: Working group i contribution to the fifth assessment report of the intergovernmental panel on climate change. In (Vol. 9781107057999, p. 1-1535). Retrieved from `www.scopus.com` (Cited By :5148)

Tiggeloven, T., Moel, H. d., Winsemius, H. C., Eilander, D., Erkens, G., Gebremedhin, E., . . . others (2020). Global-scale benefit–cost analysis of coastal flood adaptation to different flood risk drivers using structural measures. *Natural Hazards and Earth System Sciences*, *20*(4), 1025–1044.

Van Slobbe, E., de Vriend, H. J., Aarninkhof, S., Lulofs, K., de Vries, M., & Dircke, P. (2013). Building with nature: in search of resilient storm surge protection strategies. *Natural hazards*, *66*(3), 1461–1480.

van Wesenbeeck, B. K., de Boer, W., Narayan, S., van der Star, W. R., & de Vries, M. B. (2017). Coastal and riverine ecosystems as adaptive flood defenses under a changing climate. *Mitigation and Adaptation Strategies for Global Change*, *22*(7), 1087–1094.

van Zelst, V. (2018). Global flood hazard reduction by foreshore vegetation.

VL, H. P., & Massel, S. R. (2006). Experiments on wave motion and suspended sediment concentration at nang hai, can gio mangrove forest, southern vietnam. *Oceanologia*, *48*(1).

Vo-Luong, P., & Massel, S. (2008). Energy dissipation in non-uniform mangrove forests of arbitrary depth. *Journal of Marine Systems*, *74*(1-2), 603–622.

Vuik, V., Van Vuren, S., Borsje, B. W., van Wesenbeeck, B. K., & Jonkman, S. N. (2018). Assessing safety of nature-based flood defenses: Dealing with extremes and uncertainties. *Coastal engineering*, *139*, 47–64.

WorldBank. (2020). *Gdp per capita*. Retrieved from `https://data.worldbank.org/indicator/NY.GDP.PCAP.CD`

Worthington, T., & Spalding, M. (2018). Mangrove restoration potential: A global map highlighting a critical opportunity.

Xu, B., Feng, G., Li, Z., Wang, Q., Wang, C., & Xie, R. (2016). Coastal subsidence monitoring associated with land reclamation using the point target based sbas-insar method: A case study of shenzhen, china. *Remote Sensing*, *8*(8), 652.

Yastika, P., Shimizu, N., & Abidin, H. (2019). Monitoring of long-term land subsidence from 2003 to 2017 in coastal area of semarang, indonesia by sbas dinsar analyses using envisat-asar, alos-palsar, and sentinel-1a sar data. *Advances in Space Research*, *63*(5), 1719–1736.

Part V

Appendices

A | Current assessments

Coastal flood damage and adaptation costs under 21st century sea-level rise (Hinkel et al., 2014).

This research uses SLR- and socioeconomic scenario's, different adaptation strategies and available data sets to assess the impacts that increased coastal flood risk has on population and assets. The flood risk is expressed by the Expected Annual Damage (EAD) to assets and the expected annual number of people flooded, referred to as EAP in my research. The investment costs are based on the amount of dike heightening. Different adaptation strategies include the constant protection strategy, where the dike height is **not** changed, such that the flood risk increases with SLR. For the enhanced protection strategy, the dikes are raised according to the SLR and socioeconomic developments. The damage caused by flooding is assumed 0 for flood events that have a height below the crest of the dike. The study assumes that the current protection are provided by dikes, with a height corresponding to the situation in 1995 (Hinkel et al., 2014).

Global scale benefit-cost analysis of coastal flood adaptation to different flood risk drivers (Tiggeloven et al., 2020).

This research presents a global framework by which the future cost-benefits of structural defences are evaluated. Different flood risk drivers are accounted for such as sea-level rise, land subsidence and socioeconomic changes. The framework consists of four steps; the estimation of flood risk, costs of adaptation, cost-benefit analysis and attribution of costs to the aforementioned drivers. The flood risk is calculated for scenarios without and with adaptation measures, such that the difference between the calculated EAD depicts the benefits of adaptation. The EAD is calculated by taking the integral of the exceedance probability-impact curve. The flood risk benefits are calculated by determining the EAD for every year within the dike's lifetime and subtracting from the EAD for every year without adaptation. The protection standard is included in the risk computation by taking the integral starting at the exceedance probability of the protection standard (expressed as a return period). The current protection standards for the dike systems are taken from the FLOPROS modelling approach (Scussolini et al., 2016). To determine the costs of the different flood protections, the investments costs of raising the dikes are summed. In this study, resulting water levels are used to estimate the current and future dike heights. Sea-level rise and land subsidence are taken into account to determine future dike heights, by adding the SLR directly to the current dike height. A discount rate of 5% until 2100 is used to transform the benefits and costs towards a NPV. The calculations are performed for different adaptation strategies, such as; 1) keeping protection constant, 2) keeping risk constant, 3) keeping risk as percentage of GDP constant and 4) optimize NPV. For the fourth strategy, the protection standard is only improved if the benefit-cost ratios are larger than 1. The new protection standards are taken as either 2, 5, 10, 25, 50, 100, 250, 500 and 1,000 years (Tiggeloven et al., 2020).

Global flood hazard reduction by foreshore vegetation (van Zelst, 2018).

This research presents a global mapping of flood hazard reduction by salt marshes and mangroves. To determine the wave attenuation induced by these vegetated foreshores global transects are used that are aligned perpendicular to the coast. The wave attenuation is then determined by comparing the wave height at the end of the vegetated foreshore with the wave height that would occur at a bare foreshore. The research assumes that for the current situation a dike is present. The dike height reduction induced by the wave attenuation of these vegetated foreshores is then determined by subtracting the required crest height for a vegetated foreshore from the crest height required for a bare foreshore (van Zelst, 2018).

Effectiveness of mangroves in flood risk reduction (de Koning, 2021).

This research investigates the attractiveness to use mangroves for flood risk reduction. A method is developed to define the optimal configuration of a levee with mangroves at the foreshore by determining the minimum costs for the required protection standard (de Koning, 2021).

The global flood protection benefits of mangroves (Menéndez et al., 2020).

This research determines the global benefits that mangroves provide by determining the difference in flood damages between the situation with mangroves that involves the current amount of mangroves present and the situation without any mangroves present. For different storm events the amount of land being flooded is determined for both scenario's for which the amount of people and assets being flooded is calculated based on the bathtub approach. The research does not include a current coastal protection for the flood calculations. Based on these results, the EAD for the different storm events is constructed for both scenario's. The difference in flood damage between the two scenario's then expresses the benefits that mangroves provide (Menéndez et al., 2020).

The global flood protection savings provided by coral reefs (Beck et al., 2018).

This research presents a process-based method to show the global flood protection benefits from coral reefs. The method involves different stages; 1) offshore hydrodynamics (waves and sea level) are combined, 2) the waves are transferred from offshore to nearshore, 3) the effect of coral reefs on the wave-run up are determined, 4) for storm events with different return periods up to 100 years, the flood heights are extended inland for the situation with and without coral reefs, 5) the infrastructure and people that is damaged by the flood event is estimated. By comparing the extend of flooding for the situation with coral reefs and without, the flood protection benefits are determined. The research does not include a current coastal protection for the flood calculations (Beck et al., 2018).

B | Hotspot data

B.1 Connection between available data and the hotspots

If the hotspots are located within blocks of data, in this example the sea surface temperature, the hotspots are assigned a value based on linear interpolation between the values located within the hotspot's polygon. If there is no data located within the polygon, via the nearest neighbour principle, there is a value assigned to the hotspot from the nearest data block available, where a maximum distance is used within is searched for a nearby value.
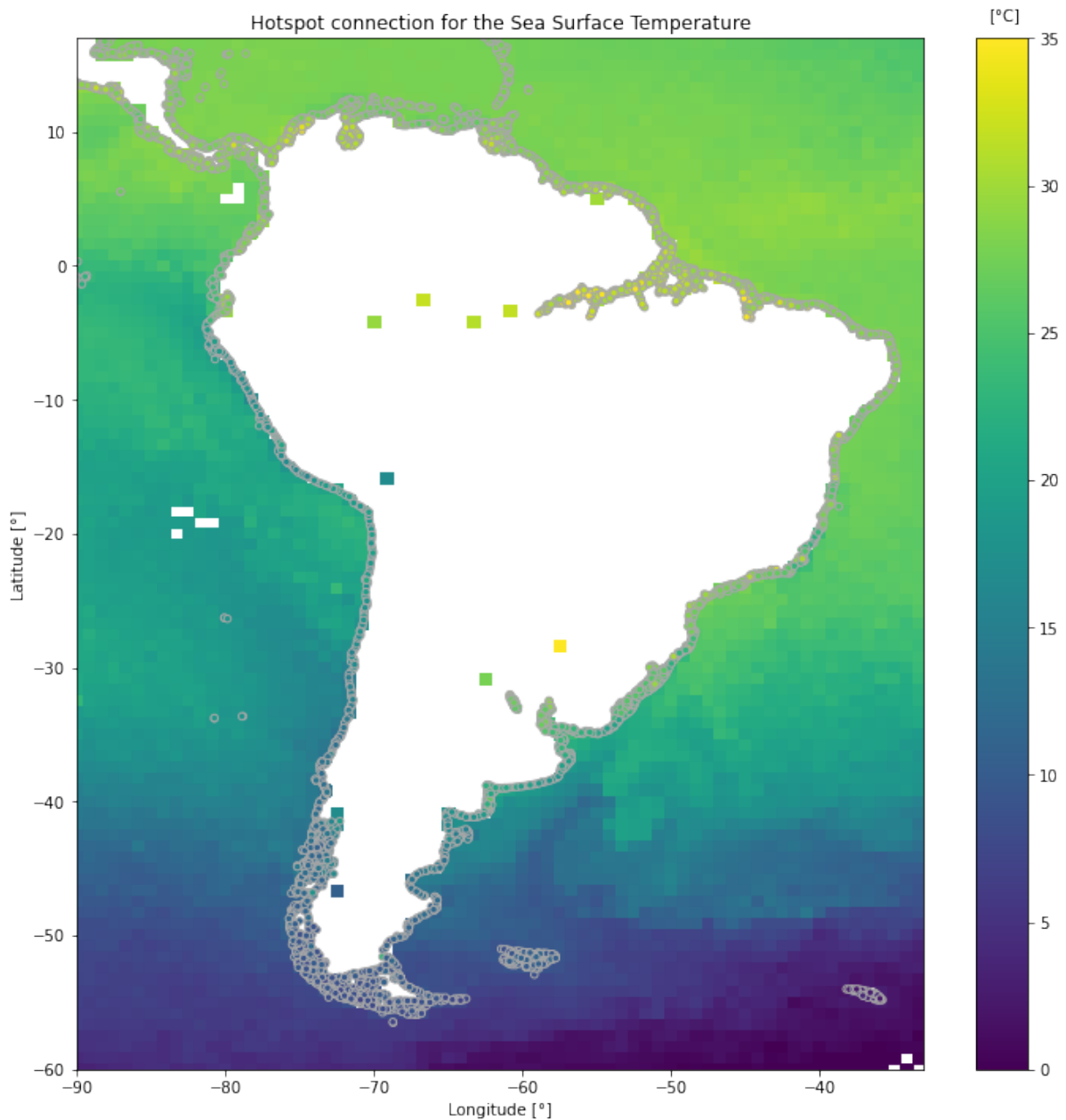
Figure B.1: *Projecting the sea surface temperature from a global map onto the hotspots.*

B.2 Storm surge data set discrepancies

The storm surge data set (GTSR) is taken from Muis et al. (2020), which determined the extreme sea levels including tide and storm surge for different return periods. The combined tide and storm surge data set is obtained from the Global Tide and Surge Model Version 3.0, where a wind speed of 10 m/s is forced in combination with the atmospheric pressure from the ERA5-data set for the historical period 1979-2017. The extremes for different return periods are obtained via a Gumbel distribution applied to the annual maxima using the maximum likelihood method.

Within this research, the data set is used to represent the storm surge for the different return periods. This is an overestimation as the data set includes a combination of tides and storm surges. The data sets are not available separately as they are interlinked by their probabilistic calculations. Because high tide plays an important role in the calculations in this research, this needs to be available separately for each location. Therefore there is also a tidal data set including the high tide that is used. As a result the calculations include conservative results as the local tide is included twice in the calculations, albeing that within the data set of Muis et al. (2020) it does not necessarily include high tide for the tidal component. This is shown by the results in Figure B.2, where locations are shown, in which the data set of Muis et al. (2020) minus the high tide results in negative values.
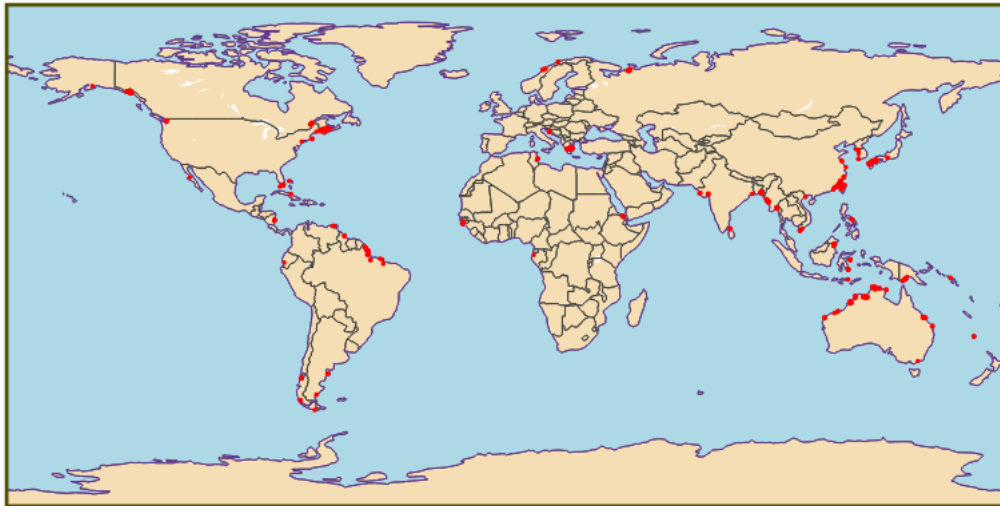
Figure B.2: *Locations where the GTSR data set minus the local high tide produces negative values.*

B.3   Data plots

Hotspots with mangrove potential and currently no mangroves.

Figure B.3: *1,759 hotspots with potential to restore mangroves and no mangroves currently present.*

Hotspots with coral potential and currently no corals.
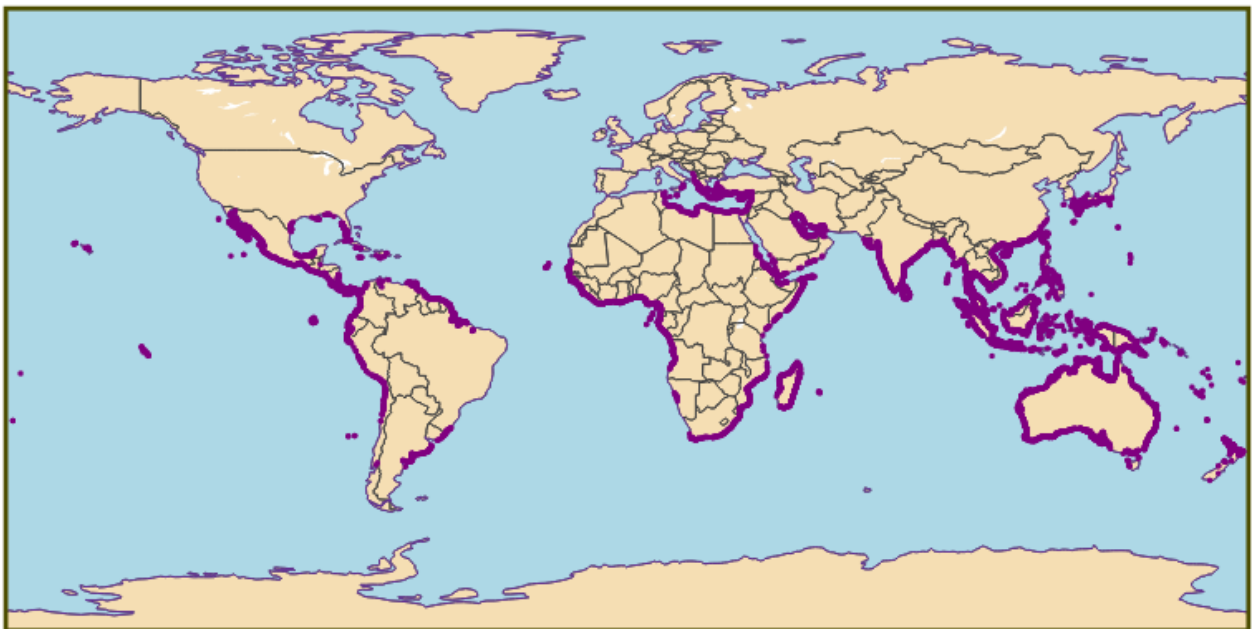
Figure B.4: *11,036 hotspots with potential to restore corals and no corals currently present.*
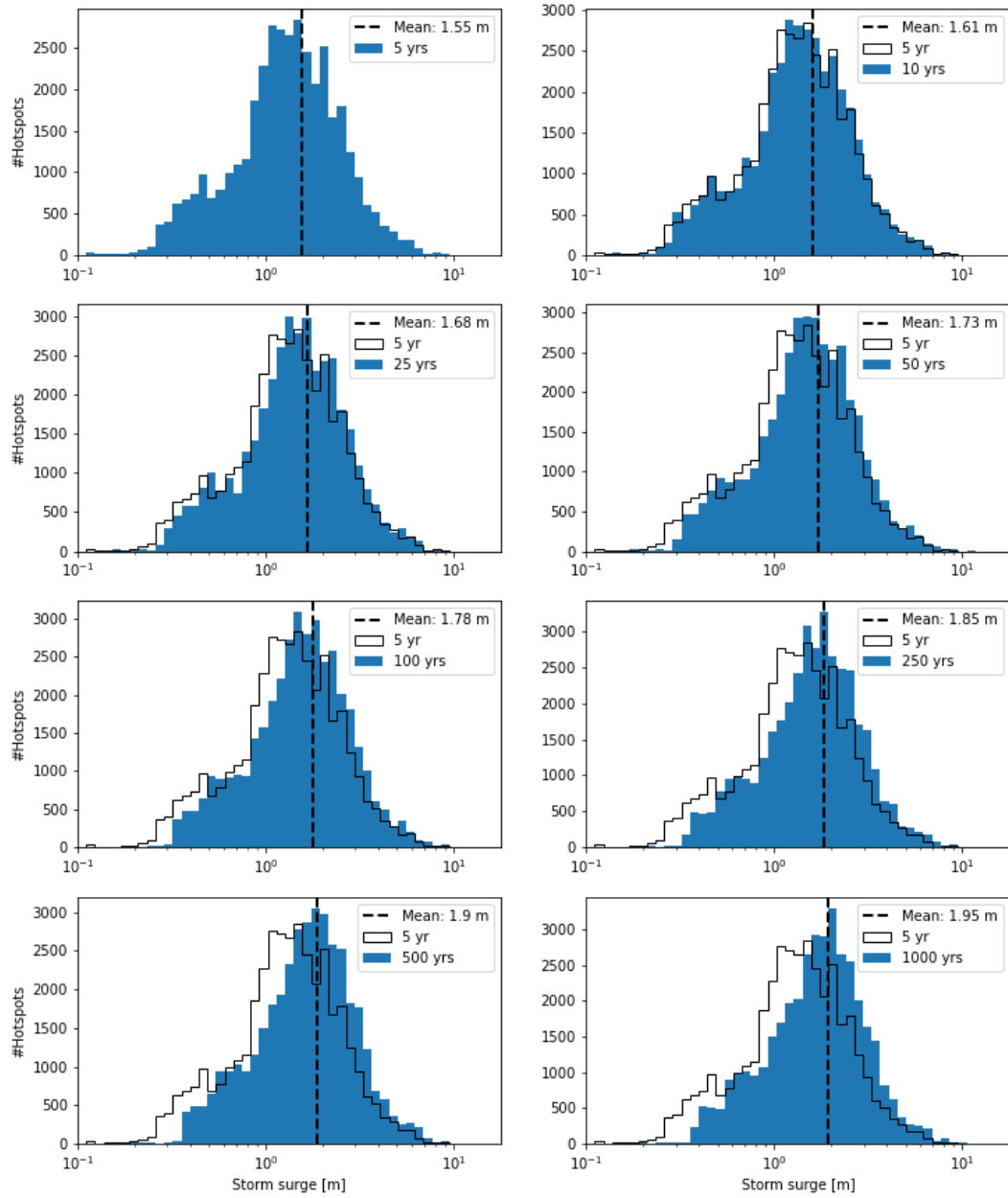
Figure B.5: *Storm surge magnitudes for the return periods of 5, 10, 25, 50, 100, 250, 500 and 1000 yrs (Muis et al., 2020). As the return periods increase, it is seen that the mean magnitudes of the storm surges over all hotspots increases as well.*
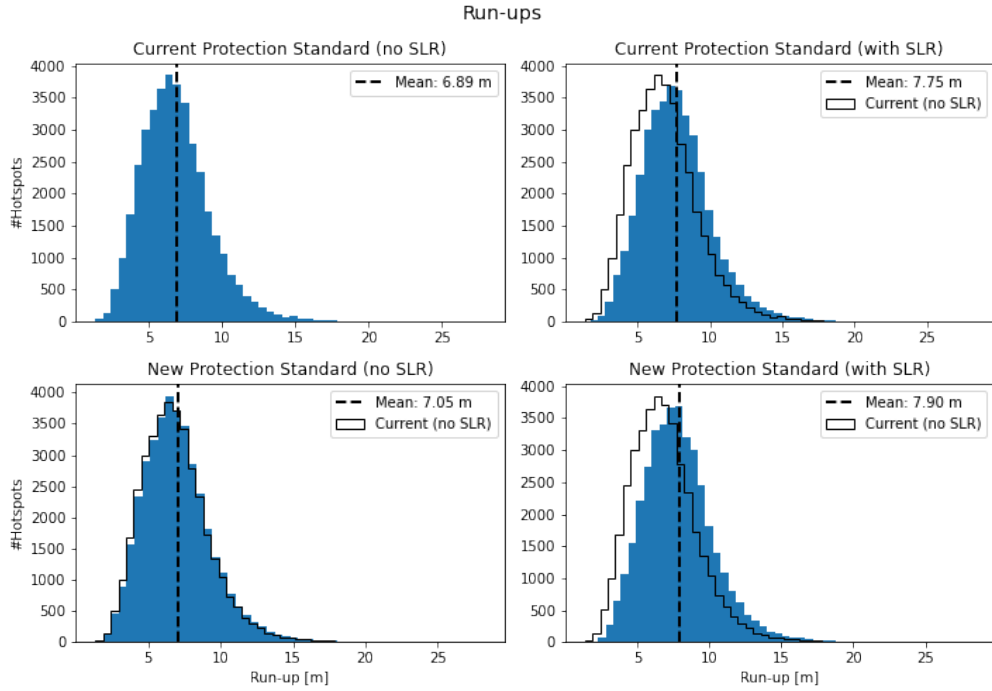
Figure B.6: *Distribution of run-ups for the current and new protection standard including and excluding SLR for all hotspots.*
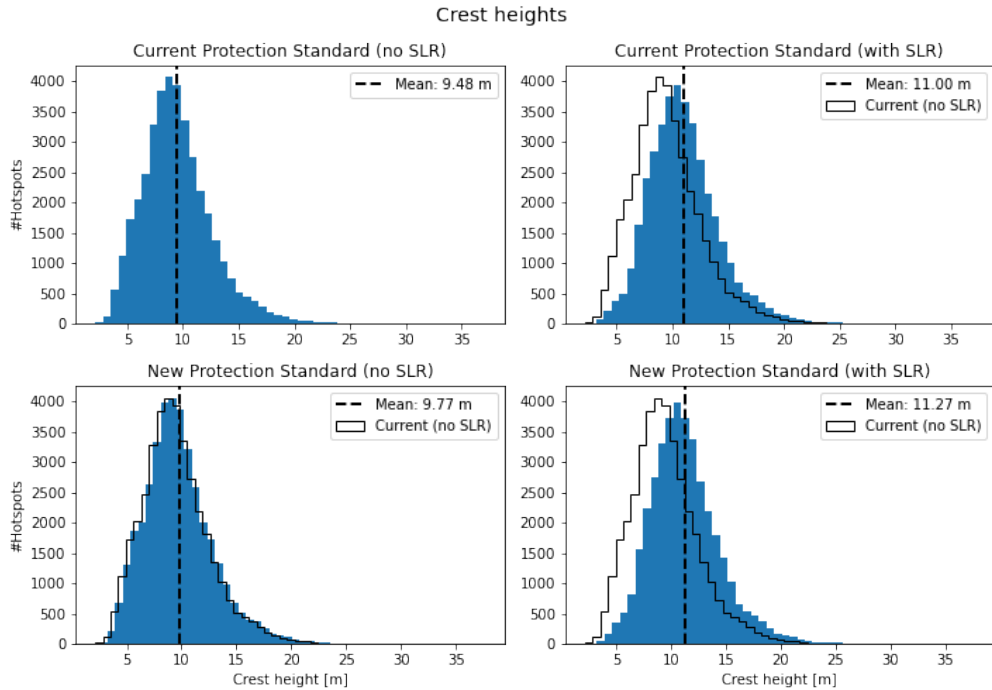
Figure B.7: *Distribution of crest heights for the current and new protection standard including and excluding SLR for all hotspots.*
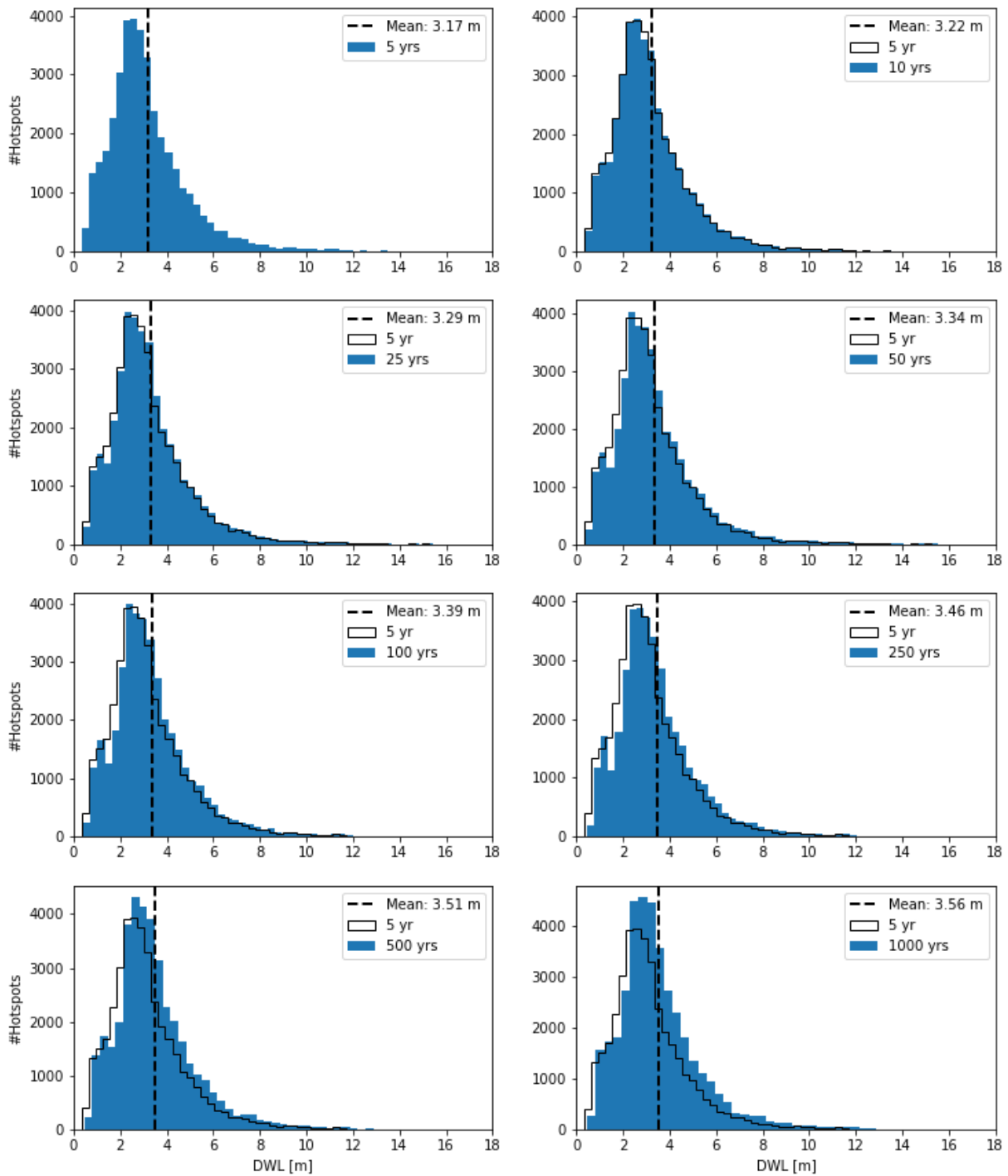
Figure B.8: *Design water levels for return periods of 5, 10, 25, 50, 100, 250, 500 and 1000 years, where sea level rise is not taken into account. It can be seen that if the return period increases the mean value of the design water levels for all hotspots also increase.*
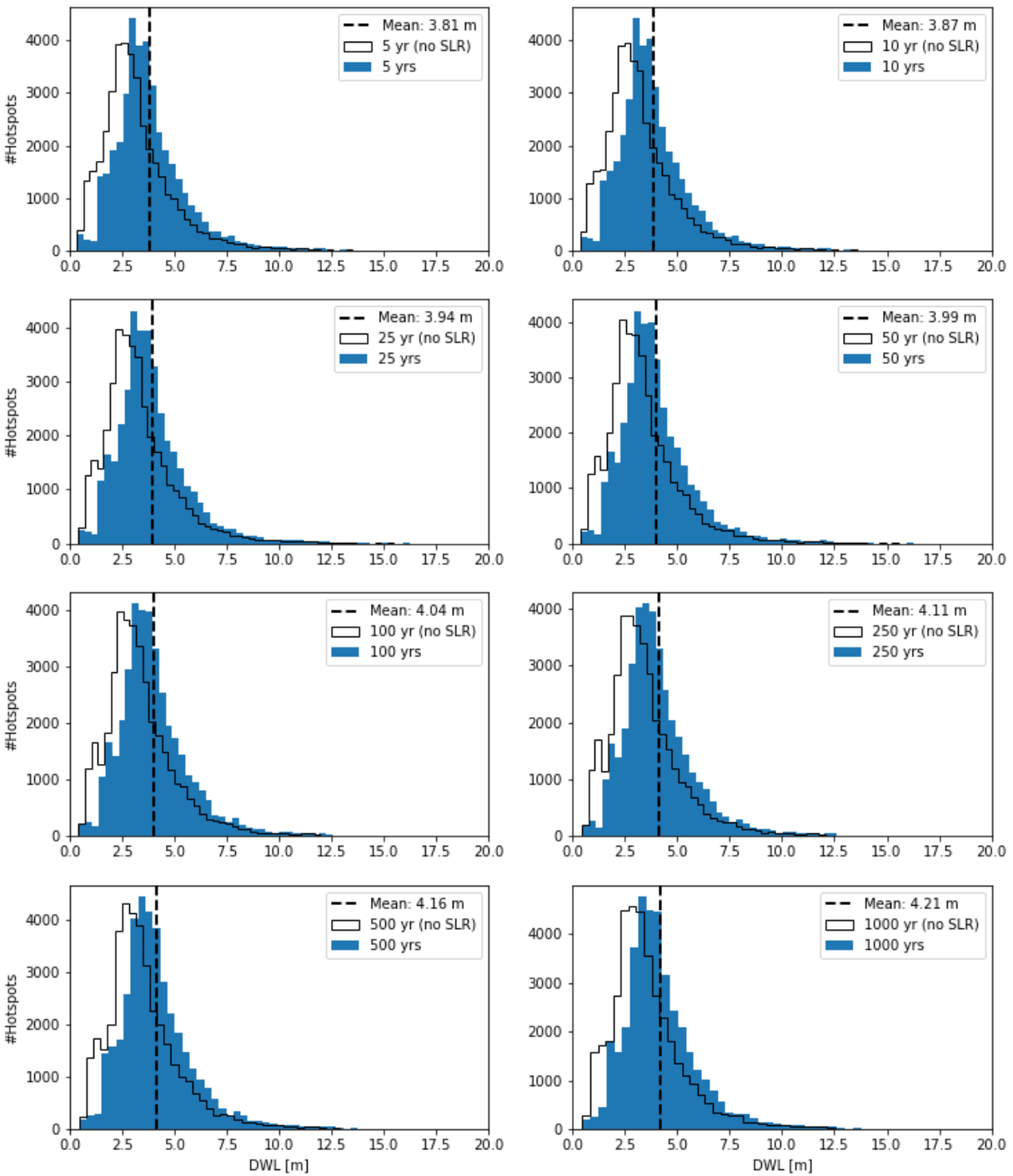
Figure B.9: *Design water levels for return periods of 5, 10, 25, 50, 100, 250, 500 and 1000 years, where sea level rise is taken into account. It can be seen that if the return period increases the mean value of the design water levels for all hotspots also increase. Compared to Figure B.8, the mean value of the design water levels is increased significantly due to the influence of sea level rise.*
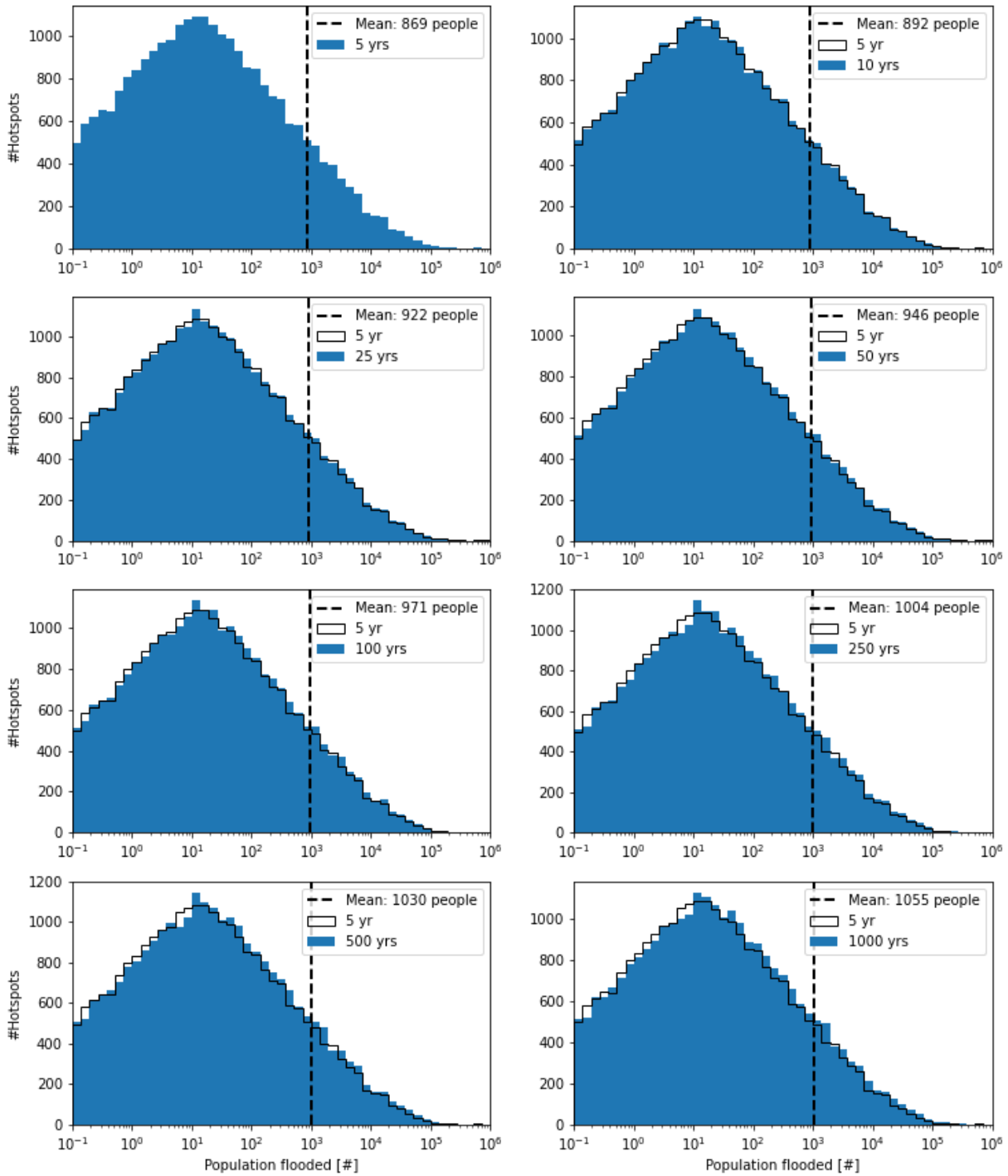
Figure B.10: *The amount of people being flooded for extreme sea levels (DWL) with return periods of 5, 10, 25, 50, 100, 250, 500 and 1000 years. Sea level rise is not taken into account for the extreme sea levels here. For extreme sea levels with larger return periods, it can be seen that the amount of people being flooded also increase.*
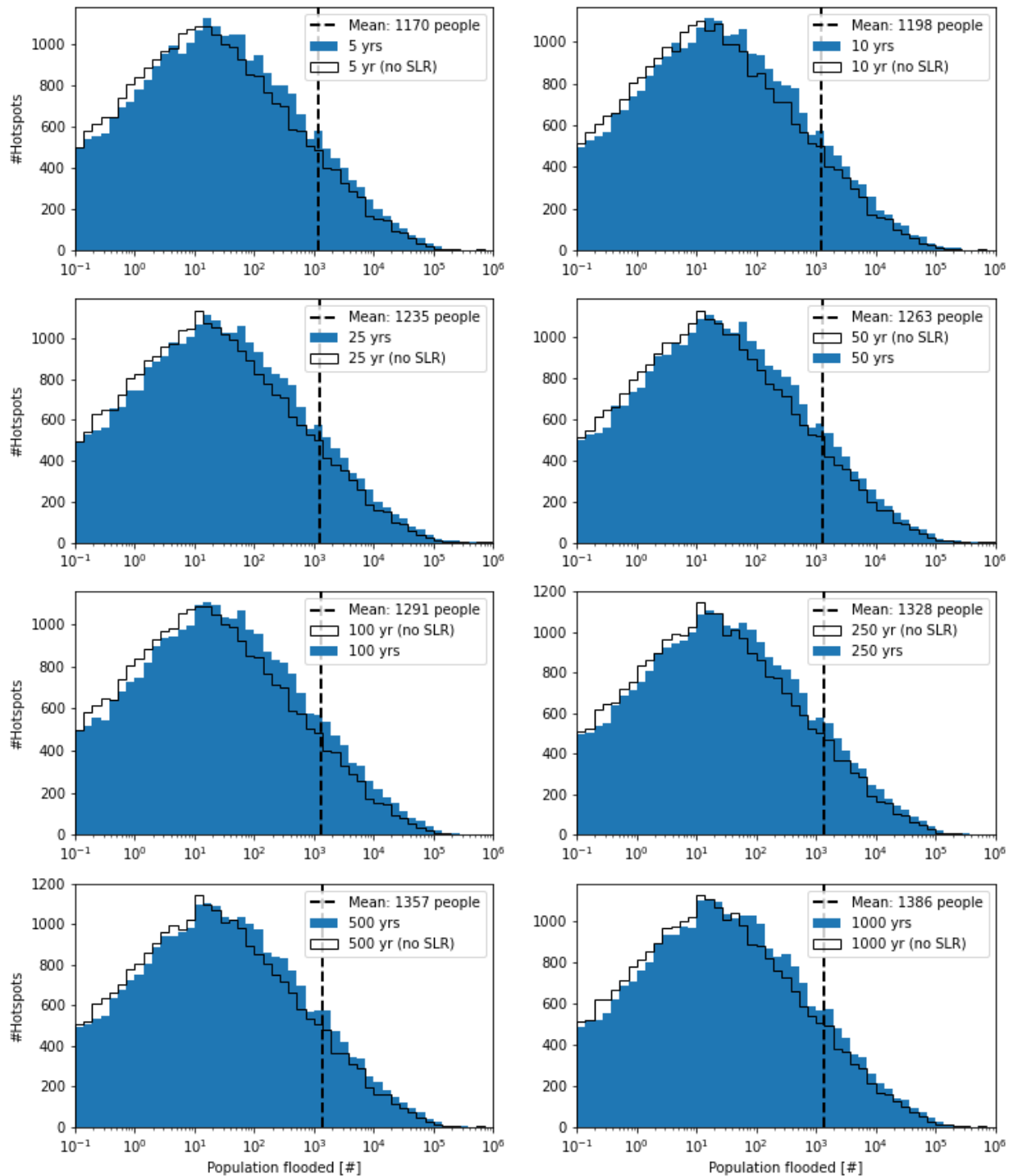
Figure B.11: *The amount of people being flooded for extreme sea levels (DWL) with return periods of 5, 10, 25, 50, 100, 250, 500 and 1000 years. Sea level rise is taken into account for the extreme sea levels here. For extreme sea levels with larger return periods, it can be seen that the amount of people being flooded also increase. Compared to the amount of people being flooded without SLR (Figure B.10), it can be seen here that the amount of people being flooded with SLR increases significantly.*

B.4 Cost optimization

Below the cost optimization calculations are shown for one location with only potential to apply corals (Figure B.12a), one location with only potential to apply mangroves (Figure B.12b) and one location with potential to apply corals and mangroves (Figure B.12c).

(a) *Thailand - 10.77° N 99.41° E. Potential for corals.*

(b) *China - 26.67° N 119.77° E. Potential for mangroves.*

(c) *Malaysia - 6.45° N 99.90° E. Potential for corals & mangroves.*
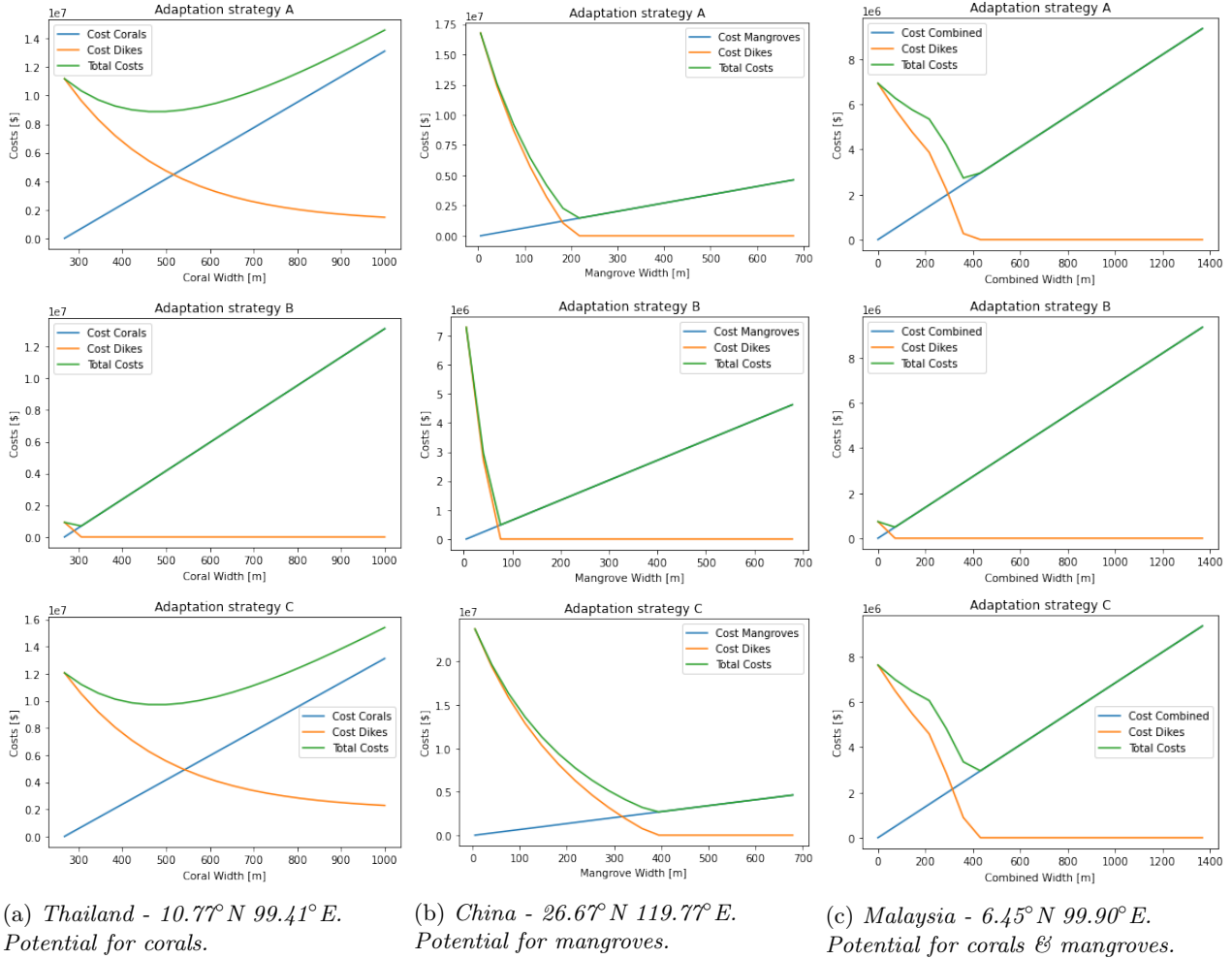
Figure B.12: *Y-axis showing the total costs consisting of dike costs and vegetation costs for all three adaptation strategies $A_{cur,slr}$, B_{new} and $C_{new,slr}$. Figure B.12a shows a hotspot located in Thailand with only potential to apply corals, hence the x-axis denotes coral width. Figure B.12b shows a hotspot located in China with only potential to apply mangroves, hence the x-axis denotes mangrove width. Figure B.12c shows a hotspot located in Malaysia with potential to apply mangroves and corals, hence the x-axis denotes Combined width.*

On the x-axis, the widths are denoted starting with the amount of corals and/or mangroves currently present in the hotspot. For the hotspot seen in Figure B.12a located in Thailand, the current width of the coral reef is 268 m. From that current width up to the maximum width of 1000 m, the costs are calculated. For the hotspot seen in Figure B.12 located in China, the current width of the mangrove forest is 5 m. From the current width up to the maximum width possible at the hotspot (679 m) which is governed by HT (3.42 m) and the slope (0.00504), the costs are calculated. For the hotspot seen in Figure B.12c located in Malaysia, the current width of the coral reef and mangrove forest is 0 m. However, as there is potential found to apply both corals and mangroves, the calculations are performed including both nature-based solutions. The maximum mangrove width possible at the hotspot is 368 m and for the coral reef again 1000 m. This is why the x-axis shows results up to 1368 m.

If the width of the mangrove forest or the coral reef increases, more wave attenuation could be induced. This can result in smaller waves occurring at the toe of the dike, which in turn can result in smaller run-up values and hence, smaller required crest heights. This explains the decrease in dike costs when more vegetation is added (Figure B.12). For the hotspots shown in Figure B.12 and B.12c, the dike costs even become 0. Since for the corresponding vegetation widths the run-up becomes so small that the calculated required crest height for the new protection standard becomes equal to the current crest height.

Intermezzo B.4a: Total investment costs (hotspot Thailand).

- Coral potential = Yes, mangrove potential = No.
- $\$_{coral}$ = 89,269 \$/ha, $\$_{mang}$ = 1,191 \$/ha.
- $A_{cur,slr}$: ΔW_{coral} = 192 m, ΔW_{mang} = 0 m, I_{tot} = 4.4 M\$/km, cost reduction = 1.1 M\$/km.
- B_{new}: ΔW_{coral} = 38 m, ΔW_{mang} = 0 m, I_{tot} = 0.34 M\$/km, cost reduction = 0.11 M\$/km.
- $C_{new,slr}$: ΔW_{coral} = 231 m, ΔW_{mang} = 0 m, I_{tot} = 4.8 M\$/km, cost reduction = 1.17 M\$/km.

For this location only potential for coral restoration is found, which is why only optimal coral widths are found that vary for the different adaptation strategies.

Intermezzo B.4b: Total investment costs (hotspot China).

- Coral potential = No, mangrove potential = Yes.
- $\$_{coral}$ = 1,826,651 \$/ha, $\$_{mang}$ = 38,982 \$/ha.
- $A_{cur,slr}$: ΔW_{coral} = 0 m, ΔW_{mang} = 213 m, I_{tot} = 0.83 M\$/km, cost reduction = 8.7 M\$/km.
- B_{new}: ΔW_{coral} = 0 m, ΔW_{mang} = 71 m, I_{tot} = 0.28 M\$/km, cost reduction = 3.9 M\$/km.
- $C_{new,slr}$: ΔW_{coral} = 0 m, ΔW_{mang} = 390 m, I_{tot} = 1.52 M\$/km, cost reduction = 12.0 M\$/km.

For this location, the maximum amount of mangroves possible at the foreshore is 679 m. Here, there is only potential for mangrove restoration, which is why only optimal mangrove widths are found that vary for the different adaptation strategies.

Intermezzo B.4c: Total investment costs (hotspot Malaysia).

- Coral potential = Yes, mangrove potential = Yes.
- $\$_{coral}$ = 89,269 \$/ha, $\$_{mang}$ = 1,191 \$/ha.
- $A_{cur,slr}$: ΔW_{coral} = 263 m, ΔW_{mang} = 97 m, I_{tot} = 2.6 M\$/km, cost reduction = 4.0 M\$/km..
- B_{new}: ΔW_{coral} = 53 m, ΔW_{mang} = 19 m, I_{tot} = 0.47 M\$/km, cost reduction = 0.23 M\$/km.
- $C_{new,slr}$: ΔW_{coral} = 316 m, ΔW_{mang} = 116 m, I_{tot} = 2.83 M\$/km, cost reduction = 4.5 M\$/km.

For this location, the maximum amount of mangroves possible at the foreshore is 368 m. Here, there is potential for mangrove and coral restoration, which is why optimal mangrove and coral widths are found that vary for the different adaptation strategies.

B.5 Benefits and costs scatter-plot

Figure B.13 shows the benefits consisting of a reduction in flood risk (y-axis) and the investment costs (x-axis) required to obtain these benefits. The left Figures show the results for strategy B_{new} in which the protection standard is increased and SLR is excluded. The right Figures show the results for strategy $C_{new,slr}$ including SLR. If NBS are considered, which is the case for defence approach 2 (lower 4 panels), one can see that the amount of locations where the benefits outweigh the costs increase. This is seen by the increase in blue dots that lie above the black dotted line. Above the line, the benefits outweigh the costs. If additional benefits are also considered (lower 2 panels), the amount of blue dots increase even more. Hence, applying NBS where possible increases the amount of cost-effective locations.
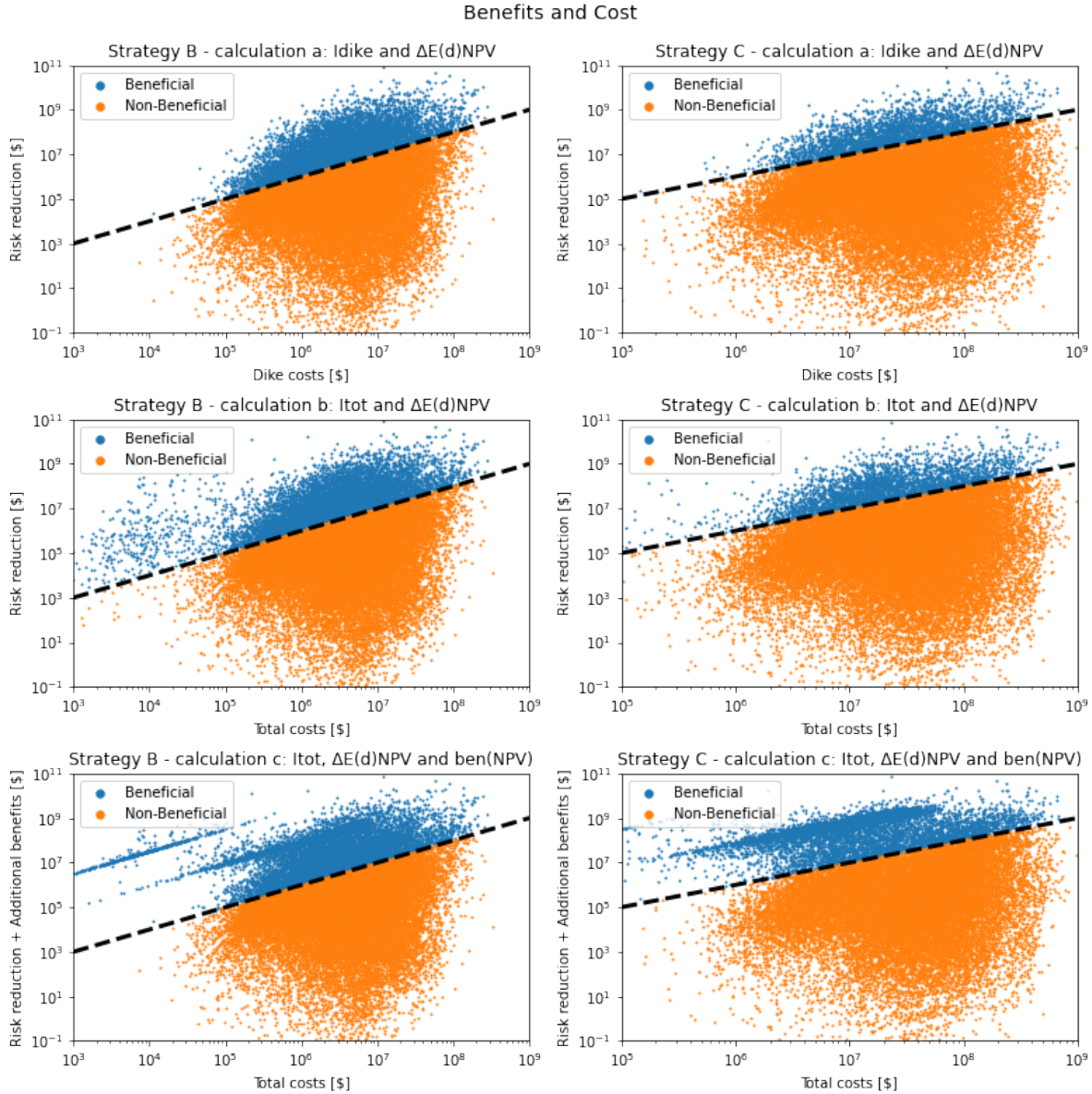
Figure B.13: *The benefits and costs for calculations a, b and c for strategies B_{new} and $C_{new,slr}$. For the blue hotspots the benefits outweigh the costs, such that it is economically beneficial to improve the protection standard of the coastal defence. The points where the benefits are equal to the costs are located on the black dotted line.*

B.6 Most cost-beneficial protection standard

As an example the calculations are shown for hotspot with id 81664 located in Brazil, with the following characteristics:

- Location: 26.17°S and 48.50°W.

- Currently no corals or mangroves present.

- Mangrove potential: Yes, coral potential: No.

- Current protection standard: 5 years.

- Dike length: 930 m.

B.6.1 a: Dike raising costs and flood risk reduction benefits.

For the different protection standards the flood risk reduction benefits ($\Delta E(d)_{NPV}$) also differ. As the protection standard is improved, the protection standard of the dike is increased. This means that for certain extreme sea levels flooding does not occur. Therefore, for higher protection standards, the flood risk decreases and the flood risk benefits between the current and new protection standard increase. For all plots, the current protection standard is chosen as the left bound, meaning that the new protection can not be lower than the current one. The flood risk reduction benefits ($\Delta E(d)_{NPV}$) for this hotspot located in Brazil are plotted with the green line in Figure B.14. As expected the line is continuously increasing for higher protection standards. The line appears to become horizontal for a certain protection standard, which is due to the site-specific depth-damage curve. For a certain protection standard, with a corresponding extreme sea level, the amount of people (and hence assets in our approach) flooded in this hotspot does not increase drastically anymore, which is why the line becomes nearly horizontal.
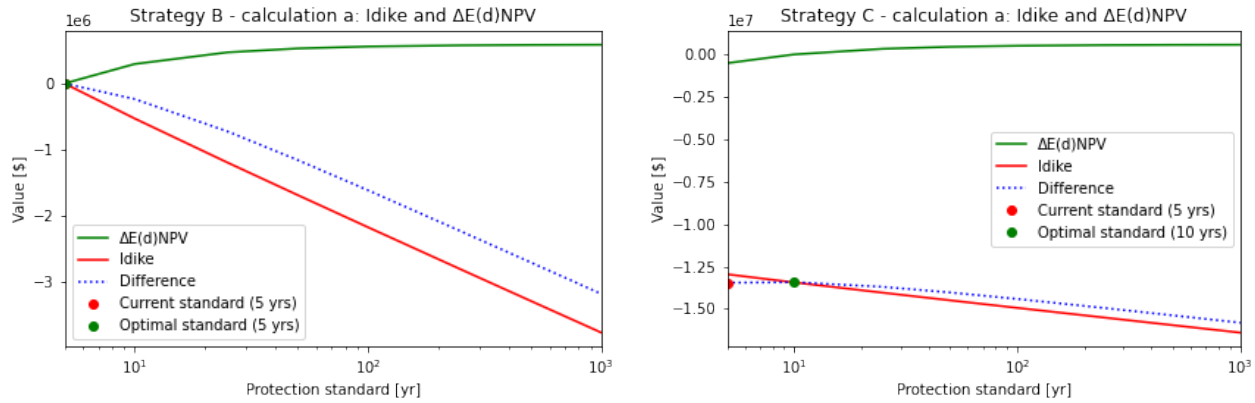
Figure B.14: *The flood risk reduction benefits ($\Delta E(d)_{NPV}$) and dike raising costs (I_{dike}) plotted against the different protection standards.*

With the red line the cost of only raising the dikes are plotted (I_{dike}). For adaptation strategy $\boldsymbol{B_{new}}$ (left Figure B.14) the costs are zero for the protection standard corresponding to the current one (red dot). This makes sense, as SLR is not taken into account and thus the dike does not have to be heightened. For adaptation strategy $\boldsymbol{C_{new,slr}}$ however (right Figure B.14) there are costs connected for keeping the same protection standard, since SLR is taken into account. For both adaptation strategies the costs are increasing (negative sign) with protection standard, as the dike is required to be more robust and the dikes need to be raised more. The blue dotted line gives the difference between the costs and benefits. At the maximum of the line, the benefits outweigh the costs most. Therefore, at this point the most cost-beneficial protection standard is achieved (green dot). This line could, however, also continuously decrease, meaning that the costs are higher than the corresponding benefits, which means that **economically speaking**, improving the protection standard is not a good choice (benefit-cost ratio < 1). This is for this location the case for adaptation strategy

B_{new} if solely the dikes are raised. The most cost-beneficial protection standard is then equal to the current one.

B.6.2   b: Dike raising costs and vegetation costs and flood risk reduction benefits.

With respect to the previous calculation, here the possibility of applying vegetation is also taken into account. This means that for each protection standard, the minimum total costs and corresponding optimal vegetation width is determined. For this location, there are currently no mangroves or corals present and there is only potential to apply mangroves according to section 2. By calculating the effects of mangrove restoration at this location, the costs for adaptation strategies B_{new} and $C_{new,slr}$ for this specific hotspot are lower compared to only raising the dikes as can be seen by the difference between the red (I_{dike}) and dashed red (I_{tot}) line in Figure B.15. As a result, now the flood risk benefits do outweigh the costs (I_{tot}) which results in a different most cost-beneficial protection standard for adaptation strategy B_{new} (Figure B.16).
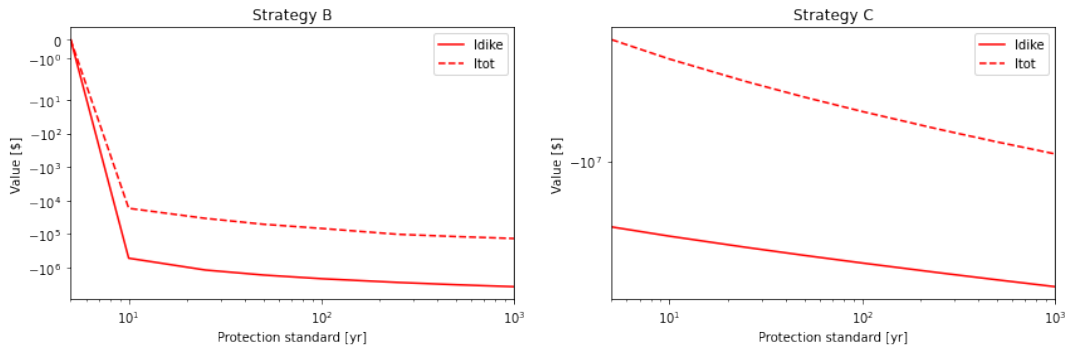
Figure B.15: *Dike raising costs (I_{dike}) and dike raising costs + vegetation costs (I_{tot}) plotted against the different protection standards.*
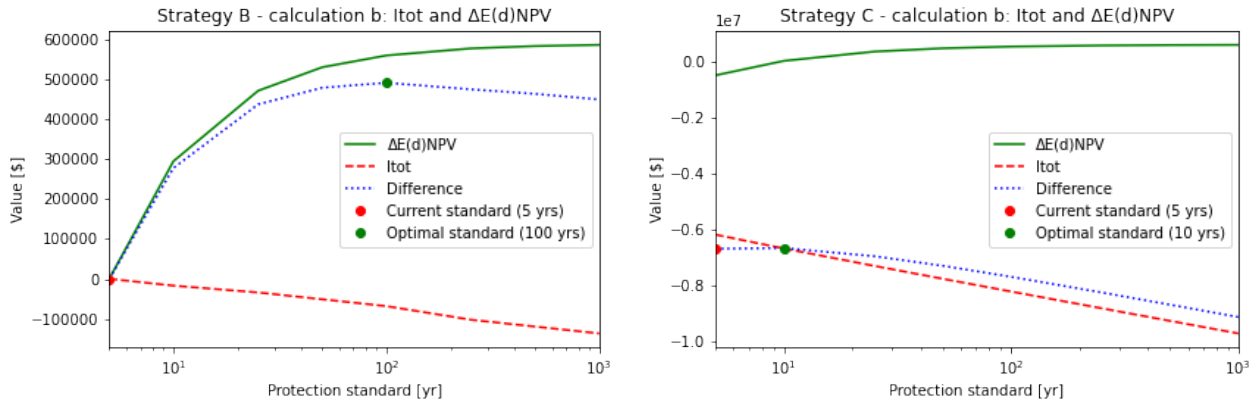
Figure B.16: *The flood risk reduction benefits ($\Delta E(d)_{NPV}$) and dike raising + vegetation costs (I_{tot}) plotted against the different protection standards.*

B.6.3   c: Dike raising costs and vegetation costs, flood risk reduction benefits and additional benefits.

For each protection standard the vegetation width for which the total costs are lowest are determined. Based on the vegetation width added the additional benefits (ben_{NPV}) are then calculated as explained in section 5.3.

For this specific hotpot in Brazil, for each protection standard there is a certain optimal amount of mangroves found for which the total costs are lowest. The corresponding additional benefits of the mangrove restoration width is plotted with the dashed black line in Figure B.17. Since there is no potential for corals at this hotspot

there are no additional benefits connected to the corals. For strategy B_{new}, the optimal mangrove restoration width increases with higher protection standards, resulting in increasing additional benefits. For strategy $C_{new,slr}$ the optimal mangrove restoration width is constant for the different protection standards. In this case this is the result of SLR, causing the optimal mangrove width to be equal to the maximum vegetation width possible at this hotspot (90 m). Taken into account the additional benefits that mangroves provide, the most cost-beneficial protection standard increases for adaptation strategy B_{new} towards 1000 years.
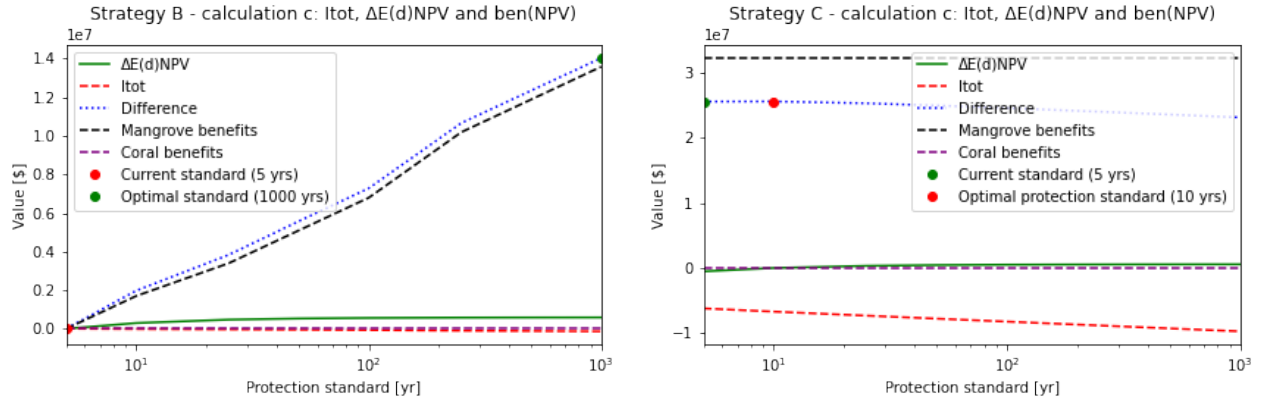
Figure B.17: *The flood risk reduction benefits ($\Delta E(d)_{NPV}$), additional benefits ($ben_{tot,NPV}$) and dike raising + vegetation costs (I_{tot}) plotted against the different protection standards.*

Originally the new protection standard was chosen according to Figure 3.3, where based on the current protection standard a fixed new protection standard was chosen. Those protection standards distributed over all the hotspots are seen in Figure B.18.
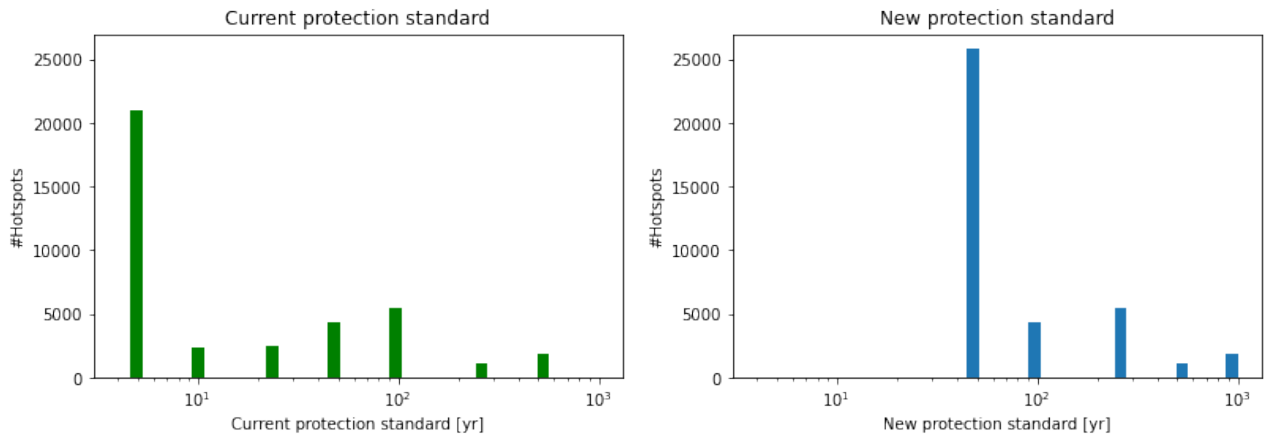
Figure B.18: *The current and new protection standards for all hotspots as determined in section 3.*

For method 2, the most cost-beneficial protection standards are calculated for all hotspots for calculations a-c and adaptation strategies B_{new} and $C_{new,slr}$. The results are given in Figure B.19.
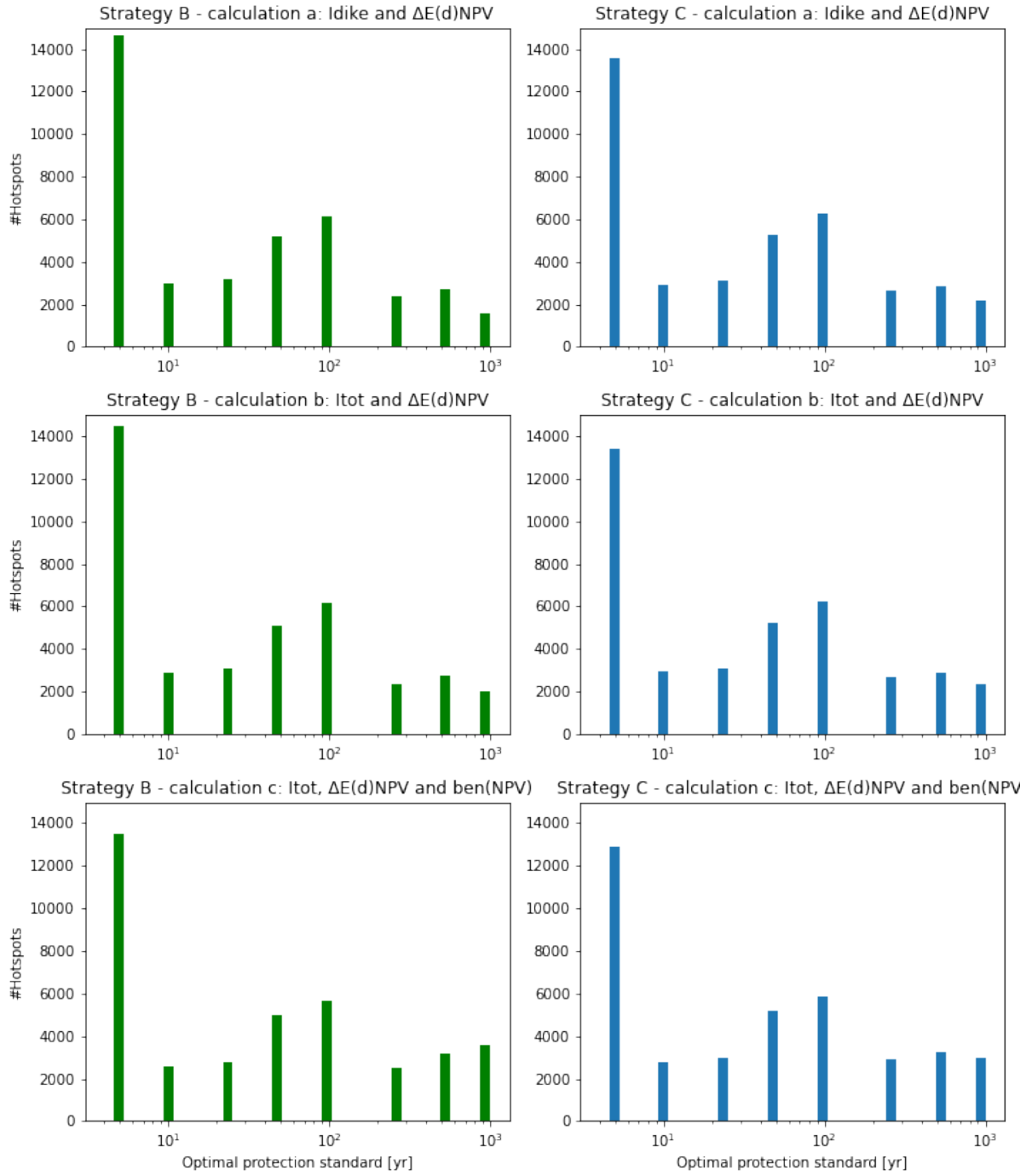
Figure B.19: *The most cost-beneficial protection standards for calculations a, b, c and d for strategies B_{new} and $C_{new,slr}$.*

Overview Python modules

Data_connection.ipynb

- Merging individual data sets
- Calculating mangrove and coral widths
- Assigning protection standards and foreshore slopes
- Determining design water levels corresponding to protection standards
- Assigning unit costs based on GDP

38773 * 45

Sensitivity_analysis.ipynb

Data_calculation.ipynb

- Determining potential mangroves and corals
- Nearshore wave height calculation
- Run-up calculation
- Dike investment costs
- Vegetation costs
- Minimum total costs

38773 * 106

Risk_connection.ipynb

- Calculating design water levels for all return periods
- Loading depth population curves for people flooded with certain depth
- Calculate amount of people flooded for all design water levels

38773 * 138

Risk_calculation.ipynb

- Calculate expected annual people (EAP) being flooded
- Convert EAP towards damage/yr
- Calculate net present value of the risk for design lifetime coastal defence

38773 * 152

Benefit_costs.ipynb

- Calculate additional benefits for restored area of mangroves and corals
- Determine benefit-cost ratios for fixed new protection standards
- Re-calculate benefits and costs for all protection standards
- Determine most cost-beneficial protection standard
- Benefit-cost ratios for most cost-beneficial protection standards

38773 * 346

Figure B.19: All calculations in this research are performed within six different modules that use the results of the previous modules. The yellow diamonds explain the size of the matrix obtained from each module, where 38,773 is the amount of coastal hotspots (rows) and the number on the right is the number of data sets (columns).

C | Case studies

C.1   Field study sites Mangroves

C.1.1   Kantang & Palian Thailand

The two sites Kantang and Palian (Figure C.1C & D) are located in the Trang Province at the west coast of southern Thailand. This part of the coast consists of numerous island and embayments, which in combination with the hydrodynamic forcing offer perfect mangrove habitat (Horstman et al., 2014).
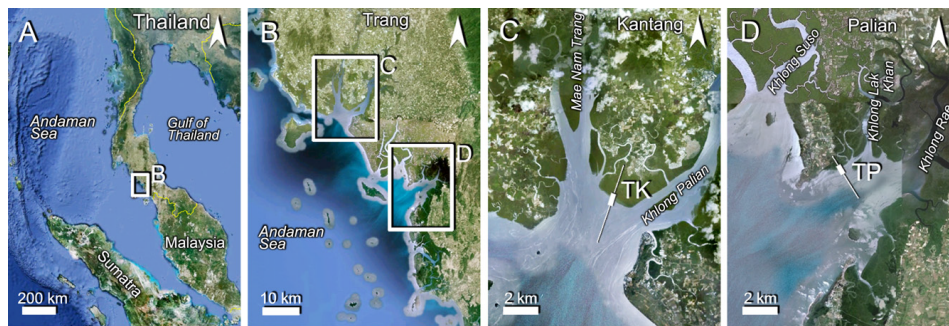
Figure C.1: *Study sites located at the west coast of southern Thailand (Horstman et al., 2014).*

Bathymetry cross-shore transects

Within the study of Horstman et al. (2014) two cross-shore transects are defined, one located in the Kantang estuary (TK C.1C) and one in the Palian Estuary (TP C.1D). The transects are aligned with the prevailing wave direction within the shallow coastal area. Both transects TK and TP feature a gradually sloping foreshore with slopes averaging 0.0033 and 0.006 respectively. Figure C.2A represents transect TK and C.2B represents transect TP.
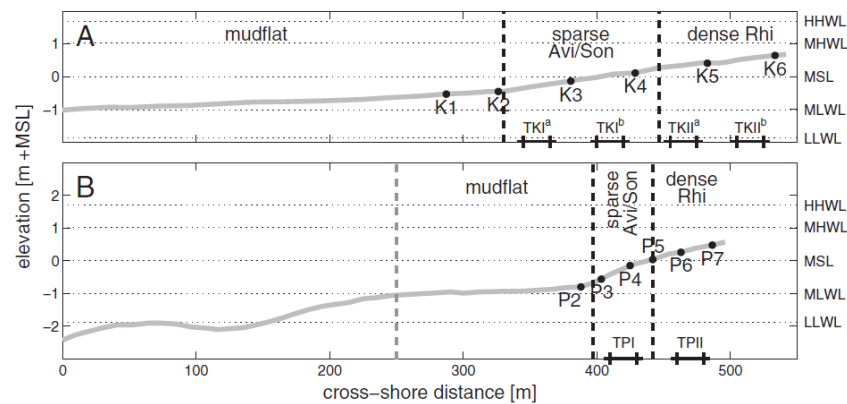
Figure C.2: *A: Kantang transect, slope K4-K4 is 0.0053, K4-K6 is 0.0056 (Hendriks, 2014). B: Palian transect, slope P3-P5 is 0.0162, slope P5-P7 is 0.0103 (Hendriks, 2014). Distinct vegetation zones bounded by dotted lines (Horstman et al., 2014).*

Mangrove characteristics

The Kantang transect consists of a mudflat, a lightly vegetated area with *Avicennia* and *Sonneratia* trees, and a densely vegetated area with *Rhizophoras*. The Palian transect also consists of a mudflat, a lightly

vegetated area with *Avicennia* and *Sonneratia* trees and a densely vegetated area with *Rhizophoras*. For the vegetated areas, the average physical parameters are taken to apply in the empirical approach. The average drag coefficients (C_d) are taken from Hendriks (2014) who calculated the drag coefficients based on the field data (see Table C.1).

	First Area					**Second Area**				
	C_d [-]	N [m^{-2}]	b_v [m]	h_v [m]	W [m]	C_d [-]	N [m^{-2}]	b_v [m]	h_v [m]	W [m]
Kantang	3.3	0.7975	0.07	2	104.8	2.4	0.215	0.19	2	100.03
Palian	4	0.01	0.66	2	43.82	2.7	1.005	0.076	2	52.60

Table C.1: *Average physical parameters for mangrove species Avicennia, Sonneratia and Rhizophoras specific to the field area. The first area for both transects corresponds to the vegetated area located seaward, whereas the second area corresponds to the landward vegetated area.*

Hydrodynamics

During the field study, the observed wave spectra for Kantang was uni-modal. Both sites are dominated by a mixed semi-diurnal tide with a mean tidal range of 2 m and a maximum of 3.6 m. Maximum observed wave heights and corresponding water depths at three stations for the Kantang and Palian transects are given in Table C.2.

	H_1 [m]	H_2 [m]	H_3 [m]	h_1 [m]	h_2 [m]	h_3 [m]
Kantang	0.151 (K2)	0.109 (K4)	0.086 (K6)	1.52 (K2)	0.97 (K4)	0.41 (K6)
Palian	0.268 (P3)	0.211 (P5)	0.097 (P7)	1.95 (P3)	1.25 (P5)	0.71 (P7)

Table C.2: *Hydrodynamic data from the field study (Horstman et al., 2014).*

C.1.2   Vinh Quang Vietnam

This study site is located in northern Vietnam (see Figure C.3), and consists of wide mud flats. The bottom slope of the foreshore is around 0.001, which results in drying up of the mud flats at low tide up to several km offshore (Mazda et al., 2006). A part of the coast is protected by a mangrove belt of 100 m wide consisting of *Sonneratia sp.* that were artificially planted (see dotted area in Figure C.3). The vegetation characteristics of these species are given in Table C.3 (Mazda et al., 2006).

Trees				**Pneumatophores**			
C_d [-]	N [m^{-2}]	b_v [m]	h_v [m]	C_d [-]	N [m^{-2}]	b_v [m]	h_v [m]
3.3	0.008	0.117	0.82	0.6	131	0.0073	0.138

Table C.3: *Physical parameters for mangrove species Sonneratia sp. specific to the field area. The parameters are specific to the trees and the roots (pneumatophores) (Mazda et al., 2006).*

The observed wave heights and the water depths at Stations 4 and 6 are extracted from the data set and given in Table C.4. Stations 4 and 6 can be seen in Figure C.3 and represent the stations at the beginning and the end of the mangrove belt.

	H_1 [m]	H_2 [m]	h_1 [m]	h_2 [m]
Vinh Quang	0.16 (Station 4)	0.14 (Station 6)	0.92 (Station 4)	0.82 (Station 6)

Table C.4: *Hydrodynamic data from the field study (Mazda et al., 2006)*
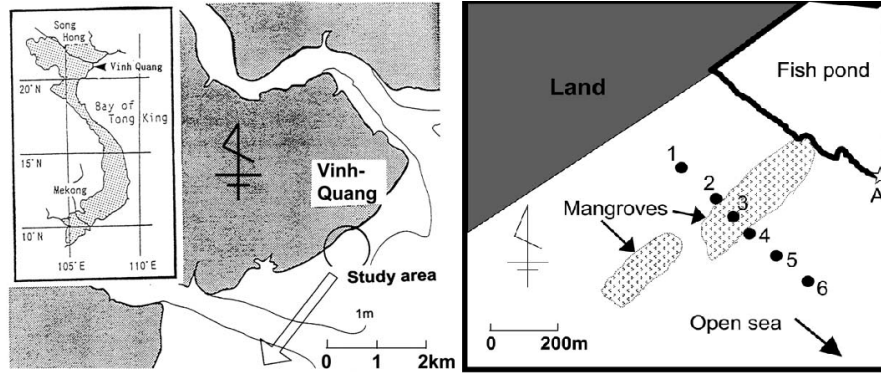
Figure C.3: *Study site along the coast of Vinh Quang (Mazda et al., 2006).*

C.1.3 Nang Hai study site

This study site is located at the mouth of the Dong Tranh estuary (Figure C.5) between the Rach Trung and Khe Ca creeks (Vo-Luong & Massel, 2008). The mangrove belt present at the study area consists of mixed mangroves of *Avicennia sp.* and *Rhizophora sp.* (VL & Massel, 2006). The physical parameters are taken from Pinsky et al. (2013) as no specific data is available for the study site (Table C.5). The bathymetry is measured at 2 m intervals along a 88 m long transect (Figure C.4). The wave heights and water depths at station 2 and at the end of the transect are given in Table C.6.

Avicennia				*Rhizophora*			
C_d [-]	N [m^{-2}]	b_v [m]	h_v [m]	C_d [-]	N [m^{-2}]	b_v [m]	h_v [m]
0.42	0.06	0.4478	3	0.42	0.39	0.1245	3

Table C.5: *Physical parameters for mangrove species Avicenia sp. and Rhizophora sp. (Pinsky et al., 2013).*

	H_1 [m]	H_2 [m]	h_1 [m]	h_2 [m]
Nang Hai	0.27 (Station 2)	0.23	1.3 (Station 2)	1

Table C.6: *Hydrodynamic data from the field study (VL & Massel, 2006).*
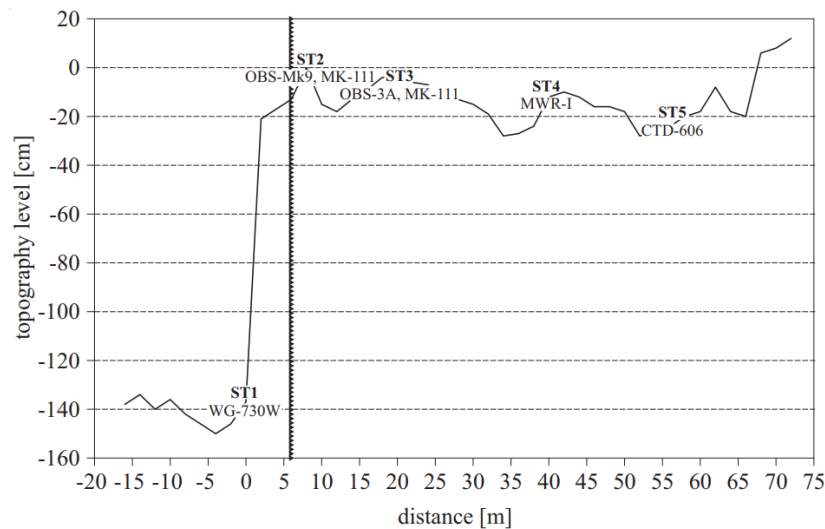
Figure C.4: *Bathymetry of the foreshore and layout of the instruments (VL & Massel, 2006).*

108
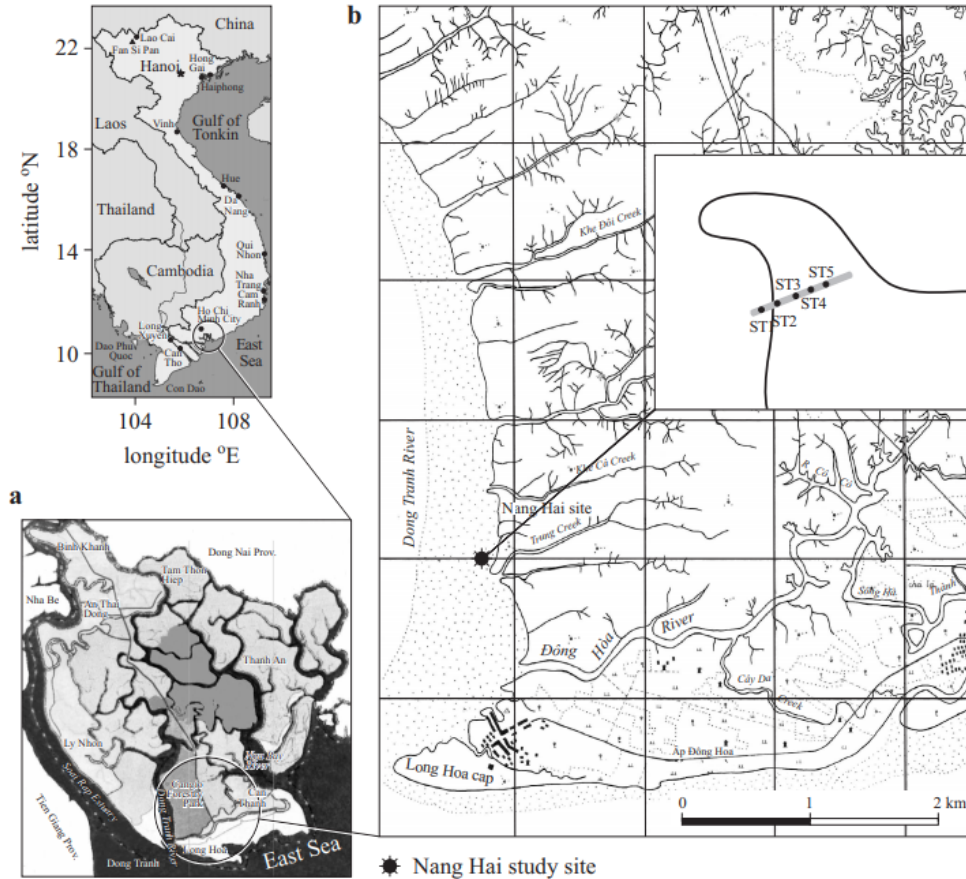
Figure C.5: *Ho Chi Minh, Vietnam (a), Nang Hai study site and transects of stations (b) (VL & Massel, 2006).*

C.2 Coral case studies

C.2.1 Warraber Island

The Warraber coral reef is located in the southern part of the Warrior Reefs within the Torres Strait (Figure C.6a). The reef flat is orientated from east to west with a maximum width of 2500 m (Figure C.6b). The island experiences a mixed semi-diurnal tidal regime with a mean spring tidal range of 2.4 m. At the time of the field study, waves where characterized by heights of 1.4-1.8 m with corresponding periods of 8-10 s (Kench & Brander, 2006).

C.2.2 Lady Elliot Island

Lady Elliot Island is the most southerly island of the Great Barrier Reef and is located around 80 km from the Australian coastline (Figure C.6a). The coral reef is orientated from north-east to south-west with a width of 800 m (Figure C.6b). The study site experiences a diurnal tidal regime with a mean spring tidal range of 1.7 m. The wave climate is characterized by swell waves with heights of 1.15 m that are exceeded 50% of the time (Kench & Brander, 2006).

C.2.3 Cocos (Keeling) Islands

The Cocos (Keeling) Islands are located in the eastern Indian ocean around 3000 km northwest form Perth (Figure C.6a). The coral reef deviates in width between 80 m in the east and 1500 m in the south (Figure C.6b). The study site experiences a micro-tidal regime with a mean spring tidal range of 0.7 m. The wave climate is characterized by wave heights in the order of 2-3.5 m (Kench & Brander, 2006).
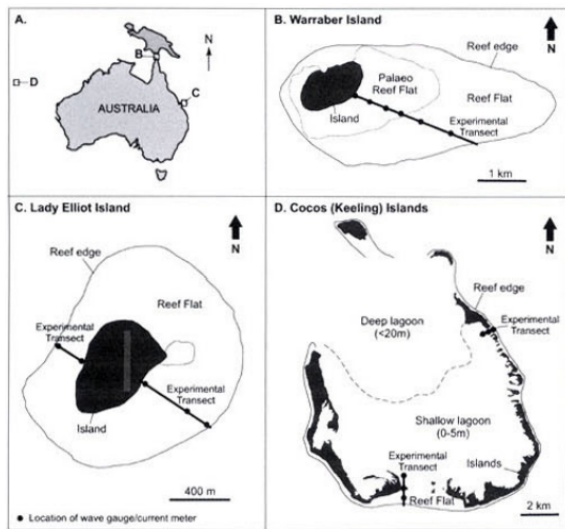
(a)
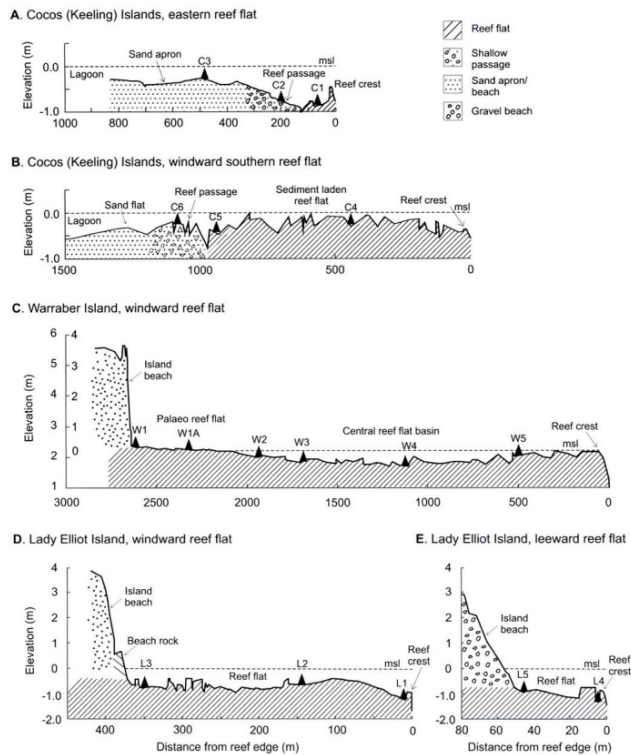
(b)

Figure C.6: *Location of the studied reefs (Figure C.6a), the black lines indicate the transects as seen in Figure C.6b. The morphology of the reef flats from the studied reefs. The triangles denote the wave gauges and current meters (Figure C.6b).*

C.3   Land subsidence

Below, two case studies are shown that provide accurate local data of land subsidence, by monitoring land subsidence in the area for a certain period of time (Yastika et al., 2019; Xu et al., 2016).

C.3.1   Case study Semarang Indonesia

Between the year 2003 and 2017, the subsidence is monitored in the coastal city Semarang. It is found that the northern part of the city, located close to the coast is experiencing severe subsidence with values as high as 16 cm/year as seen in Figure C.7 (Yastika et al., 2019). The magnitude of subsidence is closely related to the geological conditions as can be seen in Figure C.8.
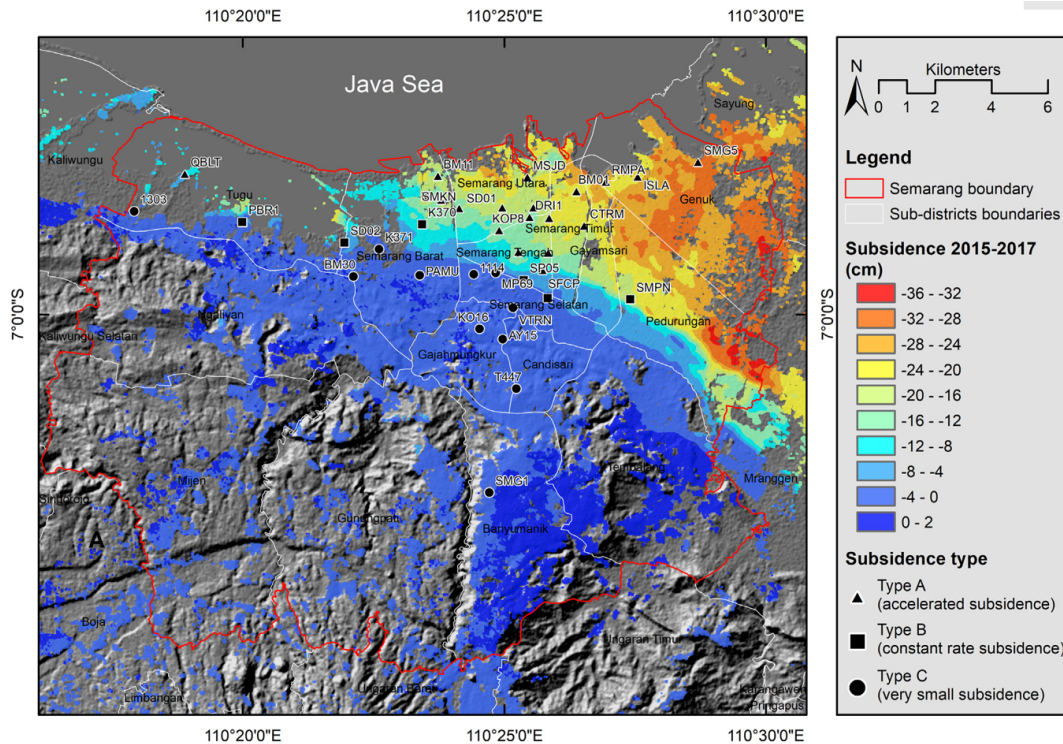
Figure C.7: *Subsidence map of Semarang (Yastika et al., 2019).*
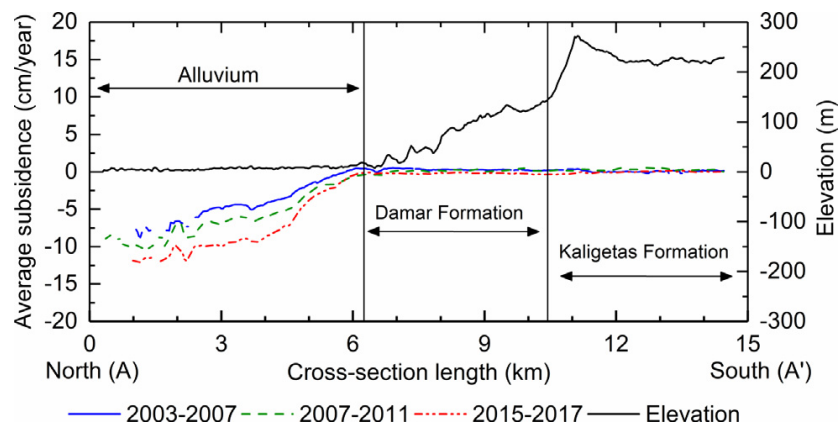
Figure C.8: *Subsidence measured in Semarang (Yastika et al., 2019).*

C.3.2 Case study Shenzhen China

The coastal city of Shenzen is built on weak alluvial clay, which compacts due to the pressure from buildings and the self-consolidation of the clay (Xu et al., 2016). Figure C.9 shows the locations in the Shenzhen area where land subsidence rates are monitored. Table C.7 gives subsidence rates for the areas indicated by respectively A, B, C and D.
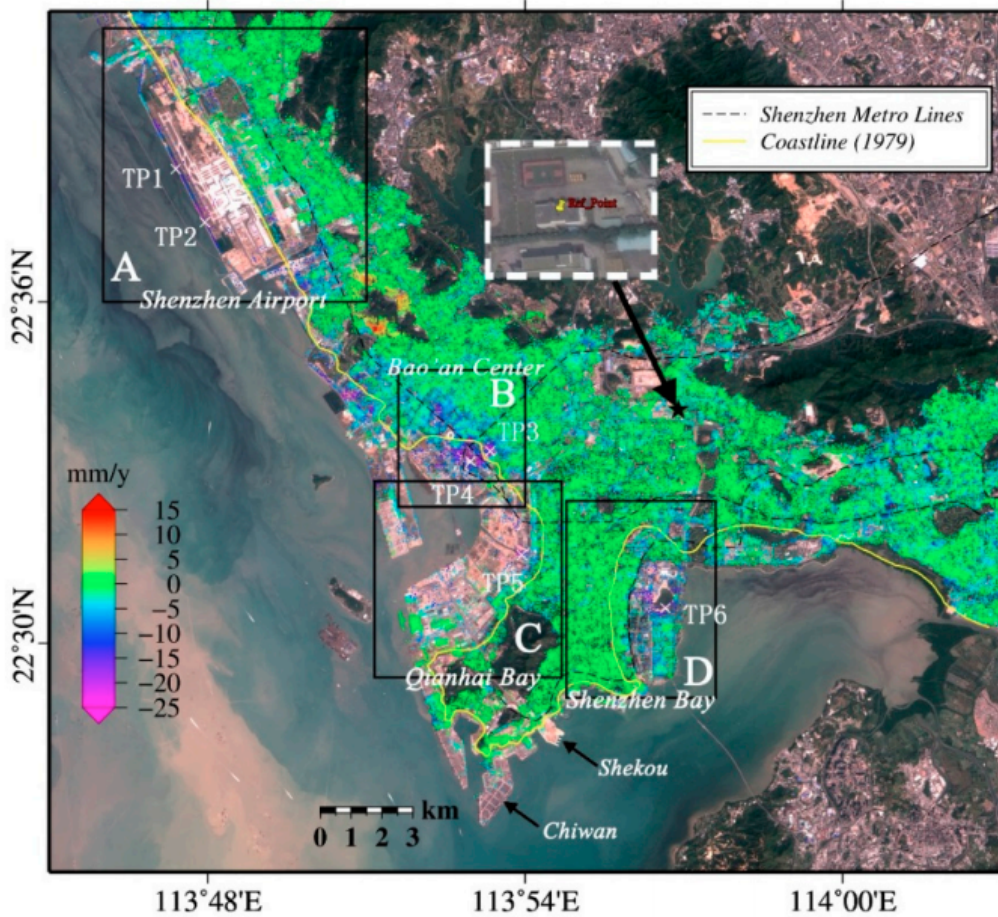
Figure C.9: *Subsidence map of Shenzhen area (Xu et al., 2016).*

Region	Subsidence rate (mm/year)
Shenzhen Airport (A)	-10.7
Bao'an Center (B)	-12.4
Qianhai Bay (C)	-5.5
Shenzhen Bay (D)	-3.9

Table C.7: *Subsidence rates of Shenzhen areas (Xu et al., 2016).*

D | Habitat requirements flowcharts

D.1 Mangrove forests
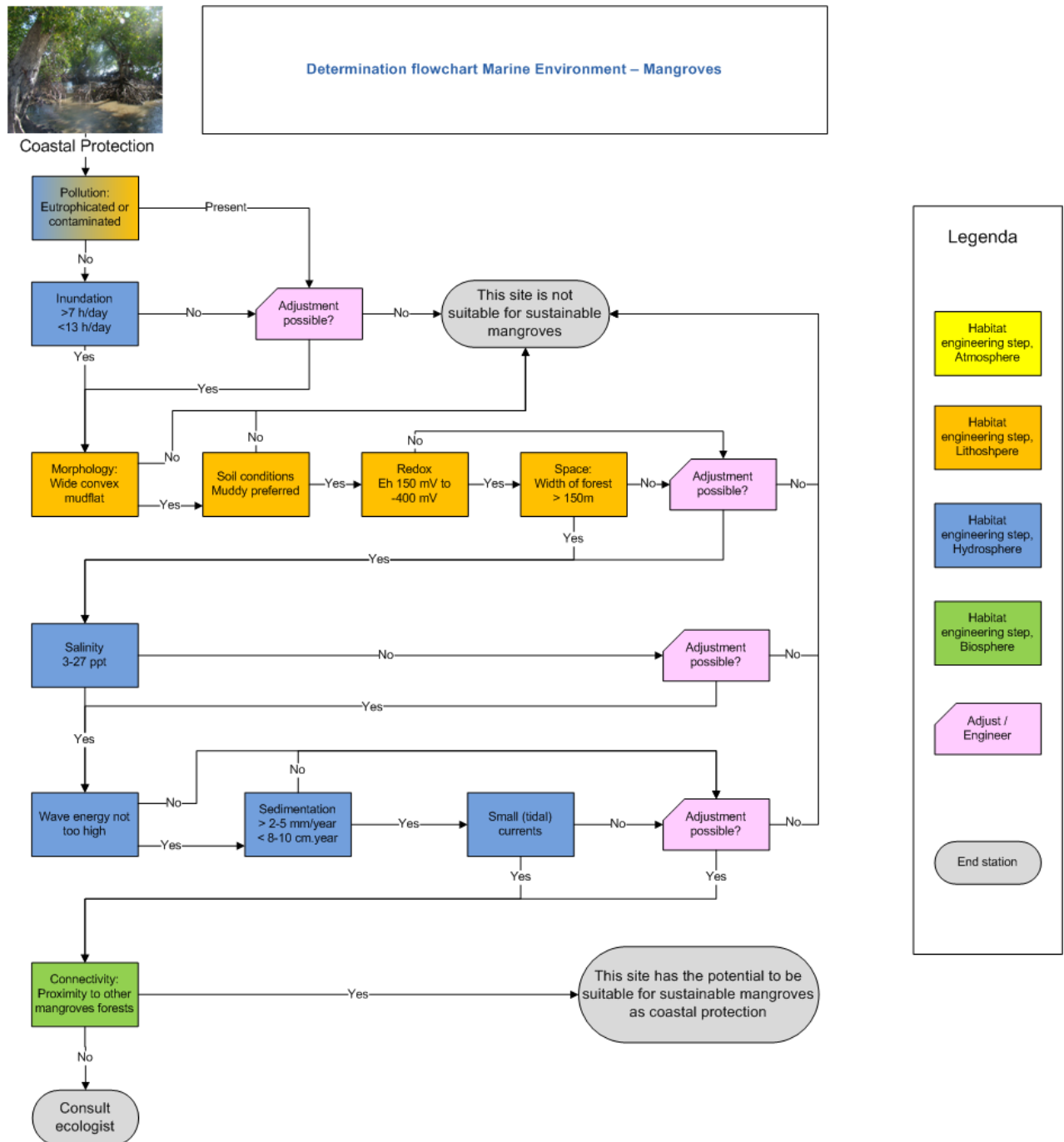
Figure D.1: *Flow chart for development of mangroves (ecoshape, 2020).*

D.2   Coral reefs
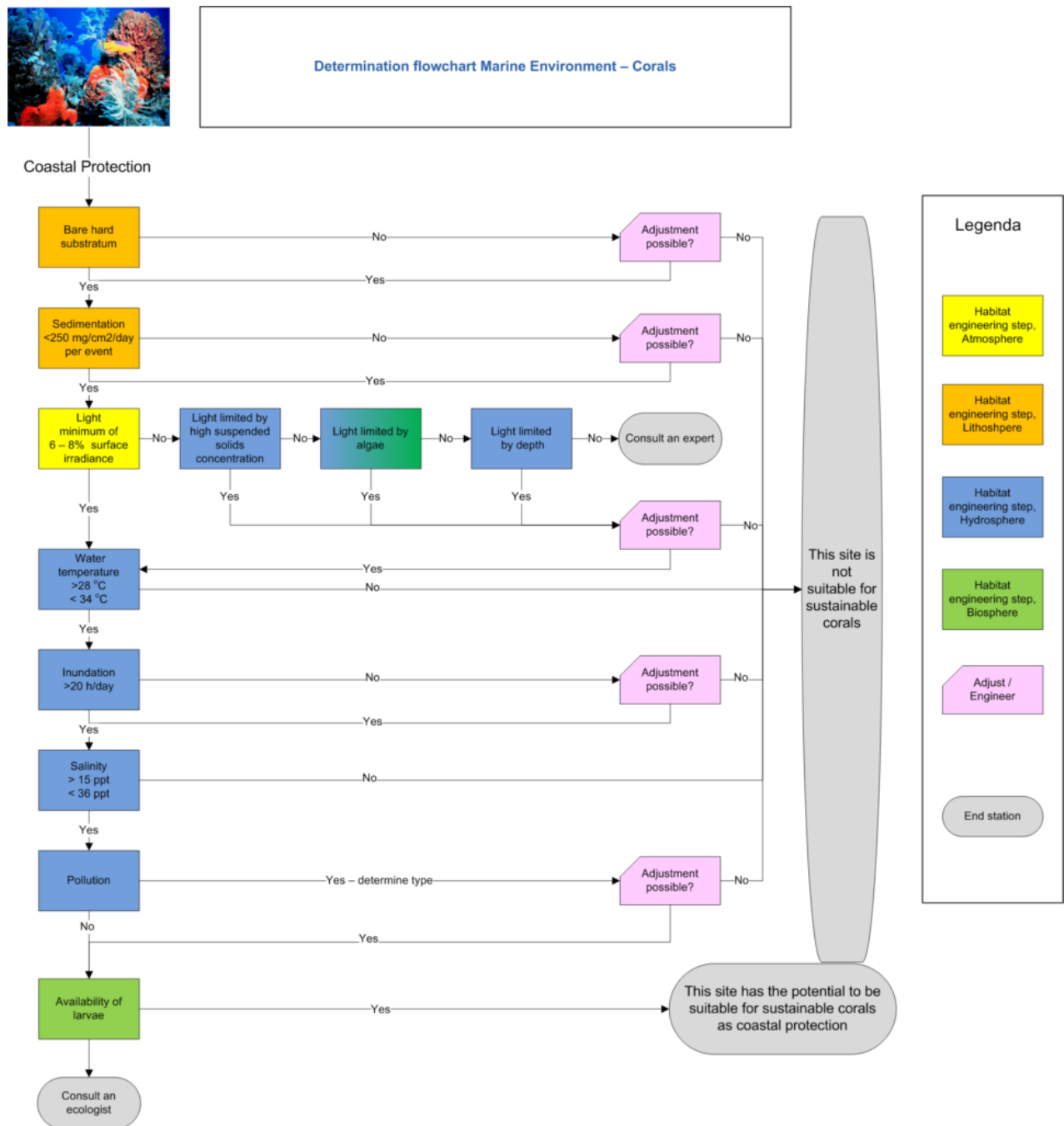
Figure D.2: *Flow chart for development of corals (ecoshape, 2020).*